The effect of alloy composition and heat treatment on the mechanical and stress-corrosion behaviour of Al-Zn-Mg alloy.

Miller, W. S.

Award date:
1977

Awarding institution:
University of Bath

The effect of alloy composition and heat treatment on the mechanical and stress-corrosion behaviour of Al-Zn-Mg alloy.

Submitted by W.S. Miller
for the degree of Ph.D.
of the University of Bath.
1977

W S Miller

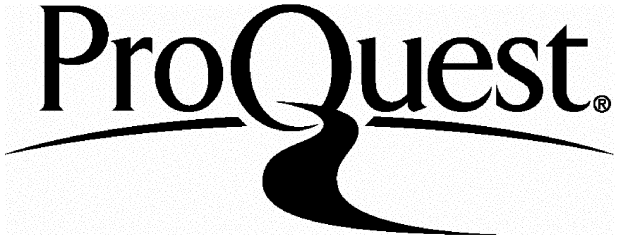

INDEX

SUMMARY

The tensile properties of a range of alloys based upon the Al 4.5% Zn 2.5 Mg system have been studied both in air and in a salt-water environment. The influence on properties of small changes (±0.5 wt%) in the zinc and magnesium contents and also minor additions of copper (< 0.3 wt%), have been investigated as well as the effect of different precipitation ageing treatments. In addition to the mechanical tests a detailed analysis of the microstructures has been carried out. Particular attention has been paid to obtaining quantitative data on precipitate dissemination in the various alloys and to characterise the nature of fracture surfaces. Correlations are drawn between alloy composition, ageing treatment, microstructure and the influence of environment on tensile properties. A new model of stress-corrosion cracking in this alloy system is proposed and suggestions are made for improving the stress-corrosion resistance of Al-Zn-Mg alloys.

1. INTRODUCTION

Al-Zn-Mg alloys belong to the precipitation-hardening group of materials, wherein the composition andheat-treatment schedule is prescribed such that a fine distribution of precipitates are produced in the matrix to confer hardening. These alloys are attractive commercially due to their high strength - to - weight ratios and have been widely applied in industry. Two major fields of use have been in aerospace technology and marine construction. In aerospace applications the alloys have been used in the construction of small aircraft, helicoptors, jet aircraft, rockets and satellites. In marine applications these materials have been employed in above-deck constructions such as superstructures and deckhouses and, also, as a primary material for the construction of hydrofoils, surface-effect ships, fast-patrol boats and hovercraft.

Oneof the chief limitations, however, of AlZnMg alloys has been their susceptibility to stress-corrosion attack, a phenomenon whereby the material can fail catastrophically at stresses of 'sufficient' magnitude and in a damageing environment. Damaging environments for stress-corrosion cracking in AlZnMg alloys include water vapour, aqueous solutions, organic liquids and liquid metals; where stresses causing crack initiation and propogation may be far below the stresses required for gross yielding. This has limited the use of aluminium alloys in a number of fields and an intensive research effort has been undertaken to develop alloys with improved resistance to stress-corrosion cracking, and at the same time to try and understand the basic mechanisms of the phenomenon.

However, before discussing the work and results of this study it isnecessary to understand the microstructure, mechanical properties and the influence of these andother variableson the stress-corrosion cracking behaviour. It is also relevant to consider proposed models of stress- corrosion cracking and to try and understand why themodels are not fully accurate. The following sections review the current state of knowledge of the Al-Zn-Mg system.

2. The Al-Zn-Mg System

2:1 Microstructure of Al-Zn-Mg alloys

2:1:1 Introduction

Aluminium alloys, containing additions of zinc and magnesium, owe their importance as structural materials to the relatively high strengths which may be achieved by precipitation-ageing treatments whilst still retaining reasonable resistance to corrosion. Precipitation-ageing treatments follow the pattern generally adopted for aluminium-based alloys (Anon 1972 a,b). Firstly the alloys are heated to a temperature between 400°C and 500°C to ensure a supersaturated homogeneous solid solution is present throughout the material. The alloys are then either quenched to room temperature and aged to an intermediate temperature to develop precipitates or, they are quenched directly to the ageing temperature and held there for an appropriate length of time. Precipitation-ageing temperatures lie in the range 100°C - 200°C, the temperature chosen playing a critical role in the development of precipitate. Double-ageing treatments may also be carried out in which the material is aged at two different temperatures to optimise specific properties.

The microstructure of precipitation-hardened alloys (Mondolfo, 1971) consists typically of a fine dispersion of precipitate within the grains together with a coarser precipitate at grain boundaries. Adjacent to the grain boundaries a thin zone devoid of precipitate is usually found, designated the precipitate-free-zone (PFZ).

The ageing sequence in AlZnMg alloys has been reported by Mondolfo, Gjostein and Levinson (1956), and Thomas and Nutting (1959/60) as:-

Supersatured Solid Solution → G.P. Zones → η' precipitate → η precipitate

i.e. the supersaturated solid solution decomposes via the sequential metastable structures to the equillibrium precipitate γ. The first-formed reaction products are spherical G.P. zones consisting of dusters of zinc andmagnesium atoms together with vacancies, within the aluminium matrix. There is evidence to suggest that the clusters start as aggregations of zinc atoms into which the magnesium atoms diffuse at a later stage (Naess; 1969). Further ageing cause the G.P. zones to elongate into thin plates identified as the intermediate precipitate γ'. The transformation to γ ($Mg\ Zn_2$) takes place gradually as the thin plates transform into laths. At ageing temperatures above 200°C a T-phase has been reported to form by Laves, Lohberg and Witte (1935) and Bergman, Wang and Pauling (1952). This phase may also occur at lower ageing temperatures at suitable sites such as grain boundaries. A further phase has been reported by Subbarao (1971) as occuring as very long laths.

2:1:2 Nucleation of Matrix precipitates

The simple picture of age hardening given by Smallman (1963) in which the major factor in the nucleation of precipitates is the degree of supersaturation is not valid for AlZnMg alloys in a number of respects. The degree of dispersion in alloys of similar solute supersaturations is frequently different and is often inhomogeneous, varying from grain to grain, in an alloy after a uniform heat treatment. The degree of dispersion is also sensitive to many other factors such as quench rate (Brown and Gourd 1964), the presence of trace elements (Baba, 1968; Bryant, 1966) and ageing sequence (Kelly and Nicholson 1963).

The investigations of Nicholson and his co-workers (Embury and Nicholson 1965; Lorimer and Nicholson, 1966a, 1966b, 1969) have made a definitive contribution to an understanding of the precipitation process.

They observed that an alloy quenched to 180°C and aged at that temperature had a much coarser precipitate distribution than the same material quenched to room temperature prior to ageing at 180°C. The interpretation of this result involved the concept of an additional phase boundary above which the G.P. zones are unstable (Polmear, 1959/58). Nicholson's concept of the G.P. solvus is based on a 'thermodynamic' approach in which the critical temperature is that below which the solid solution is metastable with respect to G.P. zones. Pashley, Jacobs and Vietz (1967) and Jacobs and Pashley (1969) have disputed this 'thermodynamic' approach and have proposed a kinetic theory in which the critical temperature is that above which homogeneous self-nucleation of clusters does not occur andas such is dependent on the vacancy concentration. Consideration of these two concepts by Starke (1970) have shown that the critical temperatureis equivalent for both theories.

Embury and Nicholson (1963) also considered the role of vacancieson the nucleation of the precipitates. A thermodynamic model was proposed in which the vacancies act as a chemical constituent of the nucleating site and reduce the critical nucleus radius for precipitation. A kinetic model was also considered in which the vacancies act as a means of transport for the solute atoms andincrease the rate of decomposition of thesolid solution into precipitate nuclei. They concluded, as did Holl (1967), that kinetic effects play the dominant role and they defined three precipitation-ageing sequences:

a) Quenched andaged above the G.P. solvus: in this case there are no G.P. zones formed and there are no easy sites for nucleation of precipitates. This results in a coarse distribution of particles nucleated on imperfections.

b) Quenched at room temperature and aged below the G.P. solvus : G.P. zones form continuously as the temperature drops below the G.P. solvus andthisprocess continues during the remainder of the quench, the holding time at room temperature and the time taken to heat the material to the ageing temperature. In this case a fine dispersion of precipitate is formed, the density of which is governed by the holding time and temperature, and the initial vacancy concentration. The distribution of the precipitates will be affected by the presence of vacancy sinks such as grain boundaries and dislocations.

c) Quenched below and aged above the G.P. solvus: As the alloy is quenched the G.P. zones form as in the previous case. However as the alloy is heated above the G.P.solvus the zones will dissolve into the matrix forming solute-rich regions. These act as nucleation sites for the γ precipitate. Thus the critical factor in determining the final precipitate density is the time the alloy is held below the G.P. solvus.

However the Pashley model of the G.P. solvus gives a different mechanism. In this model the clusters formed during the low-temperature ageing can reach a size so that they are stable at higher temperatures after the up-quench. Work of DeArdo and Simensen (1973) has shown that, in principle, the mechanism of precipitate refinement suggested by Pashley, Jacobs and Vietz (1967) is the more likely.

Thus in material aged below the G.P. solvus the roleof dislocations is to act as vacancy sinks thus causing a vacancy profile around them and hence an area denuded of precipitate. In contrast in material aged above the solvus temperature precipitates will tend to nucleate on these imperfections.

This proposed model of the nucleation process in AlZnMg alloys require that the vacancy concentration profile plays an

important role. A number of workers have shown that the rate of hardening during ageing increases with an increase in the solution-treatment temperature, and this effect is attributed to the differences in vacancy concentration after quenching. However it has also been clearly established that this effect is not present during room temperature ageing (Ryum 1975a).

Ryum (1975a, 1975b, 1975c) has analysed this problem andhas reached the conclusion that the simple ageing sequence previously described is no longer valid and has proposed that there are several nucleation mechanisms in this system. This confirms the observations of DeArdo and Simensen (1973), Holl (1967), and Guiner (1956). Ryum has proposed the following mechanisms:-

Solid solution $\rightarrow \gamma$	α - reaction
Solid solution $\longrightarrow$ nuclei 'γ' $\rightarrow \gamma' \rightarrow \gamma$	β - reaction
Solid solution $\longrightarrow$ G.P. zones $\rightarrow \gamma' \rightarrow \gamma$	δ - reaction

The activation energy for the α reaction is high and nucleation tends to occur only at high temperatures on grain boundaries and dislocations.

The β reaction has been observed in alloys quenched to room temperature held for five seconds and then aged at 150°C. It is proposed that the holding time of ~5 secs was too short for the formation of G.P. zones and that these precipitates were due to a second nucleation mechanism. Whether these 'nuclei' are very small γ' particles or vacancy solute atom clusters is open to question. The rate of growth of these vacancy dependent nuclei is slow at room temperature, but they are stable at high temperatures (above the G.P. solvus). After prolonged ageing these nuclei transform to γ' andthence to γ.

The δ reaction occurs at all temperatures up to the G.P.

solvus limit. The G.P. zones formed grow on continued ageing and become unstable when the temperature is increased above the G.P solvus. The nucleation andgrowth of these zones is apparently independent of vacancy concentration. Further ageing transforms the zones into γ precipitate probably via the intermediate γ' phase, although this point is disputed by Thackery (1968).

Experimental evidence concerning the initial stages of the precipitation reaction is difficult to achieve, however, since the initial nuclei are too small for direct observation in an electron microscope. Consequently the natureof the inital reaction stages can only be infered from the mechanical properties and from microstructural observations in the latter stages of the ageing sequence.

In a typical ageing procedure all these reactions could perhaps occur, which would result in a very complex structure, and make identification of the influence of any single reaction on the changes in mechanical properties during ageing extremely difficult.

2:1:3 Structure of Matrix precipitate phases

The initial growth of G.P. zoneshas been suggested as being due to the clustering of Zn atoms into which magnesium atoms diffuse (Naess 1969). Jurgens, Kempe and Hoffler (1974) consider that Zn-V and Mg-V pairs (V is a vacancy) are formed after the quench, but that Mg-V pairs predominate due to energetic reasons. Thus any G.P. zone formed will quickly use up the available Zn-V pairs and their growth will be controlled by the diffusion of Mg-V pairs to the zones, thus releasing a vacancy for further diffusion of unattached Mg and Zn atoms.

This influence of vacancies has also been studied by Baardham and Starke (1968). There is no distinct crystallographic structure or orientation of the zones - although they are considered to be coherent with the matrix (Graf, 1965; Dunkeloh, Kralik and Gerold, 1974) A coherent precipitate may be defined as being one in which all Burgers circuits passing through both matrix and precipitate close, when the chemical species of the atoms isneglected.

Thestructure of the intermediate precipitate γ' has been proposed by Mondolfo, Gjostein and Levinson (1956) as hexagonal with a= 4.96 Å and b = 8.68 Å with the following orientation relationship with the matrix,

$(00.1)\gamma' // (111)_{AL}$; $(11.0)\gamma' // (I\bar{1}0)_{AL}$

The precipitate probably has a coherent interface parallel to the basal plane ($2a\gamma'$ = 9.92 Å, $2d_{220Al}$= 9.91 Å) but there is a misfit of 7 per cent in the c-direction. Since the crystal structure of the matrix and precipitates are different, structural dislocations must exist at the peripheral interface of the plane and therefore the precipitate can never be completely coherent. Gjønnes and Simerson (1970) claim that γ' can be indexed as a monoclinic unit cell with a=4.97Å = b, c= 5.54Å and δ = 120°,

and the following orientation relationship:-

$(001)\gamma' // (111)_{AL}$; $(100)\gamma' // (110)_{AL}$

Thackery (1968) has studied the nature and morphology of the equilibrium precipitate in AlZnMg alloys. He concluded that the γ - phase is hexagonal with a = 5.23Å and C=8.59A° and claimed the existence of six orientation relationships of γ with the matrix. These are shown in table 2.1 along with the two other orientation relationships reported in the literature by Schmalzreid and Gerold (1958) and Embury and Nicholson (1965).

Thetype 1 relation_ship (table 2.1) is found to be associated with dislocations and grain boundaries and, tends to be present as platelets rather than laths on $(111)_{Al}$ when occuring in dense precipitate distributions. At regions near grain boundaries they have more room to grow and occur as long laths. Particles associated with types 2, 3 and 4 orientation relationships can be considered as variations of the first type with $(120)\gamma$ // $(1\bar{1}1)_{Al}$ but with $(00.1)\gamma$ rotated in $(111)_{Al}$ direction by 11°, 15°, and 25° respectively instead of lying parallel to $(110)_{Al}$. Precipitates of these three types occur in relatively small numbers. Particles of type 5 occur as hexagonal or rounded platelets lying on $(111)_{Al}$ such that the basal plane of the precipitate is parallel to the (111) planes of the matrix. These precipitates are mainly found occuring in directly-quenched or strain-aged material. Type 6 results in eight-sided platelets on $(100)_{Al}$ and these are present in air-cooled material held at room termperature for a time. Type 7 was identified by Schmalzreid and Gerold (1958) as occuring with another orientation relationship which can be identified with γ'. Type 8 was found by Embury and Nicholson (1965) as occuring in water-quenched material aged at $135^{\circ}C$. These particles showed preferential growth along the (110) matrix directions.

Mondolfo (1969) has calculated the amount of disregistry of each of the precipitate types (see table 2.1) He considered the volume changes from the aluminium solid solution to the final precipitate. Although in nucleation from a liquid the amount of disregistry is not the only factor to consider, (location and number of atoms on matching planes is important) there are indications that the larger the total disregistry the smaller is the probability of an orientation relationship being

formed (Fine 1964). This appears to agree with the results of Thackery, orientation types 1 and 6 with smaller total disregistry appearing most frequently.

Thackery (1968) has also found evidence for the existence of an x-phase. This appears as polygon-shaped particles with at least two orientation relationships with the matrix. The precipitate is probably hexagonal with a = 2.67Å and c = 4.90Å. This unit cell is very similar to that of zinc which suggests that this element is the major constituent. The nucleation of the x-phase is sensitive to quench rate, being observed only in rapidly-quenched material. Since the precipitate does not form near grain boundaries or in regions subjected to quenching strains, it is assumed that the nucleation of this precipitate is strongly vacancy dependent. The x-phase is also stable up to 300°C. It has been suggested by Auld and Cousland (1976) that this phase is some stage in the precipitation of either γ or the T-phase $(AlZn)_{49}\ Mg_{32}$.

The R-phase found by Sabbarao (1971) has a=4.96Å c= 7.02Å and has the following orientation relationship:-

$(10\bar{1}0)_R$ // $(1\bar{1}0)_{Al}$; $(0001)_R$ // $(111)_{Al}$

and grew along $(110)_{Al}$ into very long laths. The phase was found in alloys directly quenched and aged at 180°C.

The T-phase itself which forms above 200°C has a cubic structure with a=14.16Å (Laves, Lohberg and Witte; 1935) or a=14.37Å (Mattoson E, 1971) and has an orientation relationship with the matrix of:-

$(100)_T$ // $(112)_{Al}$; $(001)_T$ // $(1\bar{1}0)_{Al}$

All the final phase precipitates in AlZnMg alloys are incoherent with respect to the matrix; i.e. none of the

Burgers circuits passing through the matrix and precipitate close.

2.1.4. The precipitate - free - zone (PFZ)

Alloys in the system AlZnMg are characterised by the presence of a precipitate -free - zone adjacent to grain boundaries (Starke, 1970). Early workers attributed the presence of these zones to localised depletion of solute atoms due to the preferential growth of grain-boundary precipitates. (Geisler, 1951), Later work of Rosebaun and Turnbull (1959), Taylor (1963/64), and Holl (1964/65) indicated that vacancies were important to the nucleation of precipitate and since grain boundaries act as vacancy sinks, vacancy depletion could be the cause of the PFZ. Following the work of Lorimer and Nicholson (1966), Unwin, Lorimer and Nicholson (1969), and Unwin and Smith (1969) it has become apparent that both factors may result in the formation of PFZs.

In material quenched and aged below the GP solvus a narrow PFZ is formed due to the depletion of solute caused by the rapid growth of grain-boundary precipitates. As the material ages, the grain-boundary particles grow at the expense of the smaller, less stable, GP zones, causing the PFZ to increase in width with time. Thus the PFZ is solute depleted. In alloys quenched and aged above the solvus the nucleation of precipitates is heterogenous and the PFZ width is controlled by vacancy depletion occuring during the quench. The PFZ width is thus independent of ageing time.

Recent work by Doig andEdington (1973, 1975), and Doig, Edington and Hibbert (1973) has somewhat modified these conclusions. They used an electron microscope fitted with an electron energy analyser to measure the magnesium solute concentrations within the PFZ in an Al 6.0Zn 3.0Mg alloy. They found that in material

quenched rapidly into cold water a magnesium-enriched region was present which extended approximately 700Å on either side of the boundary (Doig and Edington, 1974). In oil-quenched and air-cooled material, however they observed a magnesium-depleted region extending ~1,000Å either side of the grain-boundary. Thus in rapidly-quenched material a solute-rich (vacancy-depleted) region is formed, but with a slower quench grain-boundary precipitates are nucleated during the quench. These cause solute depletion of the region adjacent to the grain boundary.

As the rapidly-quenched material is aged the magnesium supersaturation is diminished and the PFZ width is controlled by the magnesium profile. These results are in accord with the theories of Unwin, Lorimer and Nicholson (1969) and further suggest that similar zinc segregation profiles may also occur.

Thus any factor which tends to reduce the vacancy depletion or increase the rateof precipitation will narrow the PFZ. Such factors are high quenching temperatures, rapid quenches, high alloy content, low ageing temperatures and the presence of precipitate-nucleating agents (Mondolfo 1971).

These conclusions are valid for all grain boundaries except those low-angle boundaries with misorientations less than 2°. Below this the PFZ is considerably narrower indicating that the adsorption of vacancies by the boundary is now the rate - controlling process (Unwin, Lorimer and Nicholson 1969).

2.1.5 Grain-boundary precipitation

In the grain-boundary two distinct types of precipitate are able to form, γ ($MgZn_2$ and the T-phase ($AlZn)_{49}$ Mg_{32} (Thackery 1968; Kelly and Nicholson 1963); the latter tends to occur in slowly-quenched materials and in alloys aged at

high temperatures. In addition two distinct types of precipitates are found, thelarge type being nucleated during quenching and the smaller nucleated during ageing (Unwin and Nicholson 1969).

The number and distribution of quench-nucleated precipitates depends on two factors, the solution-treatmenttemperature and the quench rate. The quench-nucleated precipitate becomes finer as the solution-treatmenttemperature is raised. It has been implied by Cundy, Metheral, Whelan, Unwin and Nicholson (1968) that the absolute vacancy concentration is important, and that segregation of solute occurs during the quench, thus increasing the solute supersaturation at the boundary and hence, increasing the precipitation nucleation rate. The effect of quench rate is insignificant when quenching to ageing temperatures above the solvus. When quenching to temperatures below thesolvus, however, the rateof cooling is important and the density of precipitates isaffected. This factor is of importance due to the high rate of diffusion and the reduced activation energy for nucleation of precipitates at grain-boundaries compared with thematrix. As a consequence grain-boundary precipitates grow at low supersaturations and during rapid quenches. If thenucleation rate is high and the cooling rate low, the supersaturation will be reduced so that no further nucleation of precipitate occurs during ageing and a single-peaked size distribution results. If the quenching rate is high, solute denudation along the boundaries may not be complete, and further precipitates nucleate during ageing to give a bimodal size distribution. The precipitates nucleated during ageing tend to besmall and of high density, congregating in boundaries with few quench-nucleated precipitates.

Cornish and Day (1969), Unwin and Nicholson, (1969) and

Butler and Swann (1976) have studied the effect of the grain-boundary misorientation on the nucleation and growth of these particles. At high supersaturations all boundaries tend to produce a similar precipitate distribution, but with low or medium supersaturations variations occur according to the grain-boundary misorientation; low-angle boundaries show copious nucleation, except for the case of boundaries with misorientations less than 2^{o}, where little or no precipitate is nucleated. On low-angle boundaries with small misorientations, the precipitates grow in the form of sharply-pointed crystals along dislocations. In other low-angle boundaries growth is more difficult, probably because the growth directions for the γ precipitate in the matrix are not close to theboundary plane. In thiscase the precipitate morphology resembles that of random boundaries.

Randomly-orientated high-angle boundaries allow copiousnucleation to occur (Phumphry,1973). These precipitates resemble the lath-like particles in the matrix which lie on the (111) habit planes. For high-angle boundaries, where the misorientations are close to that of a coincidence site lattice, little precipitation occurs and, as the precipitates grow, they orientate with respect to oneor other of the boundary crystals. Theprecipitate shape is determined by local anisotropy of the solute diffusion profile along the boundary. These results may be explained by proposing that in material where the supersaturation is low, precipitates nucleated during quenching tend to form on dislocations and imperfections with the grain-boundary.

The rate of growth of theseprecipitates can be divided into three stages. Initially the kinetic influence of the boundary is most important with precipitates growing rapidly in the plane of the boundary to adopt a plate-like appearance.

The second stage occurs as the precipitates increase in size due to the diffusion of solute from the matrix, and growth takes place in the direction normal to the grain-boundary plane. The final coarsening stage occurs when compositionalequil_ibrium is reached in the vicinity of the precipitate and their area fraction ceases to increase significantly. The precipitates become irregular as the effect of interfacial structure becomes increasingly important.

2:1:6 The effect of copper additions.

The addition of small quantities of copper (less than 1%) i.e. below the amount necessary for the formation of new phases, has been studied by Thomas and Nutting (1959/60) in Al 6.0Zn 2.5 Mg with the addition of 0.5% copper. It was found that copper decreased the ageing rate and lowered the hardness maximum. The ageing sequence remained as in the ternary alloy, with changes in therate of formation of the various phases. The G.P. zones were found to belarger than in the ternary alloy, but of lower density (approximately one quarter that of the ternary alloy when aged at 160°C). The duration of the G.P. zone stage was longer in the ternary alloy, but once the γ' phase started to form the G.P. zones rapidly disappeared. The γ phase precipitates were much larger than those found in theternary alloy at equivalent ageing times. As in theAl-Zn-Mg alloy thegrain-boundary region showed the same sequence of changes during ageing, but with the development of coarser, more widely-spaced particles.

Parker (1972) has studied the effect of the addition of 1% copper on Al4OZn3.OMg and has found that the G.P. Solvus is raised by approximately 20°C above that of the ternary alloy.

At 120°C the ageing sequence was more rapid than that of the ternary material and the peak-hardness increased. Ageing above the G.P. solvus at 190°C decreases the ageing rate and raised the peak hardness. The precipitate structure was similar, although electron diffractions patterns of material aged at 190°C suggested that G.P.B. zones and the S-phase of the AlCuMg system (Peel 1975) were present.

In conclusion it appears that insufficient work has been done on theaddition of small quantities of copper to draw any firm conclusions as to its effect on the ageing behaviour. However reference to thephase diagram work of Zakharov (1961) and Fink and Willey (1937) suggest that the addition of copper to ternary alloys reduces the solubility af zinc and magnesium in the matrix. Hence the supersaturated solid solution would tend to decompose more readily at a given quenching rate than a corresponding alloy without copper. It isthus possible that the effect of copper is simply additive to the magnesium rather than alternating the nature of the precipitation sequence.

2.2. The Mechanical properties of AlZnMg alloys.

2.2.1 Precipitation hardening.

Al-Zn-Mg alloys show an increase in strength with time of ageing. A maximum hardness is reached due to the interactions between the fine-scale precipitates and mobile dislocations, and this is followed by a decrease in strength as the precipitate distribution changes and becomes less effective as a dislocation barrier. Recent views of precipitation hardening by Kelly and Nicholson (1963) and Fine (1975) have discussed the various mechanisms which may operate in these alloys.

Several dislocation theories of precipitation hardening have been advanced and it is probable that several mechanisms

simultaneously contribute to the total resistance to dislocation movement.

Initial hardening is due to solid-solution hardening from dissolved atoms in the metal lattice (Fleischer and Hibbard 1963). This may be due to either pinning of dislocations in their initial positions or by raising the friction stress resisting their movement over a slip plane, or by making it difficult to avoid obstacles by cross slip. Treatments of this problem by Mott (1950) and Friedel (1964) in which they assume that the solute atoms always attract the dislocation, indicate that theyield stress depends on the binding energy of the dislocation and the solute atom, U and the number of obstacles per unit volume,Ns. Ns, for atomic obstacles, is equal to the volume fraction of solute divided by the square of the atomic separation in the metal.

The interactions between a dislocation and a precipitate can be divided into short-range and long-range interactions, the former occuring as the dislocation passes through the precipitate and the latter when the dislocation is about the same distance away from the precipitate as the precipitate spacing. The long-range interaction factor was first considered by Mott and Nabarro (1940,1948) in which the internal stress created by misfitting solute atoms are taken into account. These long-range stresses are due to coherency stresses of the precipitate lattice with that of the matrix and must be overcome before a dislocation can move through the lattice. The theory of Mott and Nabarro leads to the conclusion that the flow stress of the material, τ due the precipitates is dependent on the volume fraction of precipitate, f, according to the equation:- $\tau = 4G\epsilon f$

where G is the shear modulus of the matrix and ϵ is dependent on the difference in atomic volume between the matrix and the precipitate, the bulk modulus, and Poisson's ratio of the matrix.

In the case of short-range interactions the dislocations can either pass through the precipitates or bow out round them. The former case is termed chemical hardening and the later case dispersion hardening.

The case of chemical cutting is considered according to the theory of Kelly and Nicholson (1963). Suppose a dislocation is moving in its slip plane and this slip plane is pierced by coherent precipitates which are spherical in form. As the dislocation moves forward a distance equal to its Burgers vector b, it displaces atoms in the precipitates lying above and below the slip plane by a distance b, and this occurs over a length of the dislocation lying within the precipitate as shown in Fig. 2.1. If γ is the energy of the interface produced when a precipitate is sheared by the dislocation we obtain for the flow stress:

$$\tau = \frac{\gamma}{\alpha} \frac{f^{1/2}}{b}$$

where f is the volume fraction of precipitate and α is a constant equal to 1.13. The term γ, the interfacial energy, consists of two terms; the energy of the additional particle-matrix interface produce by slip and the interfacial energy due to the order within the precipitate..

Two theories have been advanced to account for the yield stress of a material containing particles which are not sheared by the initial dislocations crossing their slip plane. Orowan (1948) pointed out that if a soft and ductile matrix contains hard particles of a second phase intersecting the glide plane of dislocations between the particles, and if the stress is large enough to bend the dislocations into a semi circular shape between the particles, the dislocations can pass by them leaving encircling loops of dislocations at the particles as

shown in fig 2.2. The final form of Orowan's prediction is that the flow stress is given by $\tau = \frac{1}{L} \frac{Gb}{2\pi} \phi \ln \log \frac{L}{2b}$ where G is the shear modulus of the matrix, b is the Burgers vector of the dislocation, L is the spacing between precipitates and ϕ is a constant equal to $\frac{1}{2}(1 + \frac{1}{1-V})$, where V is Poissons ratio.

Ansell and Lenel (1960) suggest that the Orowan bowing mechanism is inapplicable and that the pile-up of dislocations behind the precipitates eventually cause the fractureof the second-phase particles However the problem of the theory is that it assumes the matrix does not yield until the fracture of the second-phase occurs. The final form of prediction given by Ansell and Lenel (1960) and Ansell (1961) is:-

$$\tau = \frac{G'}{4c} \frac{f^{1/3}}{(0.82 - f^{1/3})}$$

G' is the shear modulus of the precipitate, c is a constant approximately equal to 30 and f is the volume fraction of precipitate.

In the case of AlZnMg alloys very little data has been gathered as to which mechanism isoperating at the various stages of theageing process. It has been shown by Thomas and Nutting (1959/60), Thomas (1959) and Kelly and Fine (1957) that the increase in hardness on ageing is associated with the increase in number and size of the particles, with a corresponding decrease in particle spacing. It was shown that it is easier for dislocations to cut through the precipitates than pass around them, and that the stress required to do this is inversely proportional to the particle spacing. However, this relaionship is in agreement with the Orowan mechanism rather than a cutting mechanism. Fine (1975) has shown that GP zones can be cut by dislocations and Holl (1967) and Ryum (1968) have shown that semi-coherent γ' precipitates can be cut by dislocation. Embury, Wilcox and Clauer (1972) have shown evidence for the Orowan mechanism occuring in overaged alloys. However there has been no quantitative study on precipitation-hardening mechanisms in these alloys.

2.2.2. Fracture in AlZnMg

It has long been thought that the brittleness of AlZnMg alloys was due to the presence of a weak precipitate-free-zone adjacent to the grain boundaries causing intergranular fracture (Varley, Day and Sendorek; 1957/58). Cornish and Day (1971) found a fall in ductility with an increase in the PFZ width. They concluded however, that since an increase in grain-boundaries precipitate size and area-fraction of precipitate accompanied this increase in PFZ width, the distribution of grain-boundary precipitate was the major contributing factor.

A number of workers have suggested that a fracture of these alloys is associated with build-up of deformation in thin bands within the matrix (Ryum, Haegland, and Lindtviet; 1967, Ryum (1969). The concentration of dislocation movement into these bands may be expected if the matrix precipitates are sheared by dislocations the effective cross sectional area of the particles decreases, thus offering less resistance to further defomation. In regions when these bands impinge on the grain-boundary, high tensile stresses are built-up when the tensile stress exceeds the cohesive stress of the boundary fracture occurs (Ryum and Baardseth, 1968).

Lynch(1973) doubts that slip bands within the matrix are caused by shearing of coherent and semi-coherent particles, since simikr slip-bands are observed in overaged material containing only incoherent particles. He suggests that these discrete bands are caused by slip introduced during quenching, locally modifying the subsequent precipitation. Dislocation movement is easier in bands with lower than average precipitate density and preferential deformation within these bands of tangled dislocations. Lynch also consider that they play no part in the fracture process.

Pugh and Johns (1961), Forsyth and Wilson (1963/64) and Sedriks, Slattery and Pugh (1969) have proposed a different mechanism for the concentration of stress in the PFZ. Dislocations are generated of sources at the grain boundary and move across the soft solid solution within

the PFZ until motion is inhibited by the presence of the fine matrix precipitate. Under increasing stress they move into thematrix (Abe, Asano and Fujiwara; 1973). The increase in stress leads to decohesion of the grain-boundary precipitates and ductile rupture of the PFZ causing fracture.

A basic model of the fracture of AlZnMg alloys given by Lynch (1973) is that deformation withih the grain interiors is small and that the low overall ductility is mainly associated with deformation in and near the PFZ. Deformation of the PFZ leads to decohesion of grain-boundary precipitate/matrix interfaces causing the growth and nucleation of voids. When the area fraction of voids is large enough, intercrystalline failure occurs over the remainder of the specimen. The area fraction of voids will be related to the relative displacement of the grains and the overall elongation. If the fracture toughness is low failure will occur when the area of coalesced voids is small (Hahn and Rosenfield, 1975; Van Stone and Psioda 1975). Thus large local strains are necessary in only a few favorably orientated PFZ's and ductility is consequently low. If the fracture toughness is high, large areas of coalesced voids can be tolerated before failure occurs. Thus defomation can occur in a large number of PFZ's resulting in improved ductility.

2.2.3 The influence of microstructureon the mechanical properties.

As discussed above, brittle inter-crystalline failure occurs by decohesion of grain-boundary precipitate/matrix interfaces and by fracture of the PFZ between particles. The first process requires little plastic defomation since the cohesive strength of these interfaces is low and therefore the majority of energy expended is due to the plastic deformation of the PFZ. Calculations of the size of theplastic zone indicate that it is larger than the PFZ for most materials. However, since the energy expended in deforming the soft PFZ is large cf the hard grain interiors, it is expected that the fracture toughness should depend on the PFZ width and the area-fraction of grain-boundary precipitates.

If the area-fraction of precipitate is large the decohesion will readily occur on the weak precipitate/matrix interface and the fracture toughness will be low and be little affected by changes in the PFZ width. The fracture toughness will increase with decreasing area-fraction of precipitates as observed by Unwin and Smith (1969)., Increased plastic deformation is associated with fracture of material between the precipitates rather than solely with interface separation. This is more likely to occur the wider the PFZ. If the PFZ is narrow little energy is expended on the plastic deformation and the amount of deformation required to fracture the precipitate/matrix interface may differ little from that associated with interface fracture. The area-fraction of grain-boundary precipitates should have little effect on fracture toughness, again observed by Unwin and Smith (1969). When the area-fraction is small fracture will occur primarily between the precipitates and the fracture toughness should increase with increasing PFZ width. This has been observed by Ryum and Baardseth (1968) who found an increase in ductility with increasing PFZ width.

For material with a constant grain-boundary structure a decrease in matrix precipitate density will be associated with an increase in overall ductility, because more deformation is able to occurin the grains adjacent to the PFZ during unstable crack propogation.

2.3 The stress-corrosion of AlZnMg alloys.

2.3.1. Introduction.

Aluminium and its alloys can fail by cracking along grain-boundaries when simultaneously exposed to specific environments and to stress of sufficient magnitude (Speidel 1971; Parkins, 1964, and 1972). The conjoint effect of stress and corrosion may result in failure of the material at a stress much lower than that expected from its published mechanical properties. Despite considerable progress in recent years in improving the resistance to stress-corrosion cracking (SCC) of aluminium alloys, the phenomen continues to be an important aspect of the development of aluminium alloys.

Intensive research effort within the past two decades directed towards an understanding of SCC in metals has been put into the mechanistic aspects of stress-corrosion. However a full understanding of them still has to be obtained (Lees, Ford and Hoar, 1973). There has been a proliferation of mechanistic processes by which stress-corrosion occurs, but no one theory to date appears to give a satisfactory explanation of all the observed facts. A number of papers reviewing thepublished literature on SCC have been published by a number of authors; Brown (1968), Brown, Sprowls and Shumaker (1972), Hyatt and Speidel (1972), and Speidel and Hyatt (1972). Any theory of SCC should take into account mechanical, metallurgical and environmental factors, and there are five points necessary for the formulation of such a theory:-

a) qualitative observation of such factors as the damaging environment and chemical reactions at the crack tip.

b) systematic quantitive measurement of SCC, e.g. stress, rate of crack growth, temperature and metallurgical variations.

c) assumption of a plausible working hypothesis.

d) development of the hypothesis into theory.

e) comparison of theory with experiment.

2.3.2. Mechanical aspects of SCC

Much of the recent work on stress-corrosion has been undertaken using a double-cantilever beam (Berry(1960); Hyatt (1969)). A short description of this technique is detailed below, because many of the results discussed in later sections are in the form obtained from these tests. However many other tests are used to determine the stress-corrosion characteristics of AlZnMg alloy e.g. (ring tests, constant-load and constant-strain - rate tests as well as service testing (Ketcham, 1972; Parkins, Mazza, Royvela and Scully, 1972).

If we consider the stresses near the tip of a crack in the opening mode in an elastic, isotropic body, fig. 2.3, it is found that they may

be fully characterised by a single parameter, the stress-intensity factor k_I. It should be noted that propagating stress-corrosion cracking in aluminium alloys is not truly elastic; a zone of plastic deformation about the crack-tip poses serious theoretical problems. However, the stress-intensity parameter has been found to correlate well with the effect of load and specimen geometry provided the plastic zone is small compared to the specimen dimensions.

The double-cantilever specimen is shown in fig. 2.4. The equation for the stress-intensity factor, provided the deflection, f , at the load line and the crack length, a, are known, may be expressed

$$K_I = Efh \frac{(4h(a+0.6h)^2 + h^3)^{\frac{1}{2}}}{4((a+0.6h)^3 + h^2 a)}$$

where E is Young modulus and h is the specimen width (see fig 2.4.) As the crack length, a, increases the crack-tip stress intensity decreases. Thus the effect of stress-intensity on the stress-corrosion crack velocity can be measured conveniently and economically by this method. A typical result is shown in fig 2.5. where the velocity of stress-corrosion cracks is plotted as a function of crack-tip stress intensity (v-k curve) for two alloys (Blackburn and Speidel,(1971), Feeney and Blackburn(1971)). This illustrates that a good corelation between crack-tip velocity and stress-intensity is observed if mechanical and environmental parameters are kept constant. It should benoted that at low stress intensities there is a strongly stress-dependent region of the v - k curve, whereas at higher stress intensities a plateau region occurs where the velocity is independent of the stress intensity. It is sometimes stated that there is a minimum stress intensity below which stress-corrosion cracking does not occur, but this may be due to tests not being carried out for sufficient time at very low intensities. Mechanical parameters other than crack-tip stress intensity e.g. state of the stress, loading rate appear to be of minor importance, but systematic investigations have not yet been performed (Scully ,1968a) However of great influence on the susceptibility to stress-corrosion is the orientation of the crack and the stress to

the processing variables of the alloys, which have not been recrystallised. (Elkington 1961/62). It has been noted by Ugiansky, Skolnick and Strefel (1969) and, Wacker and Chu (1972) that the longitudinal direction of extruded material is more resistant than the transverse direction.

2.3.3. Environmental aspects.

The general environmental aspects of stress-corrosion cracking has been reviewed by Scully (1968b). Aluminium alloys have not been found susceptible to stress-corrosion in dry gases;- dry H_2, dry N_2, dry O_2 and dry air do not support stress-corrosion crack growth (Speidel 1975). However the growth of stress-corrosion cracks commences on the introduction of water vapour, the rate of crack growth increasing as the humidity of the environment is increased (Watkinson and Scully 1971). There appears little acceleration of the crack growth rate when the environment is changed from moist gas to distilled water. However the addition of halide anions Cl^-, Br^-, I^- increases the growth rate of stress-corrosion cracks in aqueous solution above and beyond the velocity measured in distilled water. The action of these anions is important for several reasons (Speidel 1971);

a) the presence of these ions in marine environments.

b) theuse of aqueous Cl solutions in accelerated SCC tests.

c) the fact that they are unique pitting agents for aluminium and its alloys and this can influence both the initiation and propogation of S.C.C.

The enhancement of stress-corrosion crack growth by halides depends strongly on metallurgical, electrochemical, mechanical and environmental factors. Other parameters of the aqueous solution which affect the stress-corrosion crack growth rate are the ion concentration, pH, temperature, viscosity and the influence of electrochemical potential. Increasing the halide ion concentration of the aqueous solution causes a rapid increase in the velocity of the crack in the stress-independent region of the v-k curve, but in the stress-dependent region the v-k curves tend to merge together, see fig. 2.6. (Watkinson and Scully, 1972; Speidel 1971)

There is little quantitative data on the influence of pH on the crack velocity, fig. 2.7. (Sedriks, Green and Novak, 1970). It appears that the crack velocity is not affected by pH in the stress-independent region, but in the stress-dependent region the crack grows faster the lower the pH. Oneof the major problems in obtaining accurate data is that the pH at the crack tip may differ from that of the bulk solution (Sedriks, Green and Novak; 1971).

The effect of temperature is important since temperature variations during service may be significant e.g. changing from a marine polar to a tropical condition. This influence is illustrated in fig. 2.8. High temperatures cause an increase in the rate of crack growth, and the onset of the stress-independent region of the v-k curve occurs at a lower stress intensity. From these data the activation energies (Q) of the crack may be calculated for both regions. For a stress-intensity of ~ 5.5 (MN/m)3/2 the activation energy for the stress-dependent region is 27 Kcal/mole and in the stress-independent region a value of 3.8 Kcal/mole is found for stress intensities between 14 and 17(MN/m)3/2.

Fig. 2.9 shows the influence of viscosity of a salt-solution environment (Speidel 1975). The viscosity has little influence on the stress-dependent region, but in the stress-independent region the crack velocity is inversely proportional to the viscosity.

Stress-corrosion cracking of aluminium alloys can be dramatically reduced by cathodic protection (Speidel 1974; Eurof-Davies, Dennison and Mehta 1971). This is illustrated in fig. 2.10 where it can be seen that the application of a negative potential reduces the growth by a factor of more than $-X10^3$. The effect of potential is important for practical applications (cathodic protection) as well as for fundamental studies in the mechanisms of SCC (Sprowls and Brown 1969).

2.3.4. Metallurgical Aspects.

Alloy composition and heat treatment strongly affect stress-corrosion crack growth in aluminium alloys (Hyatt and Speidel 1972). The number of

quantitative results are limited and although a number of trends are apparent they are of limited value because exceptions are numerous e.g. alloys tend to become more susceptible as the yield strength increases, while alloys are more resistant the higher the fracture toughness. Fig. 2.11. demonstrates, however that both these points are not necessarily always true.

2.3.4.1. Alloy composition

SCC in aqueous solutions has been observed in Al-Ag, Al-Cu, Al-Cu-Mg, Al-Mg, Al-Zn, Al-Zn-Mg, Al-Zn-Mg-Cu, Al-Mg-Si and many other aluminium alloys (Speidel 1975). The following points appear valid.

a) pure aluminium is not susceptible

b) susceptibility increases with increase in any addition element that forms a super-saturated solid solution

c) the stress-corrosion resistance of ternary and higher order systems is influenced not only by the sum of the alloying additions but also by their ratios.

d) small additions (several tenths of a percent) of a number of metals to a high purity alloy can significantly affect its stress-corrosion behaviour e.g. Cr (Bischel, 1973; Saito and Tanaka 1972), Mn (Bryant 1966), Zr (Kulig 1973), T (Chen and Judd 1973) and V (Polmear and Scott Young 1958-59).

2.3.4.2. Precipitation hardening

A supersaturated solid-solution of aluminium in the as-quenched condition is generally resistant to SCC (Speidel 1975), although no systematic quantitative work has been done to substantiate such observations; indeed Ward and Lorimer (1973) have found as-quenched material to be susceptible to SCC. Precipitation hardening at ambient or higher temperatures can cause a severe increase in susceptibility to SCC. The maximum susceptibility is generally found before peak-hardness, see fig 2.12 (Jacobs 1965). Further ageing leads to a reduction in SCC. The effect of overageing on the v-k curve on an alloy at peak-hardness is illustrated in fig. 2.13. A small amount of overageing lowers the stress-independent plateau until a constant rate is found but the stress-dependent region continues to shift to higher stress intensities as overageing continues.

2.3.4.3. The Grain-Boundary region

The crack path in AlZnMg alloys is essentially intergranular in saline solutions and has been associated with microstructural variations within the grain-boundary region i.e. the PFZ and grain-boundary precipitation.

Various authors have made suggestions concerning the structural features that control crack growth. Sedriks, Slattery and Pugh (1969b) have found correlations between SCC susceptibility and P FZ whereas Hall (1967) and Starke suggest that the PFZ width is not a controlling factor. The solute concen ration profile within the PFZ has been put forward by Doig and Edington (1975b) as a factor producing an electrochemically sensitive path for stress-corrosion. Other work of Thomas and Nutting (1959/60) suggest that the maximum sensitivity to SCC coincides with heat-treatments that result in the formation of well defined slip bands within the matrix. Unwin and Nicholson (1969) have suggested that the size and distribution of grain-boundary precipitates may be a controlling structural feature, a view which has received support from Kent (1969), and Adler, Geschuind and DeIasi (1972). Similarly the size and distribution of matrix particles has been put forward as a controlling parameter by Speidel (1967), and Gruhl and Cordier (1968).

Thus all microstructural features have separately been proposed as a controlling factor for SCC in AlZnMg alloys. This has led to a profusion of mechanisms and theories of the phenomenon and these are discussed in the following sections with reference to the experimental observations already found.

2.3.5. Theories of stress-corrosion cracking.

Dix (1940, 1950) produced the first theory of stress-corrosion cracking in AlZnMg alloys. He proposed that potential differences would exist between the aluminium matrix and the relatively anodic precipitates. Thus in a corrosive environment the precipitates would be rapidly dissolved by electrlytic attack producing a weakened network. The conjoint effect of a tensile stress would then tend to cause the metal to crack through the depleted zones along

a line joining the holes from which the precipitate has been dissolved. This action would expose fresh metal and promote further attack. Since publication of this generalised theory, a number of mechanisms of SCC in these alloys have been proposed and they include the following critical parameters:-

a) the distribution and/or dissolution of grain-boundary precipitates. (Green and Montague (1975); Jacobs (1967)).

b) the distribution of matrix precipitates (Holl 1967); Van Leeuwen, Van der Vet and Schra (1970).

c) the preferential dissolution of deforming metal in the PFZ (Sedriks, Slattery and Pugh (1969a, 1969b); Starke (1970)).

d) repeated rupture and formation of a passive film at the crack tip (McEvily, Clarke and Bond (1967)).

e) the dissolution of solute-rich regions in the PFZ (Doig and Edington (1975b); Lorimer (1969)).

f) hydrogen embrittlement (Nielsen(1971), Haynie, Vaughan, Phalen, Boyd and Frost (1967

2.3.5.1. The distribution and dissolution of grain-boundary precipitates.

This model is a modification of Dix's original theory and has been considered by Jacobs (1969); Helfrich (1967); Day, Cornish and Dent (1969); Sedriks, Green and Novak (1973); Kent(1970); Green and Montague (1975) and Van Leeuwen, Boogers and Stentler (1975) and may be summarised as follows. $MgZn_2$, the precipitate forming at grain boundaries, is electro chemically more active than the aluminim matrix, suggesting that any exposure of the precipitates to the corrosive environment results in preferential dissolution. Since the grain-boundary precipitate is in the form of discrete particles an explanation for the removal of material between the particles must also be found. Three suggestions have been made.

a) propagation by dissolution of the intervening material. However in the absence of stress AlZnMg alloys are not susceptible to significant intergranular penetration, suggesting that simple dissolution is not a major mechanism.

b) propagation by mechanical tearing. If this model were operating then it would be expected that evidence of void-coalescence, as observed in purely tensile testing,

would be observed in stress-corrosion tests. This is not the case.

c) Plastic strain and corrosion acting conjointly. Three models have been introduced to explain these conjoint effects. The fracture of the spaces between the grain-boundary particles could be caused by the repeated fracture and passivation of the metal by an oxide film (McEvily, Clark and Bond; 1967); it could be associated with embrittlement of the area by a chemical species (Nielsen 1971), or it could be attributed to creep of the plastically deforming PFZ which prevents the formation of an effective passivating film over the crack tip so that dissolution of the material between grain-boundary particles can be sustained (Sedriks, Slattery and Pugh; 1975b). These concepts are discussed more fully in later sections.

The model in which the grain-boundary precipitates dissolve preferentially would suggest that the rate-determining step would be the size and spacing of the grain-boundary particles, and that the crack-path should follow the grain-boundary plane. Both criteria have received experimental support. Middleton and Parkins (1972) and Vaughan and Phalen (1967) have observed the crack path following the grain-boundary and not the PFZ or the PFZ/matrix interface, and a number of workers (Day, Cornish and Dent (1969); Sedriks, Green and Novak (1973)) have noted that a minimum spacing of grain-boundary particles coincides with maximum susceptibility to SCC.

Poulouse, Morral and McEvily (1974) have noted that as the number of grain-boundary particles decreases by overageing their area-fraction increase. They suggest that this observation casts the grain-boundary precipitates in a beneficial role as sacrificial anodes, slowing the passage of the crack through the PFZ.

2.3.5.2. The distribution of matrix precipitates.

A model of SCC has been put forward by DeArdo and Townsend (1970) and Adler and DeIasi (1974) based on the type, size and distribution of matrix precipitates consider 'yield-assisted electrochemical dissolution.' The model assumes that numerous anodically active sites are produced at the root of the crack and that only when dislocations intersect the root of the corroding crevice are they effective in propagating the crack.

The plastic deformation may aid crack growth in two ways: a) the slip bands that impinge on the boundary in the vicinity of the crack tip may cause deformation accelerated anodic dissolution: b) the slip bands, on reaching the boundary, cause a stress concentration which may exceed the cohesive strength of the boundary.

It would then follow that the type, size and distribution of matrix precipitates is important because the susceptibility should change with variations in the dislocation/matrix interface (c.f. effect of ageing curve on SCC fig. 2.12). Another factor which supports this model is that stress-corrosion paths tend to follow high-angle rather than low-angle grain boundaries (Cornish and Day (1969)). These high-angle boundaries have alower cohesive strength and will be less liable to stress relaxation, due to the greater dissimilarity of the respective Burgers vector. Low-angle boundaries can relax dislocation pile ups by accommodating slip through adjacent grains. Also low-angle boundaries contain closely-spaced precipitates, rather than coarse widely-spaced particles found in high-angle boundaries and are thus less susceptible to an electrochemical mechanism.

However on the basis of this model the susceptibility of as-quenched material is not explained satisfactorily, since extensive stress relaxation within the grains can occur. Also changes in matrix dissemination are usually accompanied by changes in the microstructure at grain boundaries and it is often difficult to separate the two, especially since variation in the PFZ width would effect the degree of stress relazation able to take place. Thus stress-corrosion susceptibility might vary with PFZ width which is in dispute, see following section.

2.3.5.3. PFZ Models

This model is based upon one proposed by Hoar (1963) for stress-corrosion in austentic stainless steels. In its development by Thomas and Nutting (1959/60), Robertson and Teleman (1962), and Sprowls and Brown (1969) it is argued that continuously deforming (oxide-film free) metal is anodic relative to the non-deforming metal, the increased reactivity being attributed to the disarraying

of the metal surface by the arrival of dislocations. Thus the deforming metal within the PFZ would be relatively anodic with respect to the non-deforming grains and the stress-corrosion cracks would tend to propagate preferentially here. There are a number of experimental observations in support of this model.

Sedriks, Slattery and Pugh (1969), and Sedriks, Green and Novak (1970) found that for a constant hardness the susceptibility was dependant upon the width of the PFZ, both time to initiate and to propagate the crack decreasing significantly with decreasing PFZ width. However they took little account of variations in other parameters. In point of fact Holl (1967) and Starke (1970) have found that the PFZ has little effect on the stress-corrosion behaviour.

The influence of pH on the stress-corrosion rates have been studied and found to be consistent with the above theory (Sedriks, Green and Novak, 1970). It was noted that the rate of cracking increased with decreasing pH; although the increase was not a great (x4) as that expected from the increase in corrosion (x100) for a similar change in pH. This was attributed to the fact that, irrespective of the pH in the bulk solution, the pH in a region close to the crack tip attains a value of ~3.5; probably as a result of hydrolysis of metal ions. Accordingly if it is assumed that much of the effective cathodic reaction occurs within this hydrolysis region, then the rate of dissolution would be determined primarily by the local pH and not the pH of the bulksolution.

The observation of cathodic protection against SCC in aluminium alloys has long been taken as evidence for the hypothesis that the crack-growth-rate is determined by a dissolution mechanism. However recent observations of a minimum in the crack-growth-rate as a function of potential, together with the parallel behaviour of hydrogen permeability has thrown open the question of hydrogen embrittlement as a mechnism for SCC (Speidel 1971).

Aspects of this model and the hypothesis described in the preceeding section have been formulated quantititively by Speidel (1967).
He concludes that the stress-corrosion susceptibility will increase as the

fraction of matrix precipitates increases, as their radius decreases and as the misfit parameter and anti-phase boundary energy of the grain boundary increase. This theory was found in agreement with many of the observations of the influence of alloy additions and heat treatment schedule. However Shastry and Levy (1973) have studied this model and have found it inconsistent with observations on the susceptibility of as-quenched material and the influence of grain-boundary precipitates.

2.3.5.4. Solute Distribution in the PFZ

Doig and Edington (1974, 1975b, 1975c) have measured solute concentrations in the PFZ of a number of AlZnMg alloys and have put forward the following model as have Cornish and Day (1971), and Taylor and Edgar (1971).

The overall corrosion potential of aged alloys is controlled by that of the large matrix regions containing precipitates. However for finite conductivity solutions the localised grain-boundary corrosion will be mainly controlled by the polarisation behaviour of the grain-boundary regions. It has been shown previously that grain-boundary precipitates dissolve preferentially, the rate of their dissolution depending on the nature of the cathodic region adjacent to the anodic precipitates. It is concluded, therefore that the solute concentration profile will determine the rate of stress-corrosion crack growth.

This model gives the solute concentration profile as a critical parameter but does not really provide a mechanism since this parameter could influence a number of the mechanisms given in the preceeding sections.

2.3.5.5. Film-rupture Model.

This electrochemical hypothesis of SCC is envisaged as a periodic process causing discontinuous crack advance, Vermilyea (1969, 1972) Selines, Shultz and Pelloux (1972) and Chandrasheker and Vasu (1974). The first step requires fracture of a brittle surface layer by concentrated crack tip strain. This layer need not necessarily be an oxide but, perhaps, an enriched noble metal layer. Until repassivation occurs the metal exposed by rupture is attacked at a much faster rate by the corrosive environment

than the filmed crevice sites. The path along which the crack progresses is cyclically generated as film repair and rupture alternate. This is a proven mechanism; experiments conducted on ammoniacal SCC of brasses has convincingly demonstrated that repeated cracking of a brittle film can propagate a crack through a metal (Beavers, Rosenberg and Pugh; 1973). The rate of cracking can be estimated as follows (Verymilyea 1969, 1972).

It is assumed that after fracture, as a result of oxidation of metal to a depth L, the corrosive film grows rapidly to a thickness x, at the crack tip. At a critical strain, E_c, the film fractures again and the exposed bare metal is immediately repassivated. The period of the cyclic process, t_c, is given by:

$$t_c = E_c/\dot{E}$$

where $\dot{E}$ is the crack-tip strain-rate. The crack propagation rate dl/dt is given by

$$\frac{dl}{dt} = \frac{L}{tc} = \frac{L\dot{E}}{E}$$

Evidence favouring a film rupture mechanism is summarised as follows. Many alloys exhibit SCC under thermodynamic conditions of potential and pH which favour the formation of a stable film and the model demands that the mechanical properties are important factors through their influence on film rupture and the nature of strain in the plastic zone at the crack-tip. However there are a number of factors against a film rupture mechanism (Speidel and Hyatt 1972);

a) pure aluminium is immune to SCC but passivates similarly to AlZnMg alloys.

b) the fracture surface would be expected to be striated due to be 'stop-go' aspects of the model. This has not generally been found on the fracture surfaces and indeed, where found may be alternately explained as resulting from slip.

c) the fracture of AlZnMg in aqueous chloride solutions is not thought to involve the formation of thick oxide films.

2.3.5.6. Hydrogen Embrittlement

Hydrogen embrittlement has been reviewed by Haynie, Vaughan, Frost and

Boyd (1965), Nielsen (1971) and Speidel (1974). A model of hydrogen embrittlement in AlZnMg has been proposed by Gest and Troiano (1974). They argue that hydrogen is produced by the corroding metal at the crack tip which is adsorbed and diffuses into a highly complex stress state ahead of the crack. This region of the metal becomes embrittled and readily fractures. The crack advances beyond the region of hydrogen influence where there is another incubation period and the process repeats itself. They found evidence to support their conclusions from scanning electron micrographs showing a brittle zone ahead of the crack tip and from studies of hydrogen/dislocation and hydrogen/solute atom interactions. However this model has a 'stop-start' process and many of the same objections made of the film rupture mechanism would also apply here.

A further model of hydrogen embrittlement (Van Leeuwan 1973) attempts to quantities the hypothesis. In brief in proposes that hydrogen, evolving from intergranular corrosion, precipitates into voids created by the decohesion of grain-boundary precipitates under the action of concentrated glide. This process may be aided by the occurence of slip bands at the interface as in the model of Ryum (1969) discussed in section 2.2.2. The voids grow under the action of hydrogen pressure until the cross-section area is reduced such that the stress can cause cracking. This is consistent with studies on the influence of corrosion potentials and on microscopic studies of the crack path occuring at grain-boundaries. However, the model predicts that there will be a ratio of grain-boundary particle size to spacing associated with maximum susceptibility to SCC i.e. maximum susceptibility should be associated with the peak hardness condition and hence does not explain the actual variation of SCC with hardness (fig. 2.12) or the susceptibility of as-quenched alloys.

Cherepanov (1973) has also proposed a quantitative model of subcritical crack path growth due to hydrogen embrittlement. This is based on the assumption that the crack tip is as source of H^+ ions; that the rate of the source is directly proportional to the crack opening displacement, the coefficient of proportionality being determined by the electrochemical

reaction; and that the effect of H^+ ions is dependent of their local concentration. A theoretical dependence of crack-growth velocity on stress-intensity factor is obtained which is approximately linear. This result is in contradiction with the observed results shown in fig. 2.5 - a stress-dependent region is observed but at higher stress intensities a stress-independent plateau region is observed.

2.3.5.7. A Capillary Model.

Smith (1972a,1972b) has proposed a capillary model for SCC of metals in fluid media. The model accounts for crack propagation velocity as a function of crack length, fluid viscosity, surface tension, contact angle, electrical potential and temperature. It is postulated that SCC is inhibited at large negative electrical potential in some instances due to the accumulation of hydrogen at the crack tip which prevents the corrosive fluid reaching the exposed metal. The model predicts the correct relationship of crack velocity with temperature, viscosity and electro potential but the influ-ce of both ion concentration and microstructure have not been considered.

2.3.5.8. A stress-sorption Model

A model of SCC based upon the adsorption of a damaging species entering metal at the head of an existing crack causing a reduction in the metallic bond strength (Coleman, Weinstein and Rostoker (1961); Uhlig (1969); Kaplan, Cowgill, Fritzen, Krupp, Drystkowiak and Weber (1970)). These ions are adsorbed along paths created by the action of dislocations impinging on the grain-boundary. Autoradiography has shown that chloride ions can migrate to the point of maximum stress triaxiality. These chloride ions migrate by pipe diffusion through the grains and along the grain-boundaries to the regions of triaxial stress. Fracture occurs at the grain-boundary interface due to critical combination of greatest stress and weakened metal bonds. Overageing was found to reduce susceptibility by increasing the resistance to chloride ion diffusion by reducing the planar arrays of precipitates at grain-boundaries and reducing the grain-boundary precipitate distribution or by reducing the internal stress

at grain-boundaries. This model appears to predict maximum susceptibility with maximum strength which as seen in fig. 2.12 is not the case.

2.3.6 Summary

The conclusion to be drawn from the above discussion of stress-corrosion model for AlZnMg alloys is that all the models appear to be deficient in one respect or another. However it also appears that all the models are based on certain experimental facts. Thus it may be concluded that a new model which can quantify the mechanisms of SCC, would be valid for alloys in all metallurgical conditions and environments and would enable prediction of stress-corrosion failures. The other advantage of a quantitative model would be in the design of alloys resistant to stress-corrosion cracking.

3. The Scope of the Investigation

Theresearch investigates the influence of environment on the tensile properties of a range of alloys based upon the A14.5 wt% Zn 2.5 wt% Mg composition. The effect of small changes ($\pm$ 0.5 wt%) in the zinc and magnesium levels and also of minor additions of copper (< 0.3 wt %) is studied. The variation o f properties with different heat-treatment schedules (quench rate, ageing time and temperature) is also examined. As well as evaluating tensile properties in air the behaviour of materials in a salt-water environment is investigated.

In parallel with the mechanical test programme, a detailed study of the associated microstructures is carried out.

From quantitative measurements on microstructure a better understanding of theprocesses occuring during the ageing sequence has been achieved. In particular the correlation made between microstructure and tensile properties has enabled proposed mechanisms of precipitation - hardening in aluminium alloys to be evaluated and the mechanisms which operate during the ageing sequence in the Al-Zn-Mg system to be identified. In addition studies of the morphology of fracture surfaces have been carried out in order to determine the fracture processes occuring in tensile tests.

Mechanical tests are also carriedout in a salt-water environment and the fracture surfaces examined in detail. Comparisons are made between these data and those obtained from the tests in air. The processes occuring during stress-corrosion cracking of this alloy system is then discussed in greater detail. Previously proposed models of stress-corrosion cracking are examined and, from the present investigation, are shown to be unsatisfactory. A new model of stress - corrosion cracking is therefore put forward and

is shown to account more successfully than previous theories.

Finally, the optimum alloy composition and heat treatment schedule is prescribed in order to give a combination of good tensile properties with stress-corrosion resistance.

4. EXPERIMENTAL DETAILS

4.1 Materials used in the Investigation

Seven aluminium - zinc - magnesium alloys based upon the Al 4.5Zn 2.5 Mg (weight %) composition were obtained from Fulmer Technical Services in the form of extruded rod 6mm in diameter. The alloys were manufactured using super purity aluminium with Fe $<$ 0.001% and Si $<$ 0.004%. The nominal alloy compositions are given in table 4.1; the alloy reference numbers were those designated by the suppliers.

Detailed chemical analysis of the alloys was provided by AUWE labaratories on 15 gms of machine turnings of each alloy composition; these results are given in table 4.2. It should be noted that the actual compositions are close to the nominal compositions in most cases, except for the copper level in alloy N770 (0.22 wt %) which was slightly below the nominal level(0.3%).

The extruded rod showed a high degree of preferred orientation and it was decided to produce a more isotropic structure for this investigation. This was achieved by a recrystallisation treatment carried out in a muffle furnace set at 550°C for 72 hours, the temperature being maintained to within $\pm$ 5°C of the set valve. After recrystallisation was completed the alloys were rapidly quenched into water at room temperature.

Three types of specimen were produced from the heat-treated rods:-

4.1 Materials used in the Investigation (Cont'd)

a. for optical microscopy and hardness measurements small transverse sections were cut from the re-crystallised material.

b. 3mm diameter rods were machined for the preparation of transmission electron microscopy (TEM) specimens.

c. cylindrical test specimens, see fig 4.1, for mechanical testing in both air and a stress-corrosion environment (synthetic sea-water) were fabricated at AUWE laboratories.

4.2 Ageing treatments

Prior to ageing the specimens were first homogenised by solution treatment in a muffle furnace at 460°C for 2 hours, the temperature being maintained to within ± 3°C of the set temperature. The effect of three cooling treatment temperatures was investigated:-

a. Quenching into water at room temperature (C.W.Q.).

b. Quenching into water at 80°C (H.W.Q.).

c. Cooling in air to room temperature (A.C.).

The alloys were then aged immediately in an oil bath. The effect of three ageing temperatures were studied - 120°C and 150°C (below the G.P. solvus) and 160°C (above the G.P. solvus); the temperature being held within ± 2°C of the desired valve. After ageing for the required period of time the specimens were quenched by plunging into running water at room temperature and then cleaned in chloroform.

4.3 Hardness measurements

Small transverse sections were cut from the material and after ageing were prepared metallographically by polishing on successively finer grades of emery paper. The final preparation consisted of rotary polishing using Brasso and silvo. Hardness measurements were carried out using a Vickers hardness testing machine with a 2.5 Kgm. load on a pyramidal diamond indenter. To avoid spurious readings caused by either machine/operator error or the indenter falling on a weak region of the material, eg. a grain boundary, a total of approximately 8-10 readings were taken on each sample. The Vickers pyramid number (V.P.N.) was calculated from the average of these measurements using the relationship:-

$$V.P.N. = 1.854 \frac{P}{L^2}$$

Where P is the pressure applied on the indenter and L is the average length of the diagnonal of the impression made by the diamond.

4.4 Microstructural analyses

4.4.1. Optical microscopy

For examination in the optical microscope, specimens were first metallographically polished (see section 4.3) and then lightly etched in Wasserman's reagent for $\sim$2 mins.

The specimens were cleaned in distilled water and methanol prior to examination.

4.4.2 Transmission electron microscopy (TEM)

4.4.2 Transmission electron microscopy (TEM) (Cont'd)

Thin sections were cut from the heat-treated 3mm diameter machined rod and ground on successive grades of emery paper to a thickness of $\sim$ 0.2mm. They were further thinned by electropolishing in a Tenupol apparatus using 12 volts and 0.1 amps. The electropolishing solution consisted of 10% glycerol, 20% perchloric acid and 70% ethyl alchohol maintained at 0°C. The apparatus contained a photo-electric cell which switched the current off automatically upon the initial perforation of a foil. Any electropolishing solution adhering to the specimen was immediately removed by washing in pure ethyl alchohol and the foil transferred to the electron microscope, an AEI 802 instrument operating at 100kV. Electron-micrographs were taken of the matrix precipitates and of the microstructures occuring within grain-boundary regions, precipitate-free-zones (P.F.Z.) and grain-boundary particles. Selected-area electron diffractions patterns were also recorded.

However in order to obtain quantitative information on precipitate densities and volume fractions of precipitate the thickness of the area analysed needs to be known. For this purpose a new method was developed which involved the use of a scanning transmission electron microscope (STEM) with analytical facilities. This new technique is described in detail in section 4.4.5.

As well as transmission electron microscopy on thin foils some replica studies were carried out on the fracture surfaces of stress-corroded specimens.

4.4.2 Transmission electron microscopy (TEM) (Cont'd)

Preparation of these specimens consisted of laying a piece of cellulose acetate film softened in acetone on the fracture surface. On hardening the film was stripped from the metal and placed in a vacuum-coating apparatus where it was coated with a thin layer (~few 100 Å) of carbon. In order to enhance contrast in the replica it was next shadowed with Au-Pd metal by vacuum evaporation. The cellulose acetate was then dissolved away in acetone and the remaining carbon film mounted on copper grids for examination in the transmission electron microscope.

4.4.3 Scanning electron microscopy (SEM)

Scanning electron microscopy was used to study the fracture surfaces of environmentally tested specimens. Before examining the stress-corroded samples it was found necessary to remove any traces of sea-water remaining on the fracture surfaces by washing in distilled water and then ethyl alchohol. The two fracture surfaces from each specimen were mounted on an aluminium stud using silver dag. On certain specimens a conducting coating of Au-Pd was applied to reduce charging-up effects caused by non-conducting corrosion products on the fracture surface. The mounted studs were placed in a Cambridge S4 stereoscan electron microscope for examination.

4.4.4. Electron Probe Microanalysis (EPMA)

Electron probe microanalysis was applied to study three types of feature:-

a. Elemental distributions within the bulk metal; the specimens were metallographically polished transverse sections of the rods, with the surface prepared as described in section 4.3.

b. The composition of corrosion products found on stress-corroded fracture surfaces stripped from the surface using the cellulose acetate/carbon replica technique.

c. Solute distributions and precipitate compositions in thin foils as prepared for transmission electron microscopy.

The first two types of analysis were performed using a JEOL JXA 50A microanalyser, fitted with x-ray spectrometers. Elemental distributions were recorded either as a continuous trace as the probe scanned the metal surface or as a series of measurements across the material at known distances from the specimen edge. The composition of the corrosion products was recorded as a series of x-ray pictures for each element. The relative intensities of each element was calculated using standards of known composition. The measurement of solute distributions and precipitate compositions in thin foils is shown in the following section.

4.4.5 Quantitative electron metallography.

This part of the investigation was carried out using a JEOL JEM 100C electron microscope. As well as conventional transmission electron microscopy the microscope is fitted with facilities for scanning transmission electron microscopy and energy-dispersive x-ray analysis of small areas. The first part of this programme involved the measurement of the thicknesses of thin foils to enable quantitative data on precipitate dissemination, while the second was concerned with the determination of chemical compositions and distributions within fine scale ($\sim$100Å diameter) microstructural features.

Foil thickness determination has been based on either the measurement of the projected width of known crystallographic features such as slip-plane traces or the measurement of the number and thickness of extinction contours

present in thin foils (Hirsch, Nicholson, Howie, Pashley, Whelan (1965)). This latter technique is only viable where extinction contours are present which tends to be the edge of the foil. Similarly the former technique can only be used where useable crystallographic features occur.

Foil thickness determination in this investigation was based upon recording the x-ray emission from the area of analysis at the same time as the precipitate distribution. It has already been shown by Woolf and Jay (1972) Cliff and Lorimer (1972) Jacobs and Baborovska (1972) and Hohn and Niedrig (1972) that foil thickness may be proportional to both the characteristic x-ray emission of the foil and the white radiation background level. Initially the variation of foil thickness with x-ray intensity was calculated by measuring the x-ray intensity of various pure aluminium foils of known thickness. The thickness of these foils was determined by measuring the projected width of a known crystallographic feature e.g. a slip-plane trace. By means of a simple correction taking into account the amount of aluminium present, a curve of foil thickness versus x-ray intensity can be made to apply to Al-Zn-Mg alloys. Thus any Al-Zn-Mg alloy's foil thickness may be calculated by measuring the x-ray intensity and reading the thickness from the calibration curve. It should be noted that the machine operating conditions must remain constant for all measurements. The x-ray intensity measurements were made using the aluminium K_α radiation and a portion of the continuum background between 10kV and 20kV.

A second method of estimating foil thickness was also adopted which involved depositing a small, (- 100Å) diameter, contamination spot on the foil, while inclined at a known angle to the horizontal. The foil was then tilted back to the horizontal position. The separation of the contamination spots formed on both sides of the foil and the angle of tilt enable the foil thickness to be determined as in fig.4.2.

Chemical composition analysis was made, using the energy dispersive system, on fine precipitates and the solute levels within the matrix and the grain-boundary denuded zone. Magnesium and zinc x-ray emissions were

measured from 100Å diameter areas on each of these three features, the results being obtained either in graphical or numerical form. It was found that accurate measurement of the magnesium level was difficult due to the close proximity of the aluminium kα x-ray peak masking some of the magnesium emission. It was not possible to study copper distributions due to the high copper background produced from brass components close to the specimen.

4.5 Environmental testing

After being given the appropriate heat treatment the thin gauge length of the enviromental test specimens was polished to a metallographic finish using Brasso and Silvo. The specimen was then placed in a constant strain-rate apparatus for enviromental testing, see fig 4.3. This apparatus was obtained from the University of Newcastle-upon-Tyne and embodied two tensile-test rigs which operated electrically via electric motors and worm -reduction units. The strain-rate could be varied from 2.787×10^{-8} m/sec to 6.984×10^{7} m/sec, although throughout the test programme the strain-rate was maintained at the lower rate. Each rig was fitted with a load cell and recording instruments. They could be used for mechanically testing specimens in air and also, by fitting enclosed glass tubes arround the specimen which were fed by a liquid circulating system, they could be used for determining the mechanical properties in a salt-water environment. These stress-corrosion measurements involved the use of synthetic sea-water, the composition of which is given in table 4.3. During all tests the load was monitored constantly and a chart recording of its variation with time obtained, thus enabling the time to failure of each specimen to be recorded and its tensile and yield strengths. Where possible three specimens were tested for each alloy composition and metallurgical condition, although lack of material precluded measurements to be carried out for each specimen condition referred to in section 4.2. However, the mechanical test programme was designed to allow

reliable conclusions to be drawn concerning the influence of environment on the mechanical properties in this alloy system.

5. EXPERIMENTAL RESULTS

5.1 Recrystallisation treatment

Analysis of optical micrographs of as-received material, fig 5.1a, showed a microstructure consistent with that of extruded material. After being subjected to annealing at 550°C for progressively longer times gave the results indicated in fig 5.2 for the rate of grain growth on the material. These grain growth data indicated that an equiaxed grain structure had formed after heating for 1 hour. However, it was decided to use material with a large grain size in order to observe more closely the process occurring at the grain boundaries during the environmental test programme. An annealing time of 72 hours was therefore adopted as the standard procedure for recrystallising all material; the structure thus obtained is illustrated in fig 5.1b.

Early electron probe microanalysis data obtained from metallographic sections of as-received and fully re-crystallised material are illustrated in fig 5.3 and magnesium depletion is clearly evident in the surface region although there was no change in the zinc or copper distribution. Closer inspection, fig 5.4, showed that the magnesium depletion was associated with the preferential oxidation of this alloying element. The magnesium leaching problem was subsequently cured by carrying out re-crystallisation treatments in an inert atmosphere.

5.2 Ageing characteristics

5.2.1 General observations

A typical ageing curve (hardness vs. time) is illustrated in fig 5.5 for alloy N765 (Al 4.5 Zn 2.5 Mg) cold-water quenched and aged at 120°C. The error bars indicate the scatter in hardness measurements experienced typically in the investigation. An incubation period during which the hardness stays constant at ~ 60 V.P.N. is followed by an increase in hardness to a maximum of ~140 V.P.N. After longer ageing times (~ 70 days) the hardness decreased to ~100 V.P.N. All alloys used in the investigation, irrespective of heat treatment condition, showed the same trend. Full details of the hardness data with reference to alloy composition and heat treatment are described in the following sections and in table 5.1.

5.2.2 The effect of alloy composition

Ageing curves for all alloy compositions, cold water quenched, aged at 120°C, are given in fig 5.6. Some general points emerge from these data:-

a. an increase in the total alloy content (Zn + Mg + Cu) produces an increase in the peak hardness and a slight decrease in ageing time to achieve the maximum, see fig 5.7.

b. the addition of zinc appears to have greater effect on the age-hardening characteristics than a corresponding magnesium addition, see fig 5.7

5.2.2 The effect of alloy composition (Cont'd)

c. copper additions appear to have little effect on the age-hardening behaviour. These trends were typical, irrespective of prior treatment or ageing temperature, see below.

5.2.3 Effect of quench rate

The influence of the rate of quenching from the solution-treatment temperature on the ageing behaviour is shown in fig 5.8; these curves were for alloy N765 although similar trends were observed for the other alloy compositions. In general it can be seen that air-cooling results in a decrease in the rate of ageing and a slight increase in the peak-hardness value compared with C.W.Q. alloys. Hot-water quenching leads to an appreciable decrease in peak hardness, although again this was associated with an increase in the ageing time compared with C.W.Q. material.

Full ageing curves for AC alloys are shown in fig 5.9 and two further points emerge from these data. Firstly in the brief 'incubation' time a drop in hardness from ~70 V.P.N. to ~50 V.P.N. was found for air-cooled material, which was not observed for C.W.Q. alloys. Secondly, the general influence of air-cooling was most pronounced in alloys N767 and N769, i.e. in those alloys containing low weight percentages of zinc (4%).

The complete series of age-hardening curves for H.W.Q. material are shown in fig 5.10, and contain two further points of interest:

5.2.3 Effect of quench rate (Cont'd)

a. the incubation time was increased by $\sim$ x 100 compared to both AC and C.W.Q. alloys.

b. the alloy least influenced was alloy N766, the material contained the greatest weight percent of alloy addition (Zn + Mg = 8%).

5.2.4 Effect of ageing temperature

Ageing curves for alloy N765 aged at 120°C, 150°C and 160°C after quenching into cold water are illustrated in fig 5.11. Ageing at 160°C resulted in a significantly lower hardness maximum in comparison with the other ageing temperatures, although the ageing kinetics were increased. This indicates that the G.P. solvus for these alloys is below 160°C. Ageing curves for alloys aged at 150°C are illustrated in fig. 5.12. Compared with alloys aged at 120°C (fig 5.6) the higher ageing temperature caused an increase in both the rate of ageing and a slight increase in the peak-hardness. During the incubation period certain alloys showed a small decrease in hardness, as may be observed in air-cooled material. Also of significance is the behaviour of the copper-bearing alloys, which appeared to age to a significantly higher hardness than the corresponding ternary alloy.

Peak-hardness values and ageing times to peak hardness for all alloy compositions and heat treatments are given in table 5.1

5.3 MICROSTRUCTURE

5.3.1. General observations

Figures 5.13 a-d are a series of transmission electron micrographs which illustrate typical changes in the microstructure of Al-Zn-Mg alloys during the ageing treatments; the micrographes are of alloy N765, cold-water quenched and aged at 120°C. Fig 5.13a was obtained from material prior to ageing and shows that the matrix contains many dislocations but no precipitate or second phase. The grain-boundary region shows no precipitation either. Dislocations sometimes form a banded structure within the material, Fig 5.13b. During ageing the precipitates nucleate and grow, and at peak hardness a microstructure is found similar to that observed in Fig 5.13c. The matrix contains a high density of precipitates which appear as spherical or ellip tical aggregates of ~ 15-30Å radius. (G.P. zones or η' - phase). Close to grain boundaries in this micrograph is a region devoid of precipitate (the precipitate-free-zone or PFZ). At the boundary itself there is evidence of the presence of coarse precipitate which have been subsequently etched away during the preparation of the foil. The distribution of precipitates at the grain boundary varied from one boundary to another and variations were observed within a single grain boundary.

Further ageing causes a coarsening of the precipitates both in the matrix and at grain boundaries. The width of the denuded zone next to the grain boundary also increased Fig 5.13d. It was noted that the size of the matrix precipitates was much greater in the region adjacent to the PFZ, although there were fewer here than within the matrix. Many of the particles possessed a lath-like shape which was clearly orientated with the metal lattice. Analysis of corresponding selected-area diffraction patterns indexed these partides on the basis of a hexagonal structure, $MgZn_2$ (η). The precipitates were shown to be lying on (111) planes of the matrix with the greatest length lying parallel to <110> directions in the matrix, see Fig 5.14.

5.3.2. Effect of composition

The effect of composition on the microstructures is illustrated in Fig 5.15a-d . Fig 5.15a and Fig 5.15b show the microstructure of the alloy with the highest total alloy additions (N766 5%Zn 3%Mg) at peak hardness and in the overaged condition respectively (CWQ, aged at 120°C). Figs 5.15c and 5.15d were obtained from metal with the lowest alloy content (N767 4%Zn 2%Mg) in corresponding metallurgical conditions. Comparison of these micrographs with Figs 5.13c and 5.13d and with data from the other alloy compositions, see table 5.2, indicated that:-

(a) In the peak-hardness condition the matrix precipitates are smaller the higher the total alloy content. Fig 5.16 are histograms showing the size distribution of matrix precipitates. A plot of these distributions with alloy content, Fig 5.17, suggest that zinc additions may be influencing the growth of these particles more than the corresponding magnesium addition. Copper additions reduced the size of the matrix precipitates from 25Å to 15Å radius.

(b) In the averaged condition the effect of composition on the matrix precipitate size was more marked than at peak hardness. Particles appeared to grow faster in the alloys containing low proportions of zinc and tended to exhibit a more pronounced lath-like habit, fig 5.15 e, see also the preceeding section. In addition a large number of approximately equiaxed precipates were visible, which are considered to be x-phase. Generally, however, in most of the alloys examined, it was difficult to distinguish between η' and x-phase due to the fineness of the particles.

(c) The width of the PFZ's did not vary significantly with composition for alloys in the peak-hardness condition. apart from alloy N767 (the lowest alloy content material) whose mean PFZ width was half as wide again as the alloy compositions. In the overaged condition these denuded zones approximately doubled in size, with the exception of alloy N769 (increased from 500Å - 3000Å) and alloy N767 (increased from 640Å - 11,000Å). It may be of significance that these two alloys contain

the lowest zinc content (4%) of all the alloys tested. Copper additions appear to have little effect on the width of the PFZ.

(d) Grain-boundary particle distributions in alloys showed little variation with composition in either peak-hardness or overaged conditions. Some differences were, however, observed in low alloy content material. In the peak-hardness condition precipitates are slightly smaller and more closely-spaced than other alloys, while in the overaged condition they are generally larger. Histograms of grain-boundary precipitate distributions of alloys in the peak-hardness condition are illustrated in fix 5.18. The particles are longer in a direction parallel to the grain boundary (the longitudial direction) and tend to grow in that direction and the spacing between the particles increase with ageing time.

5.3.3. Effect of quench rate

The microstructure of specimens which were air-cooled prior to ageing at 120°C are illustrated in Figs 5.19a and 5.19b for alloy N765 in the peak-hardness and overaged conditions respectively. Comparison with earlier micrographs show that matrix precipitation is finer, the PFZ wider and the grain-boundary particles coarser but less numerous in both conditions than in the corresponding CWQ material c.f. Figs 5.14c and 15.14d. It was also noted that the PFZ increased in width more slowly in air-cooled material. The variation of microstructure with alloy content produced similar but more marked effects than CWQ material, especially in the variation in the width of the PFZ with composition. Copper appeared to have little influence on any microstructural features.

Specimens quenched into hot water (HWQ.) possessed similar matrix precipitates to CWQ alloys, but a wide PFZ with coarser and more numerous grain-boundary particles, Fig 5.19c. The change of microstructure with alloy content was similar to that discussed previously with the low zinc addition alloys (N767 and N769), having wider PFZ's and coarser matrix precipitates than other compositions. Copper again appeared to have little influence on the microstructure. These data are summarised in

table 5.2.

5.3.4. Effect of ageing temperature

The effect on microstructure at peak hardness of raising the ageing temperature from 120°C to 150°C is illustrated for various alloys compositions, in the CWQ condition in Fig 3.20a-c. Matrix precipitates are much larger in material aged at the higher temperature; in addition precipitate-free-zones are an order of magnitude wider and grain-boundary precipitates are larger and more widely spaced. The influence of composition was similar to that found in alloys aged at 120°C but much more evident. The addition of copper produced a finer matrix precipitate and a narrow PFZ, but little effect of copper or the grain-boundary precipitate was observed. No result were obtained from alloys aged at 160°C due to lack of material.

5.3.5. Quantitative electron metallography

5.3.5.1. Precipitate density.

The two techniques used to estimate the thickness of foils (Slip-plane trace/X-ray intensity and contamination spot) were first evaluated. For assessing the first technique using slip-plane traces, various thin foils of pure aluminum were prepared and the thickness of areas on each foil calculated by measuring the width and orientation of slip-plane traces. The orientation of each slip-trace was found by analysing Kikuchi line patterns Fig 5.21. The X-ray intensity of each of these areas of known thickness was then measured, using both the characteristic aluminum X-ray emission from the foil and a portion of the white radiation background or continuum between 10kV and 20kV. This enabled a calibration curve, Fig 5.22, to be drawn up. The zero level was calculated by measuring the background radiation through a hole in the foil, The error bars shown in the calibration curve arise from three sources:- 1 A statistical error in microanalysis data, 2 possible error in the measurement of the slip-trace width; 3 error in determining the exact orientation of the slip trace due to slight buckling of the foil over

the analysed area. These may cause inaccuracies in individual points of up to 20%, but the statistical accuracy of the calibration curve was estemated as ~10%. Table 5.3 lists a series of precipitate measurements on electron micrographs obtained from different areas of thin foils prepared from over-aged N767 (A14.0Zn 2.0Mg). Also included are the foil thicknesses as determined from the corresponding characteristic X-ray emission and the continuum X-ray intensity used in conjunction with the calibration curve. These measurements were made under identical conditions to these of the pure aluminum foils containing slip-plane traces. Calculated precipitate densities are given in the final columns. It may be seen that agreement is very good over the range of foil thickness (4,000-12,000 Å) studied when the continuum calibration curve is used. Agreement between the results using the aluminum Kα X-ray curve is also within ± 10% for foils up to ~ 6,000 A, but for thicker foils, ~ 10,000 A, discrepancies are apparent, presumably due to absorption of aluminum X-rays within the foil. However the X-ray technique has several disadvantages:-

(a) A fresh calibration curve must be drawn up for each set of measurments

(b) The instrumental characteristics are not easy to keep constant throughout the measurments

(c) The specimen holder, if near the beam, can give spurious radiation which fogs both the aluminum emission and the continuum X-ray background.

Because of these difficulties the second technique using contamination spots was evaluated. The measured foil thicknesses and precipitate densities for a number of thin foils using both techniques are shown in table 5.4. These indicate that the contamination spot technique is as accurate as the slip-plane method (± 10.%), the main source of error arising from the accuracy with which the spacing of the contamination spots may be measured. Table 5.5. lists data obtained from all alloys aged to peak hardness; the majority of results were obtained with contamination

spot technique since it was simpler to use. From the data the following points emerge:-

(a) The matrix precipitate density increases as the alloy composition is raised; for example the precipitate density/m^3 increases from 1.4 X 10^{22} through 4.6 x 10^{22} to 12.0 x 10^{22} as the additions are increased from 4.0%Zn 2.0%Mg (N767) through 4.5%Zn 2.5%Mg (N765) to 5.0%Zn 3.0%Mg (N766). These results are for CWQ materials, but similar trends with composition were found for material in other heat treatment conditions.

(b) Precipitate densities in N767 (4.0.Zn 2.0%Mg) and N769 (4.0%Zn 3.0%Mg) were essentially the same, 1.4 x 10^{22} and 1.2 x 10^{22} particles/m^3 respectively indicating that magnesium is having little effect on the precipitate density whereas increasing the zinc content alone produces a noticeable increase in precipitate density. This trend is illustrated graphically for CWQ and AC alloys in Fig 5.23

(c) Copper appears to have little effect on the precipitate density, except when ageing is carried out at 150°C, when a small increase in density is observed

(d) alloys which have been air-cooled prior to ageing possess lower precipitate densities than CWQ alloys.

(e) Alloys which have been HWQ prior to ageing have, in general, lower densities which are two or three times lower than those measured in material aged at 120°C; also it was noted that the variation in density was less pronainced in alloys aged at the higher temerature.

5.3.52. Microanalysis of thin foils

Table 5.6 lists magnesium and zinc concentrations recorded using the energy dispersive X-ray analysis system attached to the transmission electron microscope. Measurements made from the matrix, the PFZ, and the grain-boundary precipitate on alloy N765 aged to peak hradness. Measurement of the composition of the matrix was precluded due to the presence which contributed to the X-ray emission spectrum. The results represent

spot technique since it was simpler to use. From the data the following points emerge:-

(a) The matrix precipitate density increases as the alloy composition is raised; for example the precipitate density/m^3 increases from 1.4 X 10^{22} through 4.6 x 10^{22} to 12.0 x 10^{22} as the additions are increased from 4.0%Zn 2.0%Mg (N767) through 4.5%Zn 2.5%Mg (N765) to 5.0%Zn 3.0%Mg (N766). These results are for CWQ materials, but similar trends with composition were found for material in other heat treatment conditions.

(b) Precipitate densities in N767 (4.0.Zn 2.0%Mg) and N769 (4.0%Zn 3.0%Mg) were essentially the same, 1.4 x 10^{22} and 1.2 x 10^{22} particles/m^3 respectively indicating that magnesium is having little effect on the precipitate density whereas increasing the zinc content alone produces a noticeable increase in precipitate density. This trend is illustrated graphically for CWQ and AC alloys in Fig 5.23

(c) Copper appears to have little effect on the precipitate density,

Correction

(e) alloys which have been HWQ prior to ageing have, in general, lower densities than the corresponding CWQ and AC material.

(f) Ageing at 150°C results in precipitate densities which are two or three times lower than those measured in material aged at 120°C; also it was noted that the variation in density was less pronounced in alloys aged at the higher temperature.

5.3.52. Microanalysis of thin foils

Table 5.6 lists magnesium and zinc concentrations recorded using the energy dispersive x-ray analysis system attached to the transmission electron microscope. Measurements made from the matrix, the PFZ, and the grain-boundary precipitate on alloy N765 aged to peak hardness. Measurement of the composition of the matrix was precluded due to the presence of the fine precipitates which contributed to the x-ray emission spectrum. The results represent

averaged values from six measurements. Fig 5.24a shows a typical X-ray spectrum obtained from the matrix and Fig 5.24b is an X-ray spectrum obtained from the precipitate-free-zone. Since the magnesium characteristic peak almost coincides with the aluminum $K\alpha$ peak accurate measurement of the magnesium concentration were subject to error. Errors in the zinc concentration may also occur due to the small copper $K\beta$ radiation peak adjacent to the zinc peak. However the results indicated that:-

(a) The PFZ was depleted in both magnesium and zinc, in some cases to below 50% of the matrix level. The depletion in CWQ and HWQ material was greater than in AC material

(b) Grain-boundary precipitates were rich in magnesium and zinc, confirming the results from selected-area diffraction in section 5.3.1. Quantitative data for the composition of grain-boundary particles (Zn:Mg ratio's) could not be obtained due to excitation of some of the surrounding metal matrix.

5.4 Enviromental testing

5.4.1. General comments

Fig 5.25 illustrates typical data on the tensile behaviour of an alloy tested using the stress-corrosion rig with and without the salt solution environment. The results were from tests made on N765 alloy (4.5Zn 2.5Mg CWQ) in both solution-treated and peak-hardness condition. It is clearly evident that the salt solution environment has a marked effect on properties, reducing both the life of the material and the tensile stress; little influence is shown on the yield stress of the material. The observed reduction in the stress *vs.* time curve is due to the formation and growth of a stress-corrosion crack which progressively reduces the area of load-bearing metal. For N765 material aged to peak hardness, the life has been virtually halved from $\sim$30 hours to $\sim$15 hours while the tensile stress at failure has dropped from $\sim$300 MN/m to $\sim$270 MN/m and the yield stress has remained constant at $\sim$270 MN/m^2. The solution-treated metal is softer (yield stress = 120 MN/m^2), but

also shows a reduction of mechanical properties in salt-water, the life being halved from 42 hours to 21 hours, and the stress at failure dropping from 160 MN/m^2 to 140 MN/m^2. The effect of environment on the mechanical behaviourof overaged alloys is illustrated in fig 5.26 obtained from alloy N766 (5.0Zn3.0 Mg CWQ). Again the life and load-bearing capacity of the material has been decreased by the presence of salt-water during the tests. The yield stress of the material was 280 MN/m^2 and was maintained at this value whether the environment was salt-water or air . However, it was also noted that, although the tensile stess at failure of overaged material was less than of metal at peak hardness, its life in the salt solution was longer. Full details of the environmental test programme are given in table 5.6.

Values quoted in the table were results from several tests on each material, the scatter about the mean sometimes approaching $\pm$ 10% (yield and tensile stress) and $\pm$ 25% (specimen life). The curves shown in Figs 5.25 and 5.26 represent 'averaged' data, as are all stress-corrosion data given here. It may be noted that stress-corrosion effects are present to some extent for all alloys compositions and metallurgical conditions studied.

5.4.2. Effect of alloy composition

The variation of mechanical properties in air with change in composition are shown in Fig 5.27. The results show similar variations in yield stress with composition as in the alloy ageing curves, see Fig 5.6. The variation of yield stress with total alloy content, Zn content, Mg content and the Zn;Mg ratio are shown in Fig 5.28. A correlation was found between the zinc content and yield stress; alloys with high zinc content have the highest yield stress. Fig 5.29 shows the stress vs. time curves for all alloys compositions in the salt-water environment. A comparison with Fig 5.27 shows that a simple reduction in life and tensile strength with composition does not occur. Fig 5.30 shows the variation of the reduction in life (life in salt-water/life

in air) with composition. It is apparent that the significant composition variable influencing the stress-corrosion behaviour of these alloys was the magnesium content; the lower the magnesium content the greater the resistance to stress-corrosion cracking.

The addition of 0.22 Cu increases the stress-corrosion resistance of the metals, Fig 5.31, the life being reduced by 30% with copper and 45.5% without copper.

5.4.3. Effect of quench rate

Comparison of results on cold-water quenched and air-cooled material (Fig. 5.32) indicated that there was no significant effect of quench rate on stress-corrosion life, although slightly higher tensile strengths were found in air-cooled material.

5.4.4. Effect of ageing temperature

Increasing the ageing temperature from 120°C increased the life in air slightly; the tensile and yield strengths were reduced by 22% and 25% respectively. In a salt-water environment the alloys aged at the higher temperature were less susceptible to stress-corrosion cracking (the reduction in life is only ~17% compared to 45%) and this is associated with only a slight reduction in strength.

5.4.5. Effect of microstructure

No correlations with stress-corrosion life were observed between PFZ width, and grain-boundary or matrix precipitate distributions

5.5 Fractography.

The effect of salt-water enviroments on the fracture characteristics of AlZnMg alloys may be assessed by comparing fractographs taken from alloys N765 tested in air and in sea-water.

Fig 5.33a-c are scanning electron micrographs from specimens tested in air (CWQ at peak hardness) and they show that metal failure was confined at or close to the grain boundaries. The majority of grain-boundary surfaces possess a dimpled structure, a characteristic associated with localised deformation at grain boundaries whose orientation with respect

to the specimen is such that considerable tensile force components act normally to the boundaries. It was likely that such a dimple was associated with one of the grain-boundary precipitates, although these particles could not be resolved in the micrographs. A few, relatively smooth, grain surfaces are also present and these features may be related to those grain-boundary orientations where located deformation is due to a strong shear component lying parallel to the boundary. Hence both modes of grain separation are associated with localised deformation of the softer grain-boundary regions which are denuded of precipitate (the PFZ).

A general picture of a surface fractured under tension in sea-water is illustrated in Fig 5.34d. It shows many similar features to the corresponding specimen tested in air, Fig 5.33a, in that the fracture is intercrystalline and that many of the grain surfaces possessed dimples. Close inspection of the dimples showed them to be little different in appearance from those seen in air-tested specimens. However, near the specimen edge there was marked evidence of corrosion by the sea-water. Fig 5.34b was taken from the outer surface close to the final fracture and shows localised corrosion combined with cracks which penetrate into the underlying metal and Fig 5.34c shows the crack penetrating a fracture surface. A number of deep corrosion crevices branching from the main feature surface are visible which were not present in specimens tested in air, Fig 5.34d.

Figs 5.35 a-c show that two distinct types of corrosion product were present. The first type consists of fairly large, rather angular particles identified by electron probe micro analysis as containing mainly aluminum and oxygen with some magnesium present; a series of scanning micro analysis pictures of the striped corrosion product are shown in Figs 5.36a-e. The relative intensities of alumimium and oxygen are consistent with the composition Al_2O_3 (Al:O=80:1) and the relative intensities of Al;Mg (2:1) shows that $\sim$5% of magnesium is present. The second type of

corrosion product appears as a more continuous layer on the metal. Electron-probe microanalysis data from this product, Figs 5.37a-e , indicate the presence of a film rich in magnesium and oxygen. A small amount of aluminum and zinc were also detected in the layer, which is considerably thinner than the aluminum-rich product as may be seen from the relative intensities of the oxygen emission. The magnesium-rich phase was generally found along the advancing edges of stress-corrosion cracks, whereas the aluminum-rich phase was located within established crack path, Fig 5.35c.

Similar data to that above were obtained from an examination of fracture surfaces of all alloy compositions in the peak-hardness condition. Some differences in fracture morphology were found with specimens tested in the solution-treated and overaged conditions. Solution-treated material showed very little dimpling on the fracture surface, see Fig 5.38a, due it is proposed to the lack of grain-boundary precipitates in this metallurgical condition; there was an indication that some intragranular fracture had occured, Fig 5.38b. Overaged alloys which contain fewer but coarser precipitates at the grain boundary than metal at peak hardness, exhibited fewer but larger dimples on the fracture surface. Fig 5.38c. The alloys air-cooled prior to ageing to peak hardness had fracture surface characteristics similar to CWQ alloy in the overaged condition, Fig 5.38d. Apart from these differences the nature of the stress-corrosion fracture was essentially the same as above.

6. DISCUSSION

The work may be conveniently discussed in two sections. The first part deals with the ageing characteristics of the alloy so determined by correlating both hardness measurements and tensile test data with microstructural analysis. The second section is concerned with the influence of the environment on the mechanical behaviour of the alloy.

6.1 Ageing Characteristics

6.1.1 Matrix Precipitation

Analysis of the structure of matrix precipitates as a function of the ageing sequence has given data which is consistent with those found previously by a number of workers :-

$$\text{S.S.S.S} \longrightarrow \text{G.P. zones} \longrightarrow \eta' \longrightarrow \eta\,(MgZn_2)$$

Initially the particles appear as spherical or elliptical aggregates of atoms which eventually transform into lath-like particles. An intermediate stage in which the particles appear as plates was also observed. A typical overaged structure consisted of numerous lath-like precipitates lying on close-packed $\{111\}$ planes of the aluminium matrix. These findings are in accord with those of Thackery (1968) and may be expressed :-

$$(1\bar{2}.0)_\eta \;//\; (0\bar{1}1)_{Al} \quad ; \quad (00.1)_\eta \;//\; (110)_{Al}$$

Other orientation relationships of the precipitate reported by Thackery (1968) were not identified in the present work. Not all the fine precipitate developed a lath-like morphology and these particles may be either untransformed η' or the x-phase discussed by Thackery. Few lath-like particles were found in the matrix interiors in material aged to peak hardness which suggests that high hardness in these materials is associated with either coherent GP zones or the semi-coherent η' precipitate.

Alloycomposition affected the rate of ageing. Material of high alloy content (N766; Zn + Mg = 8%) aged at a faster rate and to a higher

hardness than material of low alloy content (N767; Zn + Mg = 6%). This suggests that the ageing behaviour is controlled by the initial concentration of solute (Fine : 1964). However comparison of the transmission electron micrographs of these two alloys show that alloy N767 has more lath-like precipitate at both peak-hardness and in the overaged condition, fig. 5.15 a - d. This indicates that the rate of precipitate transformation and the ageing curve (hardness vs time) do not directly relate to each other, i.e. the microstructure of the matrix at peak-hardness is governed by the initial solute concentration. Also the precipitate diameter of alloy N766 at peak hardness is $\sim$40Å compared to $\sim$60Å for alloy N767, it appears that the transformation $\eta' \rightarrow \eta$ occurs only after a critical particle size is reached. Recent work by Love (1977) has indicated that the precipitate densities measured in table 5.6 may be subjected to a systematic error due to the presence of an oxide film on the foil surface. This oxide film is assumed to be 250Å thick on either side of the foil. If a correction is applied to the results in table 5.6 the precipitate densities increase by approximately 10 - 15%, although the amount of correction depends on the measured foil thickness. Full details of corrected values are given in table 6.1.

For a particular ageing treatment the precipitate densities at peak-hardness were progressively greater in materials of higher total alloy content. The influence of zinc was particularly marked, fig. 5.23, the higher the zinc addition the greater the precipitate density; changing either the magnesium content or the ratio of zinc to magnesium produced no significant alteration in the number of precipitates. The dominant effect of zinc on precipitate nucleation in this alloy system might be expected if, as has been suggested by Naess (1969), precipitation starts with the agglomeration of zinc atoms into which magnesium atoms diffuse later.

There appeared to be little correlation between calculated volume fractions of precipitate and either zinc or magnesium content, although the low volume fractions present at peak hardness preclude detailed comparisons. However, from measurements of precipitate volume fractions in overaged alloy N767 (CWQ) it may be estimated that approximately 1.0 - 1.5 wt % of the alloying constituents had precipitated at this stage of the ageing process. Comparing these figures with the phase diagram data given by Mondolfo (1971), where approximately 1.5 wt % Mg and 1.0 wt % of zinc can remain together in equillibrium solid solution

at 120°C, suggests that even in a well overaged structure the majority of the alloying additions remain in solid solution.

In alloys containing small quaternary additions of copper it was noticeable that, although the precipitate density remained unchanged with the addition of copper, the volume fraction of precipitate was much reduced (from 0.3% to 0.06% for cold-water quenched material). This reduction was independent of copper level within the range studied (0.22 - 0.15 wt %). These results suggest that copper may be inhibiting the diffusion of either zinc or magnesium to the precipitates. From consideration of the Al-Zn-Mg-Cu phase diagram (Zakharov, 1961) and of the relative atomic radii (Zn = 2.664Å, Al = 2.862Å, Mg = 3.196Å and Cu = 2.556Å) it would appear that diffusion of magnesium may be the more affected by either reducing the strain on the material due to the differences in atomic size and/or by blocking of diffusion paths within the material (Zener 1952). However further work needs to be done on the influence of copper on the precipitation ageing sequence.

The differences between both precipitate density and ageing response with quench rate may be explained in terms of the nucleation and growth of precipitates. Alloys rapidly quenched into cold water will contain a large proportion of quenched-in vacancies (Lorimer and Nicholson 1966a) and hence, a large number of sites for precipitation may be formed. In comparison, hot-water quenched (HWQ) alloys will have a lower proportion of retained vacancies than CWQ material due to the slower quench rate, since many vacancies are able to diffuse to vacancy sinks. Thus fewer nucleation sites will be available in HWQ alloys, giving lower precipitate densities and longer ageing kinetics as are observed. It follows that air-cooling should produce a lower precipitate density than either of the other quenching treatments, since the majority of vacancies will be annihilated during this cooling; but this was not observed. Possibly the relatively high precipitate densities found in air-cooled material may be due to the formation of atom clusters during the cooling period, when the diffusion of these atoms is relatively easy. Thereupon after ageing at 120°C these local concentrations of solute atoms can readily form GP zones to give a higher precipitate density than expected.

Supporting evidence for this view is provided by the precipitate densities of alloys containing low proportions of zinc (alloys N767 and N769). According to Naess (1969) these alloys should be less likely to contain a large number of local concentrations of atoms due to their low proportion of zinc, and therefore have low precipitate densities. This is observed, precipitate densities being lower than those found for any other alloying condition ($1.0 \times 10^{22}/m^3$). The low volume fractions of solute within air-cooled alloys at peak hardness may be due to the lack of vacancies available to assist the diffusion of solute atoms.

The ageing at 150°C produces precipitate densities lower than for material aged at 120°C. There are two possible explanations for this observation:-

1) At 150°C, the alloys are above the G.P. solvus of the material and thus the ageing sequence may be written :-

$$SSSS \longrightarrow \eta' \longrightarrow \eta$$

Nucleation of η'-precipitate would occur mainly on lattice defects, such as dislocation loops resulting from the condensation and collapse of vacancies; but transmission electron micrographs of alloys aged at 150°C, fig. 5.20, provided no evidence for nucleation concentrating on lattice defects. Furthermore the ageing curve at 150°C was more closely similar in shape to that obtained at 120°C rather than the curve for 160°C (above the G.P. solvus). These facts give little support to this concept.

2) At 150°C, the ageing kinetics are increased as evidenced from fig 5.11, and it would be expected that certain GP zones grow preferentially either because of local variations in the solute and/or vacancy concentration or due to being favourably orientated within the matrix. These fast growing zones may then set-up large concentration gradients adjacent to them, thus causing the smaller GP zones in the vicinity to dissolve. There is evidence for the rapid growth of precipitates in the high volume fractions observed in these alloys, and the relatively high precipitate densities observed are in agreement with this model.

6.1.2 Precipitation Hardening

In order to identify the mechanism of precipitation hardening it is necessary to consider the variation of matrix microstructure with the yield stress of the alloy. The most important parameters are the interparticle spacing, L, and the volume fraction of precipitate, f.

The early theories of precipitation hardening due to Mott and Nabbaro (1948) predicted that the value of the yield stress due to the precipitates, Yp, was proportional to the volume fraction according to :-

$$Yp = 4G\varepsilon f$$

where $$\varepsilon = \frac{3K\delta}{3K + \frac{2E}{1+\nu}}$$

G is the shear modulus of the matrix and E is its Young's modulus, K is the bulk modulus of the precipitate, ν is Poissons ratio for the matrix and δ is the difference in atomic size of the matrix and the solute. Thus a plot of the measured yield stress versus the volume fraction should give a slope of $4G\varepsilon$ and it should intersect the stress axis at a point corresponding to the yield stress of solution-treated material if this model is operating. A plot of Y vs f is shown in fig. 6.1 for CWQ material at peak-hardness. From the graph the intercept on the stress axis is $\sim 160 MN/m^2$ which rather high when compared to the experimental value for the yield stress of a solid solution ($\sim 110 MN/m^2$). The calculated slope of the graph, 2.7×10^4 MN/m^2 is much higher than predicted by the theory ($G \sim 25$ MN/m^2, $\varepsilon = 0.1$ - slope 10^4 MN/m^2). Furthermore the behaviour of the copper-bearing alloy cannot be explained since this would require ε to be 0.5 which is an unrealistic value.

The dispersion-hardening mechanism of Orowan (1948) indicates that the yield stress depends on the interparticle spacing, L, by the following equation :-

$$Y = Y_{ss} + \frac{Gb}{2\pi} \phi \frac{1}{L} \ln \frac{L}{2b} ,$$

where Y_{ss} is the yield stress of a solid solution, G is the shear modulus of the matrix, b is the Burgers vector of a dislocation moving past the particles and $\phi = \frac{1}{2}\left(1 + \frac{1}{1-\nu}\right)$ ν is Poissons ratio.

In the present work, L, the interparticle spacing was calculated from the precipitate density, ρ, as follows :-

$$L = \frac{1}{2\sqrt{2r\rho}}$$

where r is the particle radius.

Values of L and $\frac{1}{L}$ In $\frac{L}{2b}$ are shown in table 6.2 and fig 6.2 shows a plot of Y vs $\frac{1}{L}$ In $\frac{L}{2b}$ for CWQ material at peak-hardness.

The intercept on the stress axis is ~ 130 MN/m^2 which is comparable with the experimental value of ~ 110 MN/m^2. Furthermore the measured value of the slope 0.83×10^4 MNA/m^2 is comparable to the theoretical value of 1.42×10^4 MNA/m^2 (G = 25 GN/m^2, b = 2.86A and $\phi = 1.25$). These values suggest that an Orowan mechanism may be operating. However if individual alloys are considered discrepancies arise. For alloy N766 the Orowan mechanism gives an incremental increase in hardening due to bowing of ~ 299 MN/m^2 which compares with the experimental value of ~ 190MN/m^2 and for alloy N767 the experimental value of ~ 90 MN/m^2 compares with a calculated value of ~ 131 MN/m^2 for the incremental increase in hardening. Thus the Orowan mechanism over estimates the yield stress which might be expected since it is considered that this mechanism only operates at large precipitates spacing $\sim > 200$b.

A further theory of dispersion hardening by Ansell and Lenel (1960) predicts that the yield stress of a dispersion-hardened material should obey the relationship :-

$$Y = Y_{ss} + \frac{G'}{c} \frac{f^{\frac{1}{3}}}{(0.82 - f^{\frac{1}{3}})}$$

where Y_{ss} is the yield stress of the matrix without a dispersion, G' is the shear modulus of the particle, c is a constant approximately equal to 30 and f is the precipitate volume fraction. Following the above procedure a plot of yield stress against $f^{\frac{1}{3}}/(0.82-f^{\frac{1}{3}})$ was made, fig 6.3 for CWQ material at peak hardness. From the curve the slope is 1.45×10^3 MN/m^2 and the intercept, Y_{ss}, is approximately zero. Now taking G' = 10G the calculated slope is 2.1×10^3 MN/m^2 and if G' = 2G the calculated slope is 4.1×10^2 MN/m^2. For this alloy system a value of G' = 2G is considered more realistic (Kelly and Nicholson 1963). Thus both the intercept and the measured slope give inappropriate values. In addition there is no explanation of the influence of copper on the yield stress. It may be concluded, therefore, that a dispersion hardening mechanism is not operative in these alloys at peak hardness.

A chemical cutting model (Kelly and Nicholson 1963) gives the applied stress necessary to cut through the particles dependent on the square root of the volume fraction, f, -

$$Y = Y_{ss} + \frac{\gamma}{\alpha} \frac{f^{\frac{1}{2}}}{b}$$

where γ is the energy needed to create the new interface and consists of two terms, γ_p the energy per unit area produced by the precipitates internal ordering and γ_s the energy due to the additional particle-matrix interface created by slip, b is the Burgers vector and α is a constant equal to 1.13.

Fig 6.4 shows a plot of yield stress against $f^{\frac{1}{2}}$ for CWQ material at peak hardness. The intercept value is ~100 MN/m^2 and the calculated slope is 2.78×10^3 MN/m^2. From the measured value of the slope the interfacial energy may be calculated. Assuming that b = 2.86 A, γ is found to be 0.9 J/m^2. This value agrees well with a theoretical value of 1.0 J/m^2 calculated by Van der Merwe (1963), a value of 1.53 J/m^2 obtained by Boyd and Nicholson (1971) for θ' precipitates in Al-Cu alloys and a value of 1.4 J/m^2 for Ferrite/Cementite in plain carbon steel obtained by Kramer, Pound and Mehl (1958).

The influence of copper on the precipitation hardening mechanism may be explained if copper influences the interfacial energy of the

precipitates either by changing the internal order of the precipitates or by altering the energy of the particle-matrix interface. In fig. 6.4, a curve for copper has been drawn, assuming that the addition of copper has little influence on the solid solution hardening, which indicates that the interfacial energy is $\sim$1.87 J/m^2. This figure is high compared to the experimental value of interfacial energy given above and further work is required to substantiate this claim.

The above discussion leads to the conclusion that precipitate hardening in Al-Zn-Mg alloys at peak hardness is due to chemical hardening rather than any other proposed mechanism. As the precipitates grow they undergo a transformation and become incoherent with the matrix. Their volume fraction increases and also the inter-particle separation. A chemical cutting mechanism cannot therefore account for the accompanying drop in yield stress and it is apparent that dislocations can now pass between the particles as in a dispersion hardening theory. In accordance with this change in the interaction mechanism between dislocation and precipitate the material may now exhibit a work hardening as by a Fisher, Hart and Pry (1953), work hardening mechanism.

6.1.3 Grain Boundaries

So far the discussion of microstructure and mechanical properties has centred around the influence of precipitate distributions within the metal matrix, i.e. correlation of hardness and yield stress with the structure and growth of matrix precipitates. Attention will now be focused upon the microstructure in grain-boundary regions, since these are profoundly different from the rest of the material.

Noticeable in all alloys aged to peak hardness and beyond is coarse precipitation at the grain boundaries and an adjacent precipitate-free-zone (PFZ). The microstructure of cold-water-quenched alloys aged at 120°C will be considered first. In the peak-hardness condition the PFZ width is $\sim$500Å, the zone is depleted in alloy content and the grain boundary contains numerous elliptical particles, probably of η. In this condition none of these features is significantly influenced by alloy composition. As the alloys average the width of the PFZ increases and the size and spacing of the grain-boundary

particles also increase. These changes were most notable in alloys containing 4% zinc (N767 and N769), indicating that the zinc addition is more influential than magnesium in affecting grain-boundary microstructure, a similar conclusion to that found for matrix precipitation. These results may be explained as follows. After quenching, the region adjacent to the grain boundary is devoid of vacancies due to the grain boundary acting as a vacancy sink and upon subsequent ageing GP zones are unable to form. This effect is, of course, critically dependent on the quenching rate and explains the wide PFZ's found in slowly quenched alloys. As the material ages precipitates grow at the grain-boundary, drawing solute atoms from the supersaturated PFZ causing depletion of Mg and Zn atoms. Eventually this depleted zone extends into the matrix precipitate region and the grain-boundary particles grow at the expense of the smaller matrix precipitates causing the solute depleted zone to widen. In the case of CWQ alloys aged at 150°C the solute atoms diffuse faster and the microstructure of the region adjacent to grain-boundaries develops more quickly. Thus at peak hardness the PFZ's are approximately 10 times wider than those in alloys aged to peak hardness at 120°C and the grain-boundary precipitate more developed. The influence of composition on these features can be more clearly seen in this ageing condition.

The ellipitical grain-boundary precipitates tend to grow in the plane of the boundary; increasing the longitudinal axis of the precipitate at a greater rate than the other direction. Consequently the amount of solute in the grain boundary precipitates may be estimated. These calculations are shown in table 6.3 indicate that the amount of solute within the grain boundary is similar whatever the alloy content. Thus the variation in PFZ width with alloy composition may be understood. Fig 6.5 illustrates the variation of PFZ for alloys aged at 150°C with alloy content. A clear correlation with zinc content is observed but not with magnesium. This may be explained as follows. The precipitates within the grain boundary consist of η ($MgZn_2$) and the ratio of atomic weight of Zn : Mg within these particles is 4:1. This is a higher ratio than occuring within the matrix (5:2 to 4:3) and as these precipitates grow zinc is removed from a wider zone than magnesium. Thus the PFZ width is more dependent on the initial zinc concentration in the alloy than the magnesium concentration.

In the case of alloys containing copper the volume of material within the grain-boundary precipitates is similar to that of alloys without copper although the PFZ width has been halved. It may be proposed therefore that copper stabilises the matrix precipitates and material diffusing to the grain boundary has either to be taken from the matrix between these precipitates or that the PFZ is more devoid of solute than in corresponding alloys without copper.

In the case of hot-water quenched and air-cooled materials the growth of grain-boundary precipitates and of the PFZ will be essentially similar to CWQ metal except that the initial vacancy depleted zone may be larger because vacancies can diffuse into the grain-boundary sinks over a much wider area producing a wide PFZ. This is especially noticeable in air-cooled material where the width of the PFZ zone does not alter significantly as ageing proceeds, except in the case of alloy containing low amounts of zinc. The large widely-spaced grain-boundary precipitate occuring in air-cooled material is probably due to the nucleation of a few precipitates during cooling and the lack of vacancies precluding further nucleation. Thus the solute depletion in the PFZ's of air-cooled material is not as great as that observed for the other quenching treatments, as observed by Kent (1969).

6.1.4 Fracture in Al-Zn-Mg alloys

In all cases studied the fracture in a tensile test was essentially intergranular and must, as a consequence, be dependent upon the microstructure at grain-boundaries. The PFZ is appreciably softer than the matrix and considerable localised deformation may occur here. Moreover it would be expected that stress build-up during a tensile test could result in decohesion of grain-boundary precipitate/matrix interfaces (Lynch 1973). This is in accord with the fractographs taken from the failed material. At peak hardness the fracture path follows closely the grain-boundaries and the dimpled structure observed in fig. 5.31 is produced by, firstly, a void being formed during decohesion of the grain boundary/precipitate interface and secondly, the soft metal of the PFZ being drawn out under tensile forces. The observation that the mode of fracture does not vary with yield stress is consistent with this model, since the proportion of grain-boundary precipitate is relatively constant whatever the alloy composition.

In the case of overaged material there are larger and more widely-spaced grain-boundary precipitates. Thus the number of coalesced voids is reduced and, consequently, the number of dimples observed on the fracture surfaces is less. However, the wider PFZ allows a greater degree of tensile deformation in the soft zones, which enables the voids to coalesce. The fracture surfaces of air-cooled material in the peak hardness condition showed widely-spaced dimples as expected from the low density of grain-boundary precipitates in this material.

Where an alloy is virtually devoid of grain-boundary precipitates, as in solution-treated alloys, some decohesion at the grain-boundary still occurs, but now more of the matrix can yield easily and the final fracture surface contains portions of intragranular failure.

6.2 Environmental effects

6.2.1 The influence of mechanical properties and microstructure on the stress-corrosion characteristics

Scanning electron micrographs of the fracture surfaces of material tested in the salt-water environment showed that a number of stress-corrosion cracks had been initiated on the speciment surface. It was apparent from the tensile test data that the conjoint effect of stress and corrosive environment caused a number of these cracks to develop. This occured from the start of the tests as evidenced by the lowering of the slope of the stress vs time curve. Eventually the cracks grew and/or coalesced until the load-bearing metal was sufficiently reduced in area to give tensile failure with a similar surface to that found in an air test. The corrosion cracks observed in all specimens were always associated with intergranular attack. It was noted that ~10% of the fracture surface was covered in corrosion product, and in this situation, the 10% reduction in tensile stress at failure found for specimens tested in the corrosive environment would be expected.

The yield stress of stress-corroded material was not significantly affected by the environment as would be expected at this stage of the tensile deformation. Also no correlation was found between yield stress with the reduction in life due to the environment.

This is evidenced in fig. 6.6 for CWQ material aged at 120°C. Alloys N767 and N769 have similar yield strengths but the reduction in life due to the environment is very different; alloy N767 was relatively resistant to stress-corrosion cracking (SCC) whereas alloy N769 was highly susceptible to the environment's influence. Similarly alloys N767 and N768 were equally susceptible to SCC despite the fact that they had very different yield strengths. It can also be noted that material in the solution-treated condition is extremely susceptible to SCC whereas overaged material having a high yield stress is fairly resistant to the influence of the environment on mechanical properties.

Fig. 5.28b shows the correlation between stress-corrosion susceptibility and alloy composition. A general trend is apparent indicating that the higher the total alloy content the greater was the susceptibility; alloy N766 (Zn + Mg = 8 wt %) was very susceptible and alloy N767 (Zn + Mg = 6 wt %) was resistant. However alloys containing similar amounts of solute such as N768 and N769 (Zn + Mg = 7 wt %) behaved very differently. There was also a general trend with the Zn : Mg ratio; alloys with ratio's of Zn : Mg 2:1 were relatively resistant to SCC whereas alloys with ratio's less than 2:1 were susceptible to stress-corrosion cracking. However the effect on stress-corrosion susceptibility of magnesium content was the most significant feature in this examination. Alloy N767 and N768 with low magnesium contents of 2 wt % were equally resistant to stress-corrosion cracking whereas alloys N766 and N769 with high magnesium contents of 3 wt % were most susceptible.

These observations, taken together with electron-probe microanalysis data showing a magnesium-rich corrosion product near the head of the crack-tip and not at regions distant from the crack front, indicate that magnesium may be playing a significant role in the SCC of these alloys. However it should not be overlooked that stress-corrosion susceptibility varies with ageing treatment, which suggests that other microstructural variables may be influencing the rate of crack propogation.

Fig. 6.7 shows the variation of stress-corrosion susceptibility with matrix precipitate density and with matrix precipitate volume fraction for cold-water quenched material aged to peak hardness. There is no

correlation with either of these features. Fig. 6.8 shows the variation of stress-corrosion susceptibility with the microstructure at grain boundaries, PFZ width and area fraction of grain-boundary precipitates for alloys in the same condition as fig 6.7. Again no correlation is observed. Next the solute distribution within the PFZ adjacent to the grain-boundary down which the stress-corrosion crack travels will be considered.

In the case of solution-treated alloys the region adjacent to the grain-boundary has been shown to be locally enriched in solute (Doig, Edington and Hibbert, 1973). The high susceptibility of solution-treated material to stress-corrosion cracking may then be explained since, the higher magnesium level in this region would enhance stress-corrosion. Furthermore the lack of solute atoms in the wider PFZ in overaged alloys would explain their relative resistance to SCC. It should be pointed out that the width of the PFZ and of the region depleted in magnesium are not necessarily identical, since in section 6.1.3 it was shown that the PFZ is controlled by the zinc addition and not the magnesium addition. The effect of magnesium content on the susceptibility of alloys aged to peak hardness (CWQ) may also now be explained. It has been shown in section 6.1.3 that the amount within grain-boundary particles is relatively constant whatever the alloy composition. Thus in alloys with low magnesium contents the magnesium depletion will be greater than in alloys with high magnesium contents. It therefore follows that differences in susceptibility can therefore be related to the level of magnesium solute atoms present in the regions adjacent to the crack path.

However it is considered that magnesium solute level in PFZ's is not the only factor in stress-corrosion effects in Al-Zn-Mg alloys. For example alloy N765 exhibited similar stress-corrosion susceptibility at both solution-treated and peak-hardness, despite the fact that the magnesium levels were different; similarly air-cooled and cold-water quenched material were equally susceptible although having differing solute levels within the PFZ. It is considered, therefore, that grain-boundary precipitates may influence the susceptibility by assisting the crack to propogate, in this case by preferential dissolution in salt-water. This would explain the susceptibility of

alloys at peak-hardness where a high density of such precipitates is observed. This point will be discussed in greater detail in the following sections.

6.2.2 Mechanisms of stress-corrosion cracking

The results found in this investigation will now be discussed in terms of the models put forward in section 2.3 and will be considered in two sections. The first dealing with 'electrochemical' models in which the environment dissolves the material thus weakening it and the second, where the metal fails due to lowering of metallic bond energies due to the environment.

6.2.2.1 Electrochemical Mechanisms

Referring first to the analysis of the corrosion products it is clear that magnesium is dissolved preferentially from the metal in the chloride solution and we may write :-

$$Mg + 2H_2O \longrightarrow Mg(OH)_2 + 2H^+ + 2e^-$$

This is what would be expected from the electrode potential of the alloying constituents of - 2.3V, - 1.7V, - 0.76V and + 0.34V refer to Mg, Al, Zn and Cu respectively. Only when the metal has been exposed to the corrosive liquid for an appreciable time are substantial amounts of aluminium found in the corrosion products, for example in the 'mud-crack' material located away from the crack-tip and on the exterior surfaces of the test specimen. It may be estimated that with an $\sim$200Å thick layer of magnesium-rich corrosion product having formed on the metal surface, magnesium must have been removed from a distance of $\sim$1000Å ; the denudation may be even more extensive than this, especially when one considers the thickness of some of the corrosion products found in fig. 5.35. It also should be noted that magnesium will diffuse into the crack-tip along the grain-boundary much faster than any other region due to a high-diffusion rate along grain boundaries (Hoffman and Turnbull 1951) and thus, the corrosive attack will be concentrated along the grain-boundary region. We shall now consider various proposed mechanisms for SCC in which the crack propogates along the grain boundary by electrochemical means and see which ones fit the above experimental facts.

6.2.2.1.1 Grain-boundary precipitate mechanisms

For example, the anodic nature of these particles may cause them to dissolve preferentially (Van Leeuwen, Van der Vet, Schra 1970); Green and Montague (1975),but the results obtained from CWQ alloys in both the as-quenched and peak-hardness condition show that this is not a rate-determining step. The concept of Poulouse, Morral and McEvily (1974) in which the precipitates are believed to be beneficial in acting as sacrificial anodes may be dismissed as as-quenched and peak-hardness material have similar susceptibilities. The data on alloy N765 indicates that the grain-boundary precipitates aids the propogation of the crack since in the peak-hardness condition the corrosion rate will be slower due to the PFZ being devoid of magnesium. Thus the similarity in stress-corrosion behaviour can only be explained if these precipitates aid the cracks propagation. A manner in which this may occur is by causing the crack to advance along the grain-boundary/precipitate interface due to the difference in electrode potential between the precipitate and the PFZ, rather than by dissolution of these particles since only a small proportion of zinc is found in the corrosion products.

6.2.2.1.2. Matrix precipitate mechanisms

The model of electrochemical dissolution based on the distribution of matrix precipitates (DeArdo and Townsend : 1970) appears invalidated by the results of this investigation. The distribution of these precipitates can be clearly correlated with the zinc additions, whereas the stress-corrosion behaviour is correlated with magnesium concentration. Furthermore this model of 'yield-assisted electrochemical dissolution' would predict a dependence on yield stress which as shown in fig 6.6 is not found.

6.2.2.1.3. PFZ Models

The models proposed by Thomas and Nutting (1959/60) and Speidel (1967) in which,the precipitate-free-zone is anodic with respect to the non-deforming grains due to the disarraying of the metal surface,due to the arrival of dislocations,predicts either, a variation of stress-corrosion susceptibility with PFZ width (Thomas and Nutting) or, with

precipitate volume fraction (Speidel). Neither of these are observed nor is there any explanation in these models of either the susceptibility of as-quenched material or the influence of magnesium rather than zinc on the stress-corrosion susceptibility.

6.2.2.1.4 Solute concentration models

The conclusions of Doig and Edington (1974, 1975 b,c) that the solute concentration profile adjacent to the grain-boundary influences the rate of stress-corrosion cracking is in agreement with the present findings. However, they interpretate the data to indicate that the solute concentration profile determines the rate of dissolution of grain-boundary precipitates. The present results do not agree with this interpretation since the corrosion product found is not consistent with the dissolution of η ($MgZn_2$).

6.2.2.1.5 Film Rupture

The electrochemical hypothesis of stress-corrosion cracking as a periodic process caused by discontinuous crack growth, as a passive film on the metal is repeatedly created and ruptured has two main objections. Firstly the observed magnesium oxide film found near the crack-tip does not necessarily appear as a continuous film and secondly the fracture surfaces show little evidence of a periodic fracture process.

6.2.2.2 Mechanical Models

Mechanical models of stress-corrosion cracking consider the embrittlement of material at the head of the crack by absorption of a damaging chemical species into the metal lattice, hydrogen embrittlement or stress-sorption cracking. In the case of hydrogen embrittlement it has been shown earlier that hydrogen is evolved during the dissolution of magnesium. It would also be expected that the greater the corrosion rate the greater the rate of hydrogen-evolution. There appears evidence (Gest and Troiano 1974) that the metal lattice can accomodate hydrogen, although the amount taken up may be expected to be small, i.e. the hydrogen concentration in the salt solution would be considerably in excess of this, whatever the magnesium concentration in the metal. Hence, it is difficult to

account for the fact that high magnesium contents produce greater stress-corrosion susceptibilities on the basis of a hydrogen embrittlement model. Furthermore, any hydrogen absorbed into the aluminium lattice will tend to be concentrated at the crack-tip and at grain-boundary/precipitate interfaces. Thus, if a hydrogen embrittlement mechanism is involved in this alloy system, it would be expected that grain-boundary precipitate distribution would be a controlling factor in SCC of these alloys, but this does not appear to be the case in the present work.

In the case of stress-sorption cracking similar objections can be raised as in the case of hydrogen embrittlement. The influence of magnesium on the absorption of a damaging species of ion is not clear and, the influence of the absorbed atoms would be expected to be affected by the distribution of the grain-boundary particles.

To summarise it appears that none of the previously proposed mechanisms adequately explain the stress-corrosion results obtained in this study and a new model is proposed in the following section.

6.2.3 A Model of stress-corrosion cracking for Al-Zn-Mg in salt-water environments.

A feature that appears to have received little consideration in stress-corrosion cracking theories concerns the role of vacancies. These will be formed in the Al-Zn-Mg metal as the magnesium atoms diffuse to the crack surface and pass into solution. It has already been indicated that considerable denudation of magnesium would occur in the metal adjacent to the crack-tip and a correspondingly high vacancy fraction would hence be injected (possibly approaching $\sim$ 1% volume fraction). This value is well above the vacancy equilibrium concentration and vacancies will therefore move to suitable sites where they may either become annihilated or coalesce to form a stable void. Now the mean direction of vacancy flow would be towards regions of high tensile strain and thus the vacancies will prefer to flow into metal regions of high strain at the head of the crack-tip, where they then coalesce, either enlarging the crack or weakening the metal at the crack-tip causing failure.

The processes occuring at the crack tip according to the above hypothesis are illustrated in fig.6.9. The microstructural feature which will influence the process greatest will be the rate at which magnesium diffuses to the crack-tip and this, in turn, will be affected by the magnesium content in regions near the crack-tip. The experimental data showing that higher magnesium contents enhance the propogation of the stress-corrosion crack is in accord with this hypothesis. Using this model, the observed behaviour of these alloys may be explained as follows.

Firstly considering as-quenched material, it is of relevance to note the work of Doig, Edington and Hibbert (1973),who have shown that the grain-boundaries of solution-treated Al-Zn-Mg alloys are locally enriched in magnesium. If it is assumed that the alloys in this study are similarly enriched, it would be expected that upon dissolution of magnesium a correspondingly higher vacancy fraction would be made available to assist crack growth. Thus, the high susceptibility of alloys in this heat treatment condition may be explained.

In the case of aged alloys the crack may advance both by the above model and, by the electrochemical dissolution of the grain-boundary precipitates. However, the rate of crack advancement will be controlled by the slower of these two processes, namely the rate of crack advancement in the grain-boundary regions between precipitates. In alloys aged to peak hardness, the grain-boundary is denuded in both zinc and magnesium, the level being dependent on the original concentration within the matrix and the area-fraction of grain-boundary precipitates. Thus, although, the rate of crack propagation will be slower than in solution-treated material, the presence of grain-boundary precipitates speeds up the crack growth rate. Hence the susceptibility to stress-corrosion of material aged to peak hardness is dependent on the magnesium concentration adjacent to the grain-boundary and the area-fraction of precipitates at the grain-boundary.

In the case of CWQ alloys aged at 120^{o}C, the area fraction of grain-boundary precipitates is relatively constant and the susceptibility depends on the magnesium concentration. In air-cooled alloys aged to peak hardness the regions adjacent to grain-boundaries are richer in magnesium than in cold-water-quenched material and thus will corrode

at a faster rate. However the area-fraction of grain-boundary precipitates is less, thus reducing the rate of propagation. The combination of these two influences results in similar susceptibility in both these heat-treatment conditions. In the case of CWQ alloys aged to peak-hardness at 150°C the magnesium-depleted zone will be wider than in alloys aged at 120°C and although the grain-boundary precipitates are larger their area-fraction is approximately the same. Thus the increased magnesium depletion causes the alloys to be less susceptible to SCC, than if aged at the higher temperature.

In overaged material the grain-boundary precipitates are larger but more widely spaced. The magnesium depletion is greater and due to a corresponding reduction in the rate and number of vacancies created during electrochemical attack, the material is less susceptible to the environment.

The beneficial effect of copper additions may also be explained using the vacancy hypothesis. It has been earlier mentioned that copper atoms may reduce the diffusion of magnesium in the ageing process and hence, the rate of magnesium loss during dissolution in the salt-water may be inhibited by the presence of copper. In turn, the rate of injection of vacancies and their condensation at the crack tip is reduced, rendering the copper-bearing alloys less susceptible to the effects of stress-corrosion cracking.

From the above hypothesis it should be possible to predict the optimum composition and heat-treatment schedule for Al-Zn-Mg alloys to give the best combination of strength and stress-corrosion resistance. It has been found that high strengths occur in high zinc alloys and good stress-corrosion resistance is associated with low amounts of magnesium and small additions of copper. Thus an alloy composition such as alloy N768 (A15 wt % Zn 2 wt % Mg) with the addition of copper ($\sim$0.15%) should prove fairly resistant to SCC. It may also be feasible to introduce other minor alloying additions to slow down the diffusion of vacancies to the crack tip, such an element might be silicon or titanium. Heat treatment schedules should be aimed at producing a grain-boundary region devoid of grain-boundary precipitates and depleted in magnesium. Since the solute depletion is due to growth of these particles a compromise heat-treatment must be reached.

In this present study the best heat treatment would appear to be cold-water quenching and ageing at 150°C.

The hypothesis described above appears to explain qualitatively the stress-corrosion behaviour of Al-Zn-Mg alloys, however further work must be carried out to confirm the above observations and to try and quantify the model.

7. CONCLUSIONS

1. Detailed analysis of microstructures associated with the precipitation ageing sequence in Al-Zn-Mg alloys give results which agree well with other published work.

2. A method has been developed for determining precipitate densities in thin soils, which gives fairly good experimental reproducibility.

3. Increasing the amount of zinc in the alloys increased the density of precipitates, the peak hardness and the tensile strength; in contrast altering the magnesium content had little effect on theseproperties.

4. Additions of copper appeared to have little effect on tensile strength or on the precipitate ageing sequence, although it may be inferred from the present results that copper reduces the rate of growth of precipitates by inhibiting the diffusion of magnesium.

5. Based upon quantitative microstructural evidence precipitation-hardening mechanisms have been considered and it is proposed that a chemical interaction between precipitate and dislocation is responsible for the increase in hardness found when the precipitants nucleate and grow to peak hardness. Overageing is due to a dispersion hardening mechanism where dislocations bow around the particles by an Orowan mechanism.

6. Tensile fracture of Al-Zn-Mg alloys is associated with the formation of voids at grain-baindary precipitate/matrix interfaces and the subsequent ductile failure of the surrounding soft metal (PFZ in aged material)

7. Alloys of all compositions andheat treatment conditions studied in the present work were found to be susceptible to stress-corrosion. This susceptibility increased with increase

in magnesium content; changing the zinc level had little effect.

8. A detailed analysis of the corrosion products present on thesurfaces of failed specimens showed that a magnesium-rich product was present at freshly exposed surfaces and an aluminium-rich producton surfaces that suffered from longer immersion times.

9. Previous stress-corrosion theories cannot explain the present results and a new model is proposed which is based upon the injection of vacancies into the metal as the magnesium atoms are dissolved in the salt-water, and the subsequent condensation of vacancies at the crack-tip to increase its rate of propagation.

10. The present study indicates that the best combination of strength and stress-corrosion resistance may be achieved by maintaining a high zinc content and keeping the magnesium level to a minimum. Quaternary additions may be beneficial if they reduce the diffusion of magnesium and/or vacancies to the metal/liquid surface and provided they do not themselves readily dissolve in the salt-water. Copper has been shown to be suitable but it issuggested that other elemental additions merit investigation.

11. Although for the most part the different heat-treatment schedules adopted in this present study appeared to have little effect on stress-corrosion resistance, ageing at 150°C, after cold-water quenching, improved the properties. It was of interest to note that this particular heat treatment resulted in greater magnesium denudation at the grain-boundaries. However, more work would need to be carried out before an optimum heat-treatment specification as well as alloy composition may be prescribed.

REFERENCES

Anon., 1972a, Revue de L'aluminum, 407, p334.

Anon. 1972b, Revue de L'aluminum 407, p 416.

Abe, M., Asano, K, and Fujiwara, A., 1973, Metal trans., 4, p.1499.

Adler, P.N. and DeIasi R., 1974 Grumman Space Corp. NASA contractor report RE 468 NASA-CR-120468.

Adler, P.N., DeIasi R., and Geschwind G., 1972, Metal Trans., 3 p.3191.

Ansell, G.S., 1961, Acta Met., 9 p 518.

Ansell G.S., and Lenel, F.V., 1960 Acta Met., 8 p 612.

Auld, J.H., and Cousland, S. Mck., 1976, Met. Sci., 10 p445.

Baba Y., 1968, Sumitomo Light Met. tech rep., 9 p24.

Bardham P., and Starke, E.A., 1968 J. Met Sci, 3 p.577.

Beavers, J.A. Rosenberg I.C., and Pugh, E.N. 1973, Metals and Ceramics information contract report MClC 73-19, p57.

Bergman G., Wang, J.F. and Pauling, L. 1952, Nature, 169, p1057.

Berry J.P. 1960, J. of Mech. and Phys. of Solids, 8, p 194.

Bischel, H., 1975, Aluminium, 49 p477.

Blackburn, M.J. and Speidel, M.O., 1971, Electron Microscopy and structure of metals, Univ. of California Press, Berkeley, p905.

Boyd J.D. and Nicholson R.B., 1971, Acta Met., 19, p1101.

Brown, B.F., 1968, Met. Revs., 12, p171.

Brown R.H., and Gourd, L.M., 1964, App. Mat. Res., 3, p8.

Brown R.H. Sprowls D.O., and Shumaker, M.B. 1972 in Stress-Corrosion Cracking of Metals: A state of the Art, ASTM STP 518, p87.

Bryant, A.J., 1966, J. Inst. Met., 94, p94.

Butler, E.P. and Swann, P.R., 1976, Acta Met., 24, P343.

Chandrasheker, R., and Vasu K.I., 1974, J. Electrochem Soc. India, 23, p139.

Chen, C., and Judd, G., 1973, Mat. Div. Rensselar Polytechnic Inst., Troy, N.Y., Tech. report No. 5.

Cherepanov, G.P., 1973, Corrosion, 29, p305.

Cliff, G. and Lorimer, G.W. 1972, Proc. 5th European Conf. on electron microscopy Manchester, Inst. of Phys. London, p 140.

Coleman E.G., Weinstein D., and Rostoker W., 1961, Acta Met., 9 p491.

Cornish A.J., and Day M.K.B., 1969, J. Inst. Met., 97, p44.

Cornish A.J. and Day M.K.B., 1971, J. Inst Met., 99, p377.

Candy, S.L. Metherall A.J.F., Whelan, M.J. Unwin P.N.J., and Nicholson, R.B., 1968, Proc. Roy. Soc., A307, p267.

Day, M.K.B., Cornish A.J., and Dent, T.P., 1969, J. Met Sci. 3, p175.

DeArdo A.J., and Simensen Chr. J, 1973, Metal trans., 4, p243.
DeArdo A.J., and Townsend, R.D. 1970, Metal Trans. 1, p2573.
Dix E.H., 1940 Trans A.I.M.E. 137, p11.
Dix E.H., 1950, Trans A.S.M. 42, p1057.
Doig, P., and Edington, S.W., 1973, Phil Mag. 28, p 961.
Doig, P., and Edington J.W., 1974 Br. Corros. J. (Quart) 9, p230.
Doig, P., and Edington J.W., 1975a, Metal Trans A., 6, p 943.
Doig, P, and Edington J.W., 1975b, Corrosion, 31 p 347.
Doig, P., and Edington, J.W., 1975c, in Grain Boundaries in Engineering Materials, A.I.M.E. and A.S.M., Claitor's Pub. Div., Baton Rouge.
Doig, P., Edington, J.W. and Hibbert, G., 1973, Phil Mag., 28 p971.
Dünkeloh, K.H., Kralik, G., and Gerold, V., 1974 Z. Metallkunde., 65 p291.
Elkington, E.W., 1961 - 62, J. Inst. Met., 90 p267.
Embury, J.D., and Nicholson R.B., 1963, J. Aust. Inst. Met., 8 p76.
Embury J.D., and Nicholson R.B., 1965, Acta Met., 13 p 403.
Embury, J.D., Wilcox B.A., and Clauer, A.H., 1972, J. Inst. Metal, 100 p 153.
Eurof-Davies, D., Dennison J.P., and Mehta, M.L., 1971, Corrosion, 27, p371.
Feeney J.A., and Blackburn, M.J. 1971, in the Theory of stress-corrosion cracking, N.A.T.O., Brussells, p355.
Fine, M.E., 1964, Phase Transformations in Condensed systems, McMillan and Co., New York.
Fine M.E., 1975, Metal Trans., 6A p 625.
Fink, W.L., and Willey L.A., 1937 Trans. A.I.M.M.E., 124 p78.
Fisher, J.C. Hart, E.W., and Pry, R.H., 1953, Acta Met., 1 p 336.
Fleischer, R.L. and Hibbard, W.L., 1963, in The Relation between the Structure and Mechanical Properties of Metals, H.M.S.O., London.
Forsyth P.J.E., and Wilson, R.N., 1963-64, J. Inst. Met., 92 p82.
Freidel, J., 1964, in Dislocations, Pergamon Press, London.
Geisler, A.H., 1951, in Phase Transformations in Solids, Wiley, N.Y., p387.
Gest, R.J., and Troiano, A.R., 1974, Corrosion, 30 p274.
Gjønnes, J., and Simerson, C., 1970, Acta Met., 18 p 881.
Graf, R., 1965, Comptus Rendus 242 p1311.
Green J.A.S., and Montague W.G., 1975, Corrosion 31, p209.
Gruhl, W., and Cordier H., 1968, Aluminium 44, p403.
Guiner, A., 1956 Trans A.I.M.E., 206 p673.
Hahn, G.T. and Rosenfield, A.R. 1975 Metal Trans. 6A p653.
Haynie, F.H., Vaughan, D.A., Frost, P.D. and Boyd, W.K., 1965 Air Force Materials Laboratory report, A.F.M.L. TR 65 258.
Haynie, F.H., Vaughan, D.A. Phalen, D.I. Boyd., W.K., and Frost, P.D., 1967 Air Force Materials Laboratory report AFML TR 66 267.

Helfrich, W.J., 1967, in Stress Corrosion Testing, ASTM STP 425, p21.
Hirsch, P.B., Howie A., Nicholson, R.B. Pashley, D.W. and Whelan, M.J., 1965, in Electron Microscopy of Thin Crystals, Butterworths, London ch.17
Hoar, T.P., 1963, Corrosion, 23, p197
Hoffman, R.E. and Turnbull, D., 1951, J. App. Phys. 22 p634.
Hohn F.J., and Niedrig H., 1972 Proc. 5th European conf on Electron Microscopy, Manchester, Inst. of Phys., London, p358.
Holl, H.A., 1964-65, J. Inst. Met., 93, p364.
Holl, H.A., 1967a, Met. Sci. J., 1, p111.
Holl H.A., 1967b, Corrosion, 23, p 197.
Hyatt, M.V., 1969, Boeing Corporation, Washington, report D6-2446-6.
Hyatt, M.V., and Speidel, M.O., 1972, in Titanium and Aluminium alloys Naval Res Lab., Washington D.C., p 14.
Jacobs, A.J., 1965, Trans. A.S.M. Quart., 58 p 579
Jacobs, A.J., N.A. Aviation Inc. Rocketdyne Div, Report R-7026 1967.
Jacobs, A.J., 1969, in Fundamental Aspects of Stress Corrosion Cracking, N.A.C.E. Houston, Texas, p530.
Jacobs, M.H., and Baborovska, J., 1972, Proc.5th European Conf. on Electron Microscopy, Manchester, Inst. of Phys., London p136.
Jacobs, M.H., and Pashley, D.W. 1969, in the Mechanism of Phase Transformations in Crystalline Solids, Inst. of Met., London, p43.
Jurgens, G., Kempe, M., and Hoffler, H., 1974, Phys. status solidi, 219, pk39.
Kaplan, M.P., Cowgill, D.S., Fritzen, J.S., Krupp, W.E., Drystkowiak, S., and Weber, K.E., 1970, Corrosion, 26, p7.
Kelly, A., and Fine, M.E. 1957, Acta Met. 5, p365.
Kelly, A., and Nicholson R.B., 1963, Prog. Mat. Sci., 10 p149.
Kent, K.G., 1969, J. Inst. Met. 97 p 127.
Kent, K.G. 1970, J. Aust Inst. Met., 15, p171.
Ketcham, S.J. 1972, in Stress Corrosion Cracking in Metals - A state of the Art, A.S.T.M. Philadelphia, p79.
Kramer, J.J., Pound, G.M., and Mehl, R.F., 1958, Acta Met., 6 p763.
Kulig, Z., 1973, Polska Akod Nauk. Prace. Kam Metal., 18 p309.
Laves F., Lohberg J., and Witte H., 1935, Metallschaft, 14 p793.
Lees, D.J., Ford, F.D., and Hoar T.P., 1973, Met. and Materials, 7 p 231.
Lorimer G.W., 1969, A.G.A.R.D. Conf. Proc. No. 53, p3.
Lorimer G.W., and Nicholson R.B., 1966a Acta Met., 14, p41.
Lorimer G.W., and Nicholson R.B., 1966b, Acta Meta. 14 p1009.
Lorimer G.W., and Nicholson R.B., 1969, in The Mechanism of Phase Transformations in Crystalline Solids. Inst. Of Met. Monograph and report Series No. 33, p36.
Love, G., 1977, Private comm., Univ. of Bath.

Lynch, S.P., 1973, Metal Sci. J., 7 p93.
Mattoson, E., 1971, Br. Corros. J., 6 p73.
McEviley A.J., Clark T.B., and Bond A.P., 1967, Trans A.S.M. 60 p 661.
Middleton, W.R. and Parkins, R.N., 1972, Corrosion, 28 p 88.
Mondolfo, L.F. 1969, J. Inst. Met., 97, p95.
Mondolfo, L.F. 1971, Met. Revs., 16, p95.
Mondolfo, L.F. Gjostein, N.A. and Levinson D.W., 1956, Trans A.I.M.M.E., 206 p1378.
Mott, N.F., 1950, in Imperfections in Nearly Perfect Crystals (ed. W. shockley) Wiley, New York p173.
Mott N.F., and Nabarro, F.R.N., 1940, Proc. Phys. Soc., 52, p86.
Mott, N.F., and Nabarro, F.R.N. 1948, Rep. Conf. Strength of Solids Physical Society, London p1.
Naess, S.E., 1969, Scripta Met., 3 p179.
Nielsen N.A., 1971, Corrosion 27 p 173.
Orowan, E., 1948, Symposium on Internal Stresses in Metals and Alloys, Inst. of Metals p451.
Parker, B.A., 1972, J. Aust, Inst. of Met., 17 p31.
Parkins R.N., 1964, Met. Revs. 9. p201.
Parkins R.N., 1972, Brit. Cor.J. 7 p15
Parkins R.N., Mazza F., Royuela J.J., and Scully J.C., 1972, Brit. Cor. J. 7. p154
Pashley D.W., Jacobs, M.H., and Vietz, J.T, 1967, Phil Mag., 16 p 511.
Peel C.J., 1975, Royal Aircraft Establishment T.R. 75062.
Polmear, I.J. 1958-59, J. Inst. Met. 87 p24.
Polmear I.J. and Scott Young P, 1958-59, J. Inst. Met., 87 p 65.
Poulouse, P., Morral J.E., and McEvily A.J. 1974, Met. Trans., 5 p1393.
Pugh, E.N., and Jones, W.R.D., 1961, Metallurgica 63 p3.
Pumphrey P.H., 1973, Scripta Met., 7 p1045.
Robertson W.D., and Tetelman A.S., 1962, in Strengthening Mechanisms in Solids Seminar Ohio, 1960, A.S.M.
Rosenbaun H.S., and Turnbull, D., 1959 Acta. Met. 7 p664.
Ryum, N., 1969 Acta Met., 17, p821.
Ryum, N., 1975a Z Metallkunde, 66 p338.
Ryum, N., 1975b, Z Metalkunde 66 p344.
Ryum, N., 1975c, Metallkunde, 66 p 377.
Ryum, N., and Baardreth M., 1968, J. Inst. Met., 96 p92.
Ryum N., Haegland, B., and Lindtviet T., 1967, Z Metallkunde., 58 p.28
Saito, T., and Tanaka, T., 1972, J. Japan Inst. Light Metals 22 p47.
Schmalzreid H., and Gerold V., 1958, Z. Metallkunde 49 p 291.
Scully J.C. 1968 a, Corrosion Science, 8 p 759.
Scully J.C., 1968b, Corrosion Science, 8 p513.
Scully J.C., 1972, Anti Cor. Method and Mat., 7 p5.

Sedriks, A.J., Green, J.A.S., and Novak, D., 1970, Metal Trans. 1 p 1815.
Sedriks, A.J. Green, J.A.S., and Novak, D., 1971, Corrosion, 27 p198.
Sedriks, A.J., Green, J.A.S., and Novak, D., 1973, Metal Trans. 4, p1992.
Sedriks, A.J., Slattery P.W., and Pugh, E.N., 1969a, Trans A.S.M. 62, p815.
Sedriks A.J., Slattery P.W., and Pugh, E.N., 1969b, Trans A.S.M., 62 p238.
Selines, P.J., Stoltz, R.F., and Pelloux, R.M., 1972, Air Force Material Laboratory report, AFML-TR-72-21.
Shastry, C.R., and Levy M., 1973, Army materials and mechnaical Research Centre Report, AMMRC-TR-73 /34
Smallman, R.E., 1963, in Modern Physical Metallurgy, Butterworths, London p1963.
Smith, T., 1972a, Corrosion Science, 12, p45.
Smith, T., 1972b, Corrosion Science 12, p675.
Smith, W.F., and Grant, N.J., 1969, Trans A.S.M., 62 p724.
Speidel, M.O., 1967, Phys. status solidi, 22a, pK71.
Speidel, M.O., 1971, in Conf. Proc. on The Theory of Stress Corrosion in alloys (ed. Scully, J.G.) N.A.T.O., Brussells, p289.
Speidel, M.O., 1974, in Hydrogen in Metals, A.S.M., p249.
Speidel, M.O. 1975, Metal Trans., 6a p651.
Speidel, M.O., and Hyatt M.V., 1972, in Advances in Corrosion Science and Technology V.2, Plenum Press, N.Y. p115.
Sprowls, D.O., and Brown, R.H., 1969, in Fundamental Aspects of Stress-Corrosion Cracking N.A.C.E. Houston, Texas, p466.
Starke, E.A., 1970, J. of Metals, 22 p54.
Subbarao K.V., 1971, M. Sc. Thesis Univ. of Manchester.
Taylor I.T. and Edgar, R.L. 1971, Metal Trans., 2 p833.
Thackery P.A., 1968, J. Inst. Met., 96 p228.
Thomas, G., 1959, Phil. Mag., 4 p606.
Thomas G., and Nutting J, 1959-60, J. Inst. Met, 88 p81.
Ugiansky, G.M. Skolnick, L.P. and Stiefel, S.W., 1969, Corrosion, 25 p77.
Uhlig, H.H., 1969, Proc. Conf. on Fundamental Aspects of Stress-corrosion cracking N.A.C.E., Houston, Texas p86.
Unwin, P.T.N., and Nicholson R.B., 1969, Acta Met. 17, p 1379.
Unwin P.T.N., Lorimer, G.W. and Nicholson, R.B. 1969, Acta Met. 17 p1363.
Unwin P.T.N., and Smith G.C., 1969, J. Inst. Met., 97 p299.
Van der Merwe, J.H. 1950, Proc. Phys. Soc., 63a p616.
Van der Merwe, J.H., 1963, J. App. Phys. 34, p117 and 123.
Van Leeuwen, H.P., 1973, Corrosion 29 p197.
Van Leeuwen, H.P., Boogers, J.A.M., and Stentler, C.J., 1975, Corrosion, 31, p23.

Van Leeuwen, H.P. Van der Vet, W.J., and Schra, L., 1970, National Lucht-en Riumtevaartlaboratorium, NLR TR 70105 U.
Van Stone, R.H., and Psioda, J.A. 1975, Met. Trans., 6A p668
Varley P.C., Day, M.K.B. and Sendorek A., 1957 - 58, J. Inst. Met., 86 p337.
Vaughan D.A., and Phalen, D.I, 1969, Stress Corrosion Testing A.S.T.M. STP 425 p209,
Vermilyea, D.A., 1969, Proc. Conf. on Fundamental Aspects of Stress Corrosion Cracking N.A.C.E. Houston Texas p15,
Vermilyea, D.A., 1972, J. electrochem. Soc. 119 p405.
Wacker, G.A. Chu Huai Pu, 1972, Corrosion, 28 p233,
Ward, D.E., and Lorimer, G.W. 1973, Proc. 3rd Inst. Conf. on strength of Metals and Alloys, Inst. of Metals, London p488.
Watkinson F.E., and Scully, J.C. 1971, Corrosion Science, 11 p179.
Watkinson F.E., and Scully, J.C., 1972, Corrosion Science, 12 p 905.
Woolf R.J., and Joy D.C., Proc. 5th European Congress on Electron Microscopy Manchester, Inst. of Phys., London 1972.
Zakharov, A.M., 1961 Isvet, Metally, 1 p124.
Zener, C., 1952, in Imperfections in Nearly Perfect Crystals (Ed. W. Shockley) Wiley, N.Y., ch11.

ACKNOWLEDGMENTS

The author would like to thank the following people who have helped in the research. Dr. V.D. Scott of Bath University my superior for his help, advice and encouragement throughout the period of the research.
Dr. A. Culpan of A.U.W.E. and Dr. G.W. Lorrimer of Manchester University for many helpful discussions.
Mr. H. Perrot of Bath University for his help in using the transmission and scanning electron micorscopes, Mr. G. Love of Bath University for his help and advice in doing the quantitative electron microscopy and in the use of the electron microprobe analyser.
JEOL of London for their permission to use the JEOL JEM 100C electron microscope. A.U.W.E. of Portland for financial support during the research.
Mr. G. Lamb for assisting in the prepapation of some of the figures.

TABLE 2.1

Orientation relationships and disregistries of γ precipitates observed in Al-Zn-Mg alloy after Thackery (1968), Schmalzreid and Gerold (1958), Embury and Nicholson (1965) and Mondolfo (1969).

Type	Orientation Relationship	Disregistry
1	$(1\bar{2}.0)\gamma$ // $(1\bar{1}1)_{Al}$, $(0.01)\gamma$ // $(110)_{Al}$	+3.4%
2	$(1\bar{2}.0)\gamma$ // $(1\bar{1}1)_{Al}$, $(30.2)\gamma$ // $(110)_{Al}$	+33.2%
3	$(1\bar{2}.0)\gamma$ // $(1\bar{1}1)_{Al}$, $(20.1)\gamma$ // $(121)_{Al}$	-17.4%
4	$(1\bar{2}.0)\gamma$ // $(1\bar{1}1)_{Al}$, $(10.4)\gamma$ // $(110)_{Al}$	-15.3%
5	$(00.1)\gamma$ // $(1\bar{1}1)_{Al}$, $(10.0)\gamma$ // $(110)_{Al}$	-23.1%
6	$(10.0)\gamma$ // $(100)_{Al}$, $(00.1)\gamma$ // $(011)_{Al}$	- 2.4%
7	$(11.0)\gamma$ // $(110)_{Al}$, $(00.1)\gamma$ // $(1\bar{1}1)_{Al}$	+2.9%
8	$(10.0)\gamma$ // $(1\bar{1}0)_{Al}$, $(00.1)\gamma$ // $(110)_{Al}$	+18.2%

Table 4.1

Nominal Alloy Compositions Weight Percent

Alloy Designation	Zn	Mg	Cu	Al
N765	4.5	2.5	-	bal
N766	5.0	3.0	-	bal
N767	4.0	2.0	-	bal
N768	5.0	2.0	-	bal
N769	4.0	3.0	-	bal
N770	4.5	2.5	0.3	bal
N771	4.5	2.5	0.15	bal

TABLE 4.2

Chemical Analyses of Alloys Used in this Investigation

Alloy	Zn	Mg	Cu	Fe	Sl	Pb	Cr	Mn
N765	4.38	2.66	0.02	0.05	0.01	<0.01	<0.01	<0.01
N766	4.87	3.18	0.02	0.05	<0.01	<0.01	<0.01	<0.01
N767	3.86	2.03	0.01	0.05	0.01	<0.01	<0.01	<0.01
N768	4.87	1.89	0.01	0.05	0.01	<0.01	<0.01	<0.01
N769	3.93	2.98	0.01	0.05	<0.01	<0.01	<0.01	<0.01
N770	4.48	2.53	0.22	0.05	0.01	<0.01	<0.01	<0.01
N771	4.38	2.40	0.14	0.05	<0.01	<0.01	<0.01	<0.01

TABLE 4.3.

Composition of Synthetic Sea-water

Distilled Water	1 litre
NaCl	26.5 gms
$MgCl_2$	2.4 gms
$MgSO_4$	3.3 gms
$CaCl_2$	1.1 gms
KCl	0.73 gms
$NaHCO_3$	0.20 gms
NaBr	0.28 gms

TABLE 5.1

Details of hardness data of Al-Zn-Mg, alloys for different compositions and heat-treatment conditions (± 10%)

(a) Cold-water quenched material aged at 120°C

Alloy type	N765	N766	N767	N768	N769	N770	N771
Time to P.H. (Mins)	$6x10^3$	$3x10^3$	$7x10^3$	$4x10^3$	$6x10^3$	$4x10^3$	$4x10^3$
V.P.N at peak hardness	149	159	100	138	120	120	146

(b) Air-cooled material aged at 120°C

Alloy type	N765	N766	N767	N768	N769	N770	N771
Time to P.H. (Mins)	$4x10^4$	$4x10^4$	$2x10^5$	$8x10^4$	$1.5x10^5$	$8.5x10^4$	$8.5x10^4$
V.P.N. at peak hardness	144	153	112	137	109	147	146

(c) Hot-water quenched material aged at 120°C

Alloy type	N765	N766	N767	N768	N769	N770	N771
Time to P.H. (Mins)	$7x10^4$	$1.3x10^4$	$6x10^4$	$6x10^4$	$7x10^4$	$7x10^4$	$7x10^4$
V.P.N. at peak hardness	104	127	82	95	84	99	93

(d) Cold-water quenched aged at 150°C

Alloy type	N765	N766	N767	N768	N769	N770	N771
Time to P.H. (Mins)	$5x10^2$	$5x10^2$	$7x10^2$	$6x10^2$	$6x10^2$	$6x10^2$	$6x10^2$
V.P.N. at peak hardness	140	156	105	133	120	157	162

TABLE 5.2.

Microstructure of aged Al-ZmMg alloys in various heat-treatment conditions. All measurements in angstroms, Å . (± 10%)

(a) CWQ aged to peak hardness at 120°C

Alloy	N765	N766	N767	N768	N769	N770	N771
PFZ width	375	400	640	400	500	400	400
Grain-boundary precipitate size	x^{400}_{300}	x^{400}_{300}	x^{250}_{150}	x^{360}_{150}	x^{320}_{250}	x^{320}_{250}	x^{300}_{180}
Grain-boundary precipitate spacing	300	300	200	300	300	300	350
Matrix-precipitate radius	25	20	29	20	29	15	15

(b) CWQ aged for 2×10^4 mins (overaged) at 120°C

Alloy	N765	N766	N767	N768	N769	N770	N771
PFZ width	800	800	11000	700	3000	1000	1000
Grain-boundary precipitate size	x^{500}_{300}	x^{500}_{300}	x^{2000}_{600}	x^{600}_{200}	x^{800}_{300}	x^{600}_{300}	x^{800}_{300}
Grain-boundary precipitate spacing	600	600	800	700	600	600	600
Matrix precipitate radius	30	25	60	25	55	25	25

(c) A.C. aged to peak hardness at 120°C

Alloy	N765	N766	N767	N768	N769	N770	N771
PFZ width	1700	1500	5000	1000	1325	1200	1200
Grain-boundary precipitate size	x^{800}_{300}	x^{800}_{300}	x^{600}_{300}	x^{800}_{300}	x^{800}_{300}	x^{600}_{300}	x^{650}_{280}
Grain-boundary precipitate spacing	3000	1800	1500	2000	2500	2000	2000
Matrix precipitate radius	15	20	15	14	20	15	15

(d) Air-cooled aged 10^5 mins (overaged) at 120°C

Alloy	N765	N766	N767	N768	N769	N770	N771
PFZ width	2100	2000	15000	1500	4500	1800	1700
Grain-boundary precipitate size	x^{1000}_{600}	x^{1000}_{600}	x^{1400}_{600}	x^{1200}_{400}	x^{1500}_{500}	x^{1400}_{400}	x^{1400}_{300}
Grain-boundary precipitate spacing	3000	2500	2000	3000	3000	2500	2500
Matrix precipitate radius	20	20	60	25	50	25	20

TABLE 5.2. Continued

(e) Hot-water quenched aged to peak-hardness at 120°C

Alloy	N765	N766	N767	N768	N769	N770	N771
PFZ width	2000	2000	15000	2000	10000	2000	2000
Grain-boundary precipitate size	x^{600}_{300}	x^{500}_{200}	x^{400}_{200}	x^{600}_{300}	x^{600}_{300}	x^{600}_{300}	x^{600}_{300}
Grain-boundary precipitate spacing	400	300	300	400	350	500	500
Matrix precipitate radius	20	15	30	20	30	15	15

(f) Cold-water quenched aged to peak-hardness at 150°C

Alloy	N765	N766	N767	N768	N769	N770	N771
PFZ	6000	5000	25000	5000	16000	3250	3250
Grain-boundary precipitate size	x^{1300}_{300}	x^{800}_{300}	x^{700}_{300}	x^{1200}_{400}	x^{1500}_{500}	x^{900}_{300}	x^{900}_{300}
Grain-boundary precipitate spacing	1000	700	800	1200	1500	1000	1000
Matrix precipitate radius	50	35	60	50	60	30	30

TABLE 5.3.

Foil thickness and precipitate densities of Al4.0Zn2.0Mg CWQ and overaged at 120°C, using slip plane technique:
A are results from white radiation and B are results from the aluminium radiation.

Area	No of precipitates per unit area	thickness Å 'A'	thickness Å 'B'	density 'A' x $10^{22}/m^3$	density B x$10^{22}/m^3$
1	46	4,000	3,400	0.996	1.037
2	64	5,500	5,200	1.008	0.953
3	75	6,000	5,500	1.083	0.993
4	125	11,600	7,500	0.936	0.605
5	130	12,000	7,800	0.936	0.608

TABLE 5.4.

Comparison of slip-trace technique and contamination spot technique for measuring precipitate densities at peak hardness

Alloy	density (Slip-trace)	density (Contamination Spot)
Al 4.0Zn 2.0Mg CWQ overaged	$1.01 \times 10^{22}/m^3$	$0.95 \times 10^{22}/m^3$
Al 4.5Zn 2.5Mg CWQ peak hardness	$4.3 \times 10^{22}/m^3$	$4.7 \times 10^{22}/m^3$
Al 5.0Zn 3.0Mg CWQ peak hardness	$11.0 \times 10^{22}/m^3$	$12.4 \times 10^{22}/m^3$
Al 4.0Zn 3.0Mg CWQ peak hardness	$1.3 \times 10^{22}/m^3$	$1.2 \times 10^{22}/m^3$

TABLE 5.5

Matrix precipitate densities and volume fractions of precipitate for Al-ZnMg alloys of different compositions and heat treatments.

(a) Cold-water Quenched, aged at 120°C to peak hardness

Alloy	Precipitate density /m^3	Volume fraction%
N765	4.6×10^{22}	0.3
N766	12.0×10^{22}	0.4
N767	1.4×10^{22}	0.15
N768	6.2×10^{22}	0.2
N769	1.2×10^{22}	0.12
N770	4.5×10^{22}	0.06
N771	4.0×10^{22}	0.05

(b) Air-cooled, aged at 120°C to peak hardness

Alloy	Precipitate density /m^3	Volume fraction %
N765	3.9×10^{22}	0.05
N766	4.2×10^{22}	0.13
N767	0.7×10^{22}	0.06
N768	4.6×10^{22}	0.01
N769	0.5×10^{22}	0.02
N770	3.5×10^{22}	0.05
N771	3.6×10^{22}	0.05

(c) Hot-water Quenched, aged to peak hardness at 120°C

Alloy	Precipitate density /m^3	Volume fraction%
N765	2.4×10^{22}	0.08
N766	3.6×10^{22}	0.05
N767	1.4×10^{22}	0.15
N768	3.2×10^{22}	0.10
N769	-	-
N770	5.0×10^{22}	0.07
N771	-	-

TABLE 5.5 Continued

(d) Cold-water Quenched, aged at 150°C to peak hardness

Alloy	Precipitate density /m^3.	Volume fraction %
N765	1.4×10^{22}.	0.7
N766	3.8×10^{22}.	0.65
N767	1.3×10^{22}.	1.1
N768	2.5×10^{22}.	1.3
N769	1.4×10^{22}	1.1
N770	1.8×10^{22}	0.2
N771	2.0×10^{22}	0.22

TABLE 5.6.

Micro-analysis measurements from thin foils of Al4.5Zn 2.5Mg at peak hardness

(a) Air-cooled material

	Zn	Mg
Matrix level	42 cts	68 cts
Precipitate-free-zone	32 cts	59 cts
Grain-boundary precipitate	50 cts	73 cts

(b) Hot-water quenched material

	Zn	Mg
Matrix level	33 cts	63 cts
precipitate-free-zone	18 cts	30 cts
Grain-boundary precipitate	75 cts	85 cts

(c) Cold-water quenched material

	Zn
Matrix level	426 cts
Precipitate-free-zone	218 cts

TABLE 5.7

Enviromental test results

(1) Tests in air

(a) Solution treated CWQ

Alloy	Yield strength MN/m^2	Tensile strength MN/m^2	Life hrs
N765	110	150	42
N766	120	160	40
N767	110	150	48

(b) Peak hardness CWQ 120^{o}C

Alloy	Yield strength MN/m^2	Tensile strength MN/m^2	Life hrs
N765	280	320	27.5
N766	310	380	23
N767	200	250	45
N768	260	330	24.5
N769	210	290	44
N770	270	340	30

(c) Overaged CWQ 120^{o}C

Alloy	Yield strength MN/m^2	Tensile strength MN/m^2	Life hrs
N765	255	285	32
N766	290	360	24
N767	205	230	42

(d) Peak hardness CWQ aged 150^{o}C

Alloy	Yield strength MN/m^2	Tensile strength MN/m^2	life hrs
N765	210	250	31

(2) Test in salt-water enviroment

(a) Solution treated CWQ

Alloy	Yield strength MN/m^2	Tensile strength MN/m^2	Life hrs
N765	105	130	21
N767	105	110	27

(b) CWQ peak hardness 120^{o}C

Alloy	Yield strength MN/m^2	Tensile strength MN/m^2	Life hrs
N765	260	260	15
N766	300	320	12
N767	200	250	35

TABLE 5.7 Continued

(b) CWQ peak hardness 120°C Contd

N768	265	310	20
N769	205	240	20
N770	270	315	21
N771	270	315	20

(c) CWQ overaged 120°C

Alloy	Yield strength MN/m²	Tensile strength MN/m²	Life hrs
N766	230	275	17

(d) Air-cooled peak hardness 120°C

Alloy	Yield strength MN/m²	Tensile strength MN/m²	Life hrs
N765	270	325	16
N766	300	355	14
N767	190	220	33
N768	280	320	21
N769	230	230	18
N770	265	325	20
N771	275	340	20

(e) Air-cooled overaged 120°C

Alloy	yield strength MN/m²	Tensile strength MN/m²	Life hrs
N769	170	210	24

(f) CWQ peak hardness aged 150°C

Alloy	Yield strength MN/m²	Tensile strength MN/m²	Life hrs
N765	190	230	26
N770	210	240	29
N771	220	245	36

TABLE 6.1

Matrix precipitate densities and volume fractions for AlZnMg alloys corrected for oxide film

(a) Cold-water Quenched aged at 120°C to peak hardness

Alloy	Precipitate density	Volume fraction
N765	6.1×10^{22} per m^3.	0.4 %
N766	16.0×10^{22} per m^3.	0.53 %
N767	1.54×10^{22} per m^3.	0.17 %
N768	9.9×10^{22} per m^3.	0.32 %
N769	1.4×10^{22} per m^3.	0.14 %
N770	5.7×10^{22} per m^3.	0.08 %
N771	5.1×10^{22} per m^3.	0.07 %

(b) Air-cooled aged at 120°C to peak hardness

Alloy	Precipitate density	Volume fraction
N765	4.7×10^{22} per m^3.	0.06 %
N766	5.6×10^{22} per m^3.	0.17 %
N767	1.05×10^{22} per m^3.	0.09 %
N768	5.0×10^{22} per m^3.	0.02 %
N769	0.9×10^{22} per m^3	0.03 %
N770	4.0×10^{22} per m^3	0.06 %
N771	3.9×10^{22} per m^3	0.06 %

(c) Hot-water Quenched, aged to peak hardness at 120°C

Alloy	Precipitate density	Volume fraction
N765	2.8×10^{22} / m^3.	0.09 %
N766	4.1×10^{22} / m^3.	0.06 %
N767	1.7×10^{22} / m^3.	0.20 %
N768	3.8×10^{22} / m^3.	0.13 %
N769	-	-
N770	5.7×10^{22} / m^3.	0.08 %
N771	-	-

TABLE 6.1 Continued

(d) Cold-water Quenched, aged to peak hardness at 150°C

Alloy	Precipitate density	Volume fraction
N765	2.6×10^{22} /m^3	1.3 %
N766	5.1×10^{22} /m^3	0.9 %
N767	1.5×10^{22} /m^3	1.3 %
N768	3.3×10^{22} /m^3	1.5 %
N769	1.7×10^{22} /m^3	1.3 %
N770	2.4×10^{22} /m^3	0.3 %
N771	2.5×10^{22} /m^3	0.3 %

TABLE 6.2.

Interparticle spacing, L, and the Orowan Function, $\frac{I}{L}$ In $\frac{L}{2b}$, for CWQ alloys aged at 120°C at peak hardness.

Alloy	L	$\frac{1}{L}$ Log $\frac{L}{2b}$
N765	237 Å	0.0157 $Å^{-1}$
N766	158 Å	0.021 $Å^{-1}$
N767	483 Å	0.009 $Å^{-1}$
N768	212 Å	0.017 $Å^{-1}$
N769	509 Å	0.0088 $Å^{-1}$
N770	352 Å	0.0117 $Å^{-1}$

TABLE 6.3

Area fractions of grain-boundary precipitate for CWQ alloys at peak-hardness aged 120°C

Alloy	Area-fraction
N765	5.7%
N766	5.7%
N767	3.7%
N768	5.4%
N769	4.3%
N770	4.3%
N771	3.5%

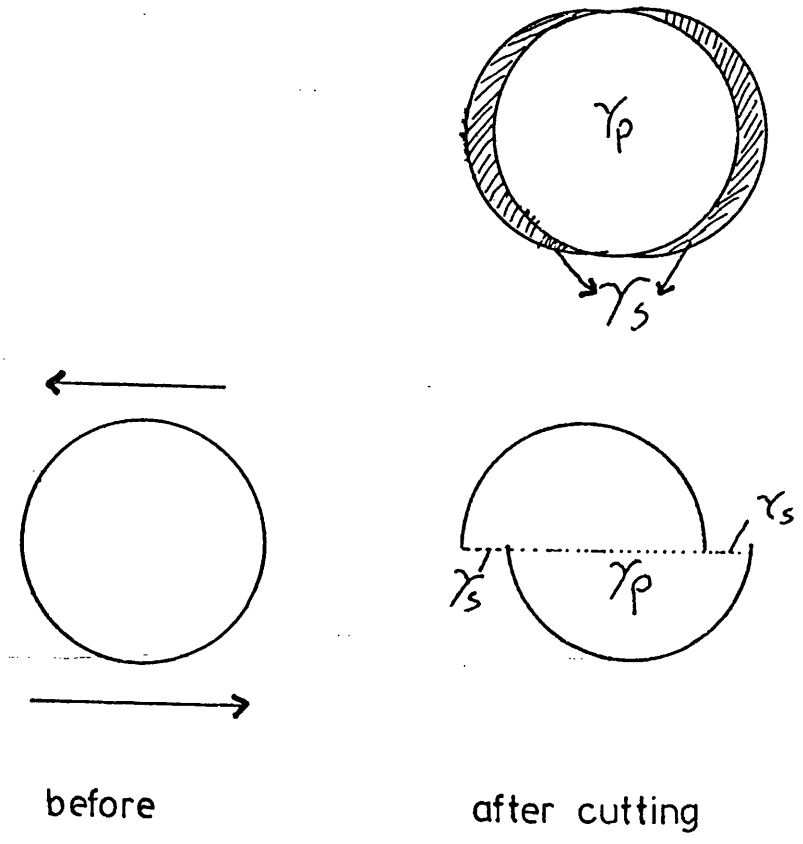

Fig. 2.1 Cutting of precipitate by a dislocation

γ_p interfacial energy due to variation in order of precipitate
γ_s interfacial energy due to increase in precipitate/matrix interface

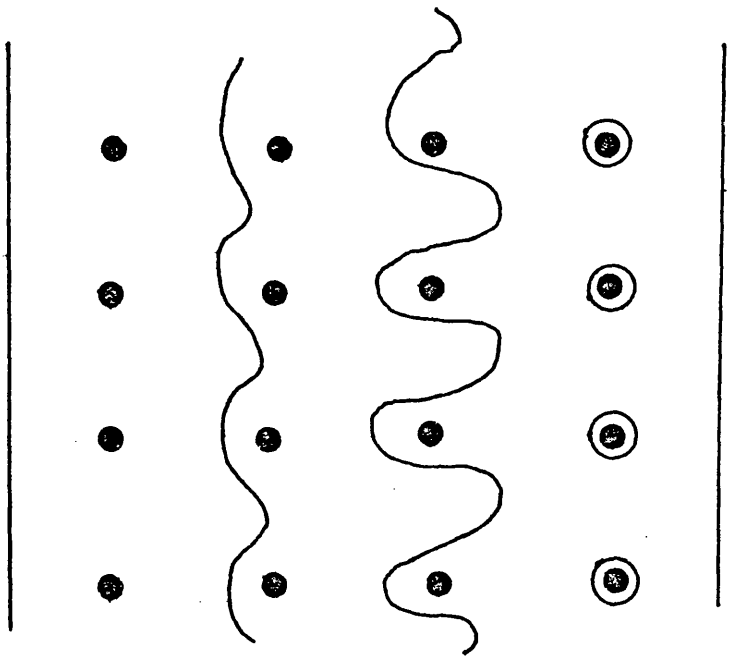

Fig. 2.2 Orowan bowing model

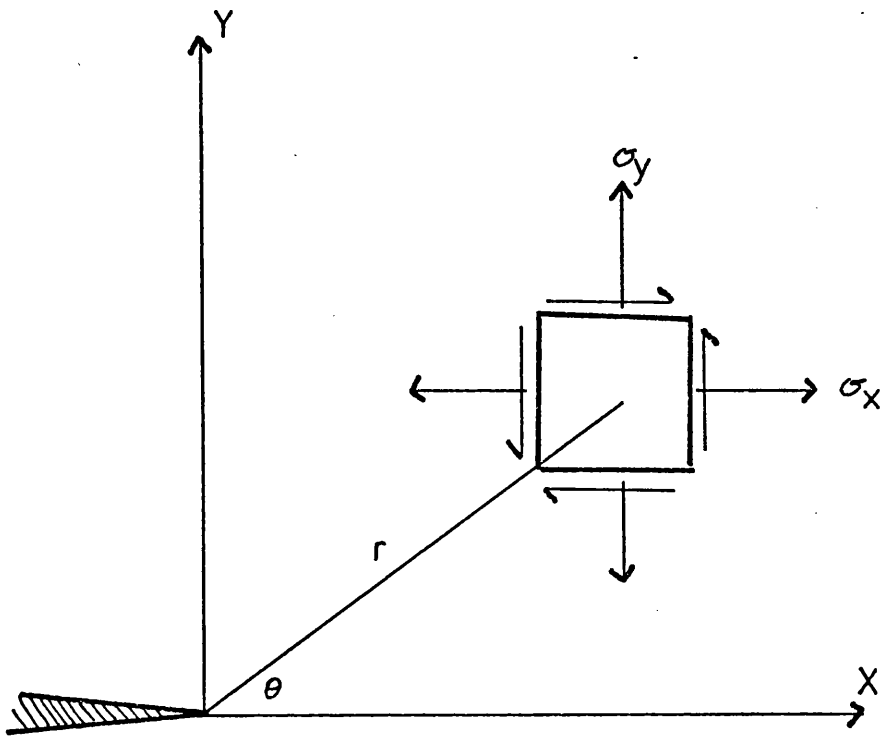

$$G_x = \frac{K_I}{\sqrt{2\pi r}} \cos\frac{\theta}{2}\left(1 - \sin\frac{\theta}{2}\sin\frac{3\theta}{2}\right)$$

$$G_y = \frac{K_I}{\sqrt{2\pi r}} \cos\frac{\theta}{2}\left(1 + \sin\frac{\theta}{2}\sin\frac{3\theta}{2}\right)$$

$$Y_{xy} = \frac{K_I}{\sqrt{2\pi r}} \sin\frac{\theta}{2}\cos\frac{\theta}{2}\cos\frac{3\theta}{2}$$

Fig. 2.3 Stresses near the tip of a crack in the opening mode in an elastic isotropic body

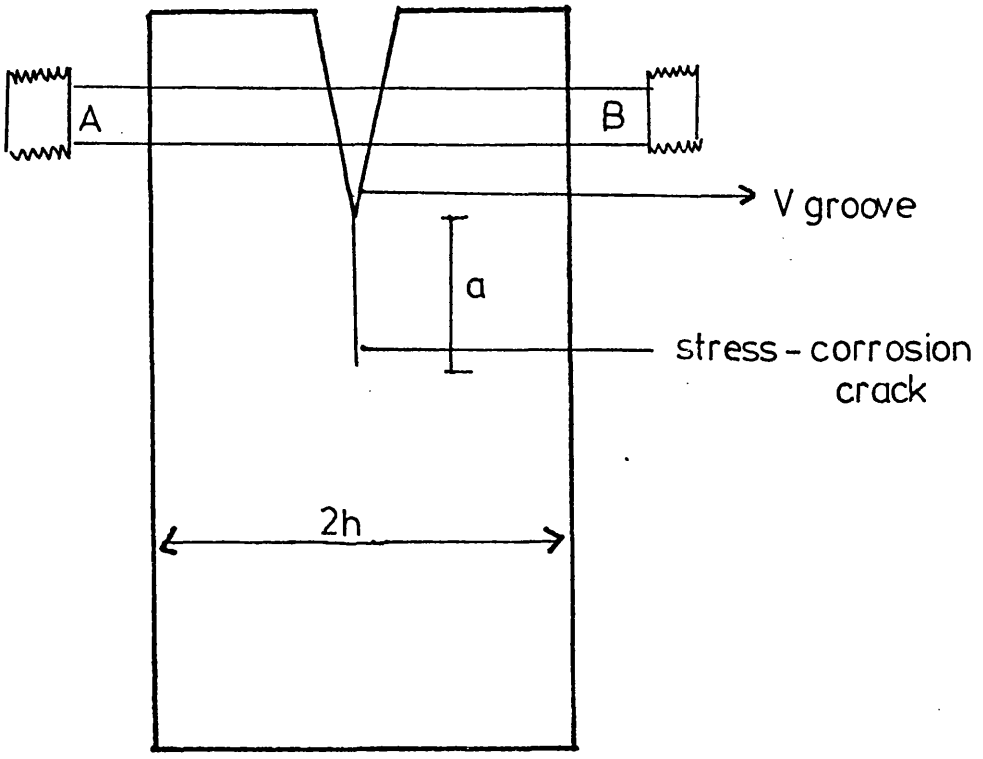

$$K_I = Efh \frac{\left[4h\,(a + 0.6h)^2 + h^3\right]^{\frac{1}{2}}}{4\left[(a + 0.6h)^3 + h^2 a\right]}$$

K_I = stress intensity at Crack tip

E = Young's Modulus

f = defection at Load Line A-B

Fig. 2.4 A Double-Cantilever beam

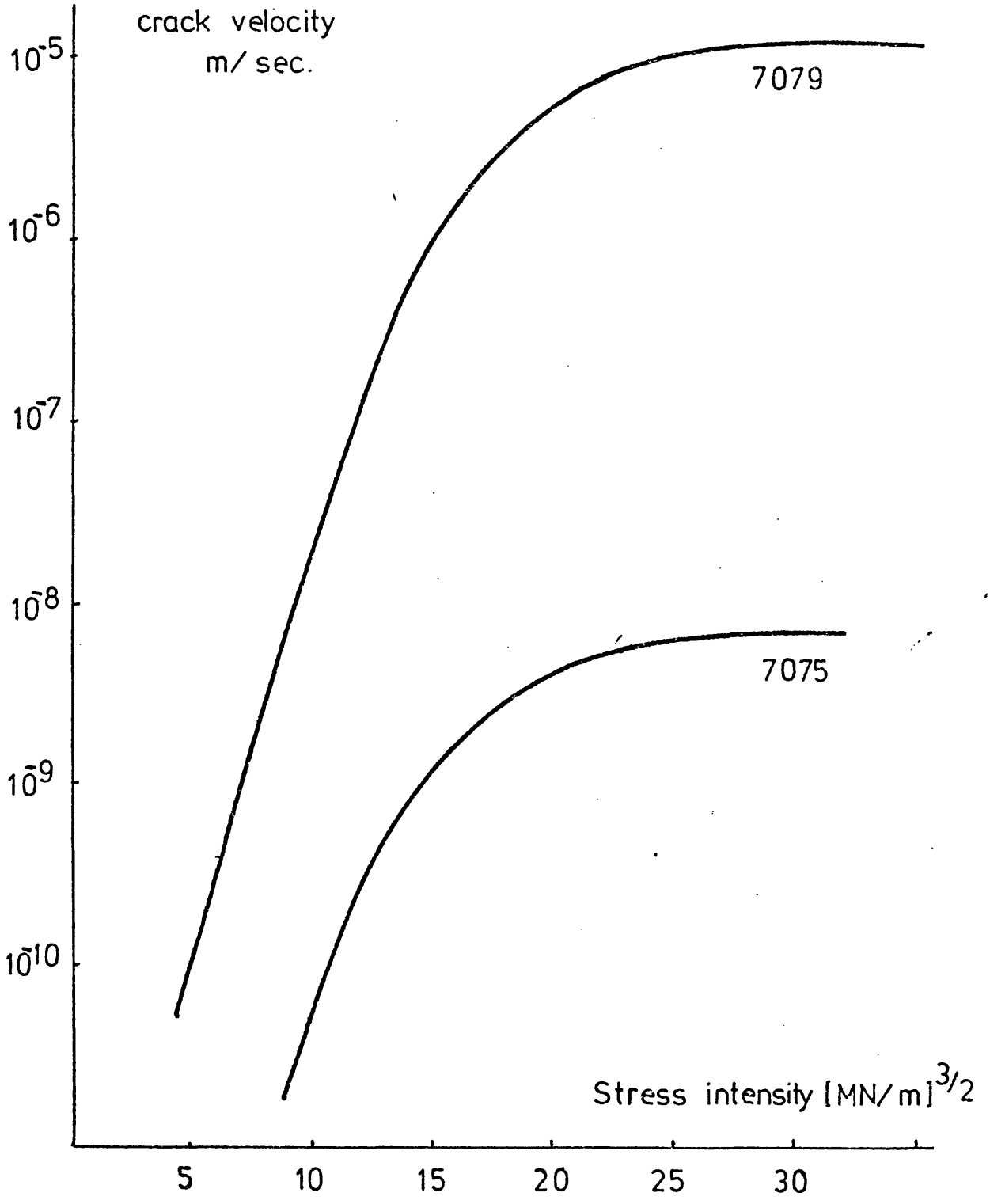

Fig. 2.5 Stress-corrosion crack velocity vs stress intensity for alloy 7079 (A1 4.3 Zn 3.3 Mg. o.6Cu.) and alloy 7075 (A1 5.6 Zn 2.5Mg. 1.6 Cu). Tests performed in aqueous NaCl at 25°C.

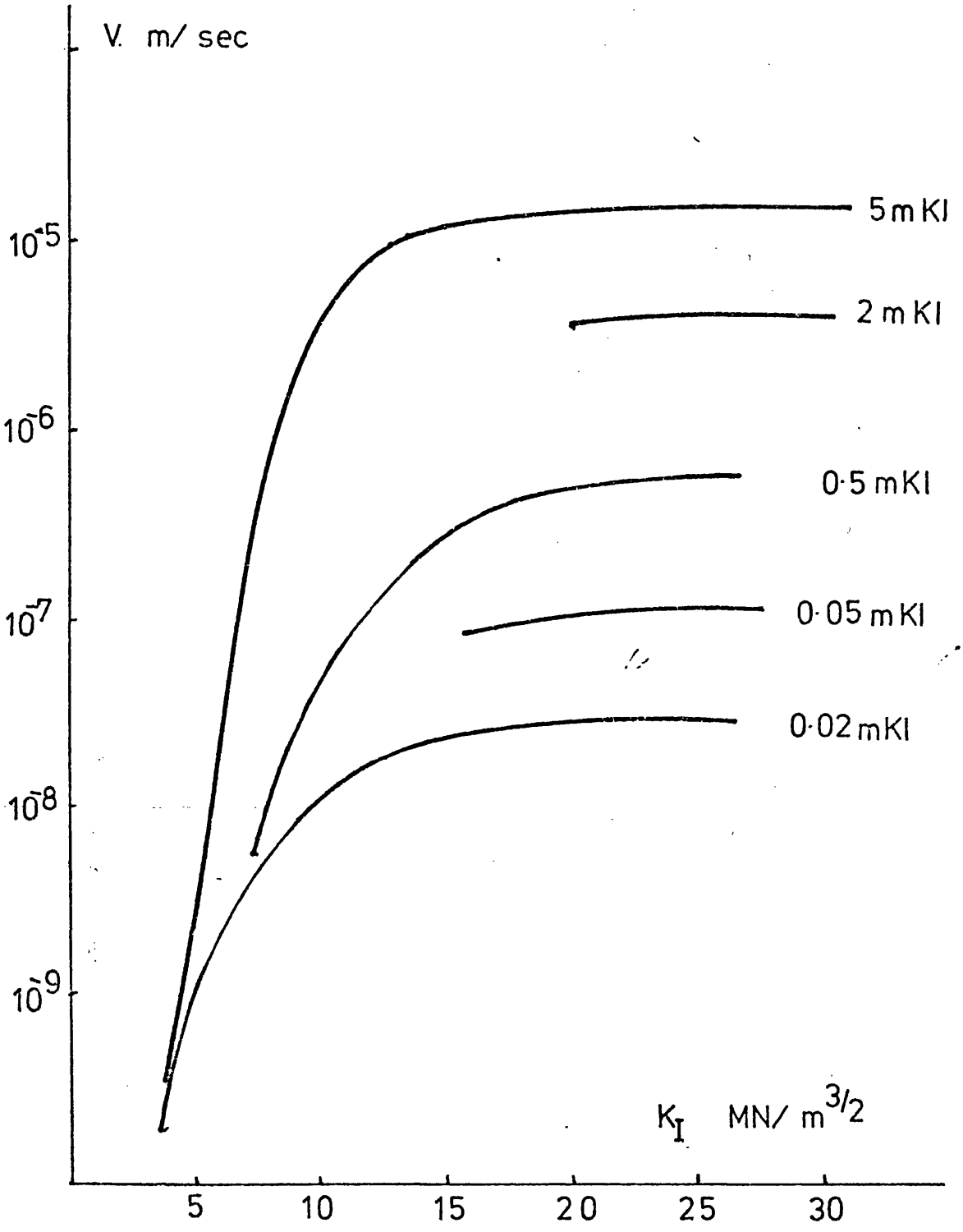

Fig. 2.6 Effect of stress intensity (K_I) and iodide concentration on stress-corrosion crack Velocity (V) in a high strength aluminium alloy (Al 4.3 Zn 3.3 Mg. 0.6 Cu.) in aqueous solution of PH = 6 at 25°C.

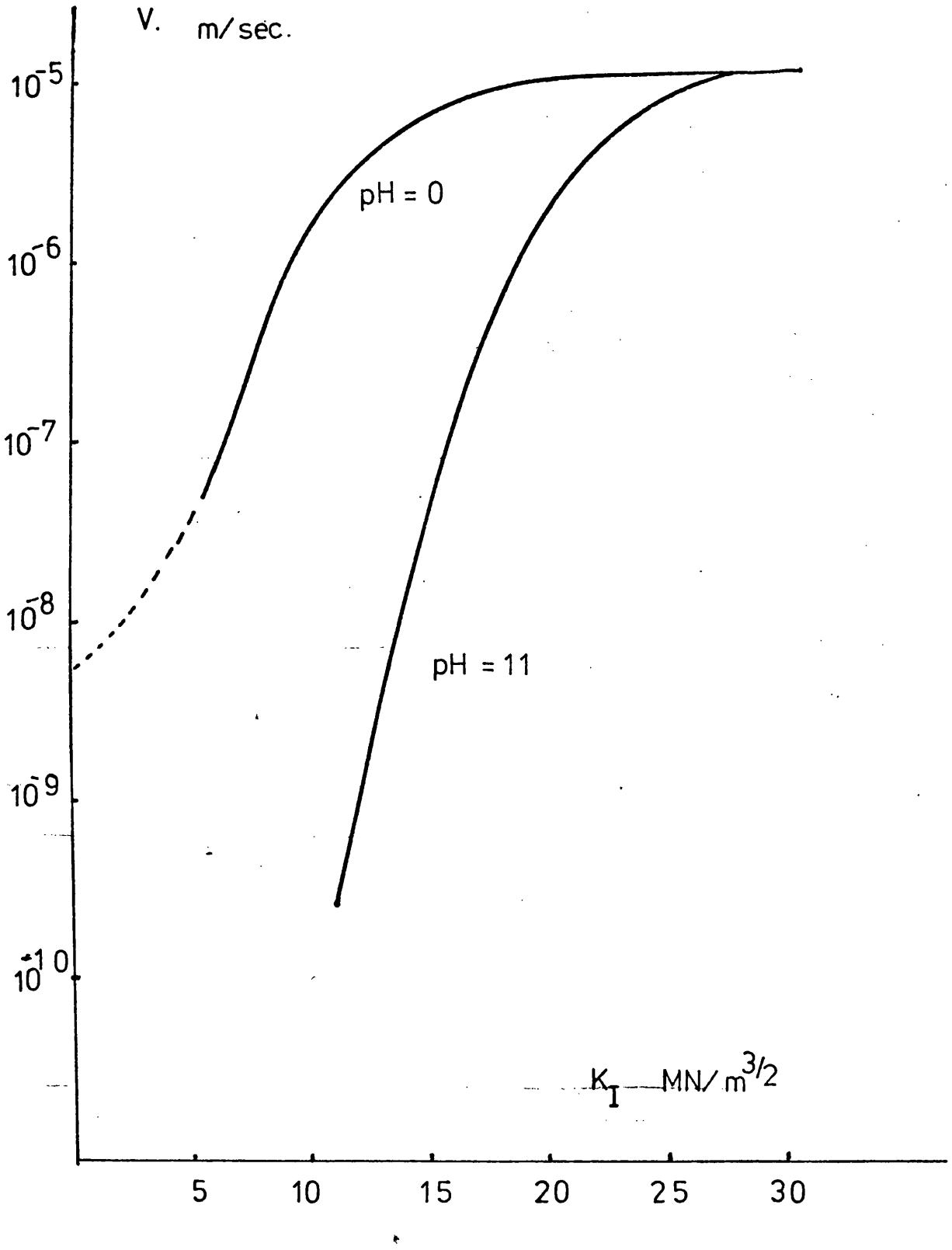

Fig. 2.7 Effect of stress intensity (K_I) and pH on the stress-corrosion crack velocity (V) of a high strength aluminium alloy in a aqueous chloride solution at 25°C.

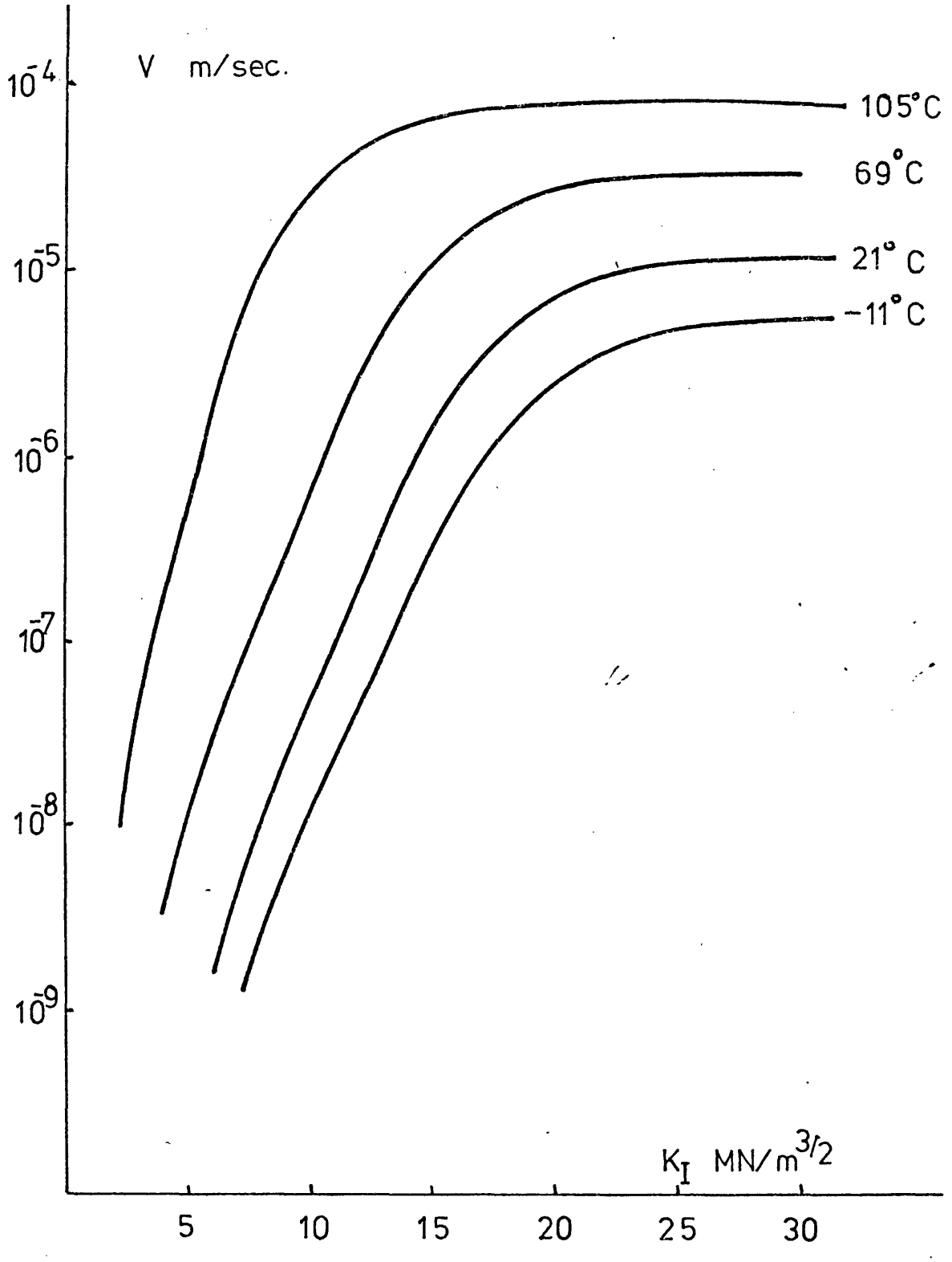

Fig. 2.8 Stress-corrosion crack velocity (V) in Al 4.3 Zn 3.3Mg. 0.6 Cu. as a function of stress intensity, K_I, and temperature. Tests carried out in aqueous iodide at 25°C.

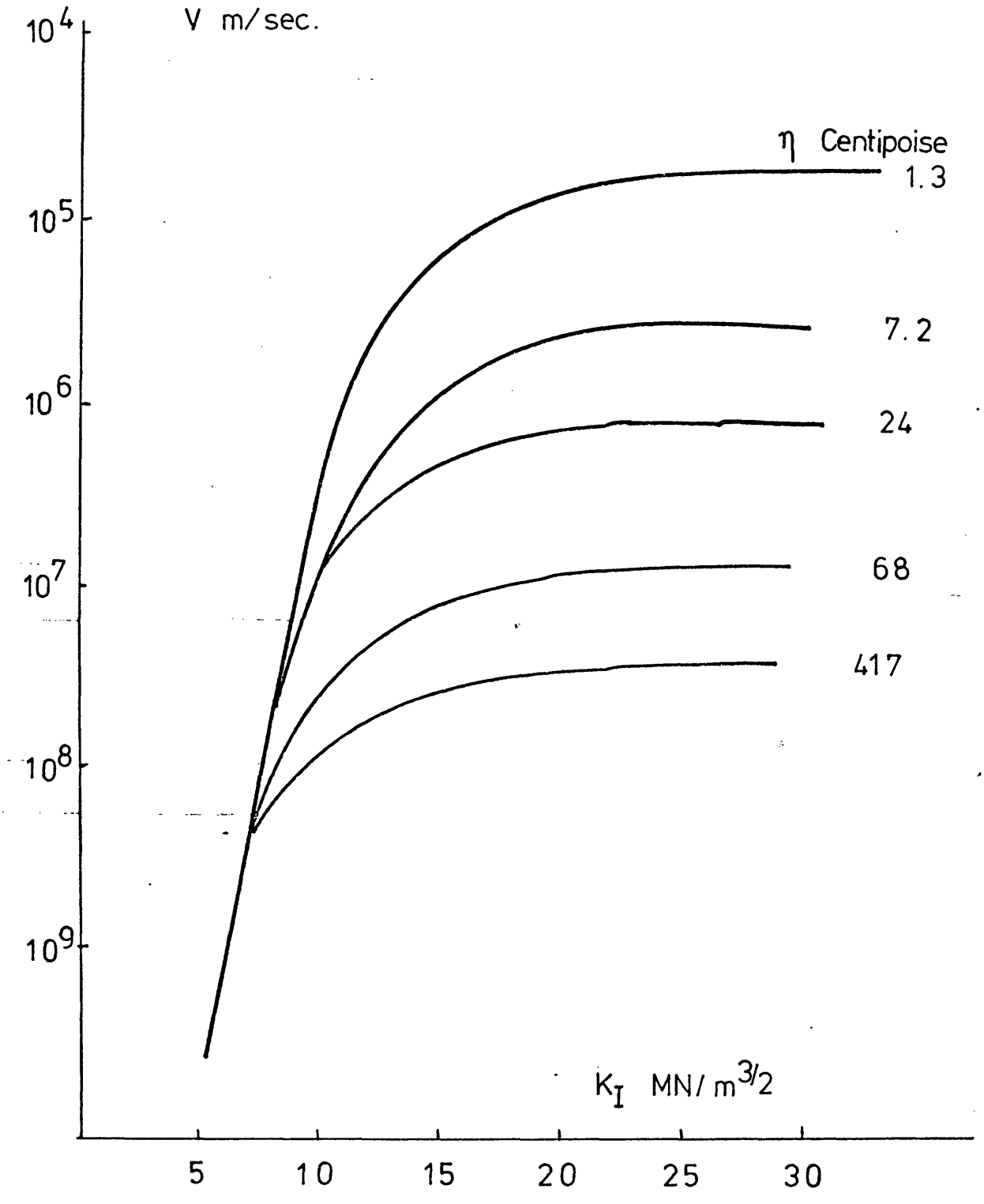

Fig. 2.9 Effect of stress intensity, K_I, and viscosity, η, on stress-corrosion crack velocity, V, in a high strength aluminium alloy.

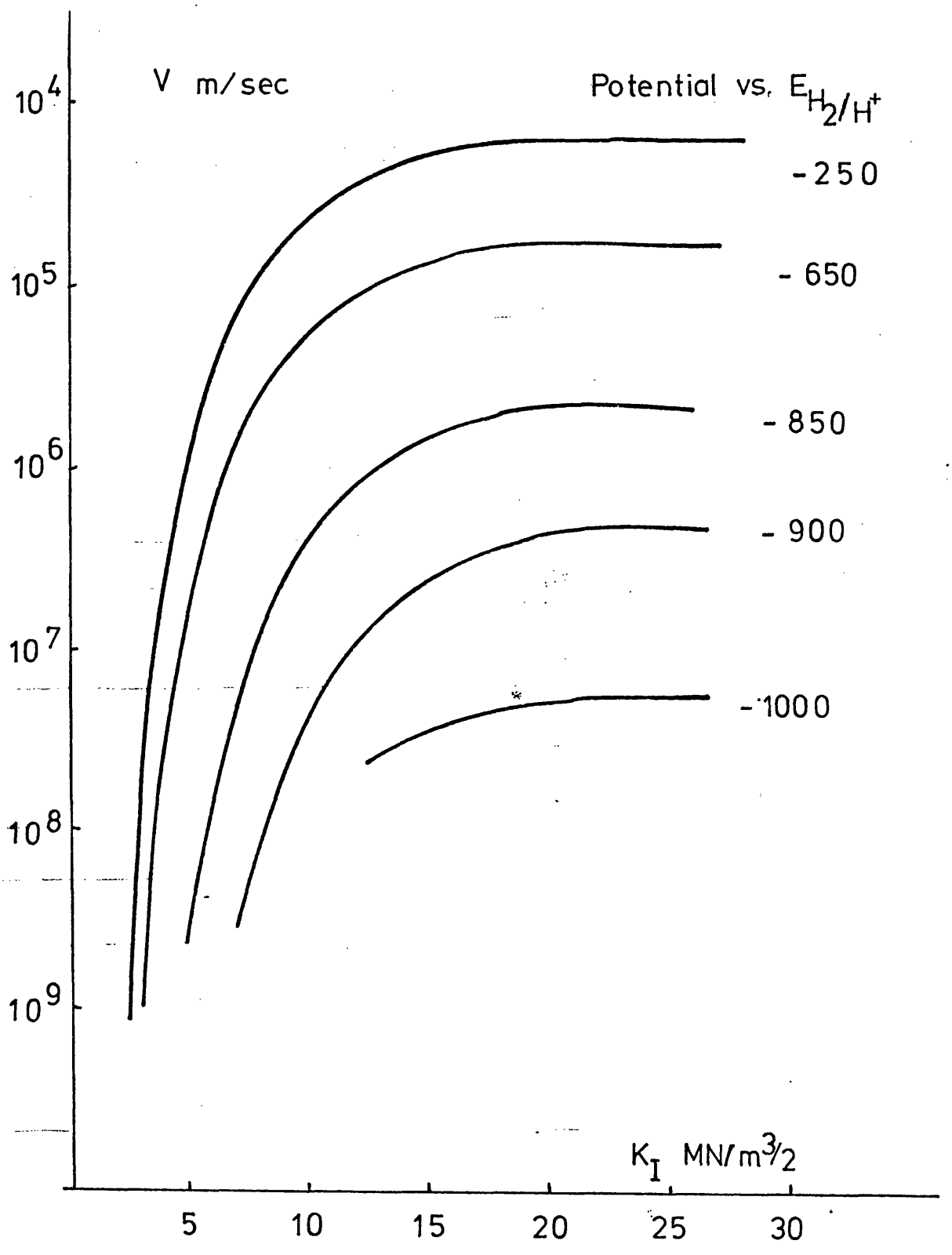

Fig. 2.10 The effect of electrical potential and stress intensity, K_I, on the stress-corrosion crack velocity in a high strength aluminium alloy in 5m aqueous KI at 23°C.

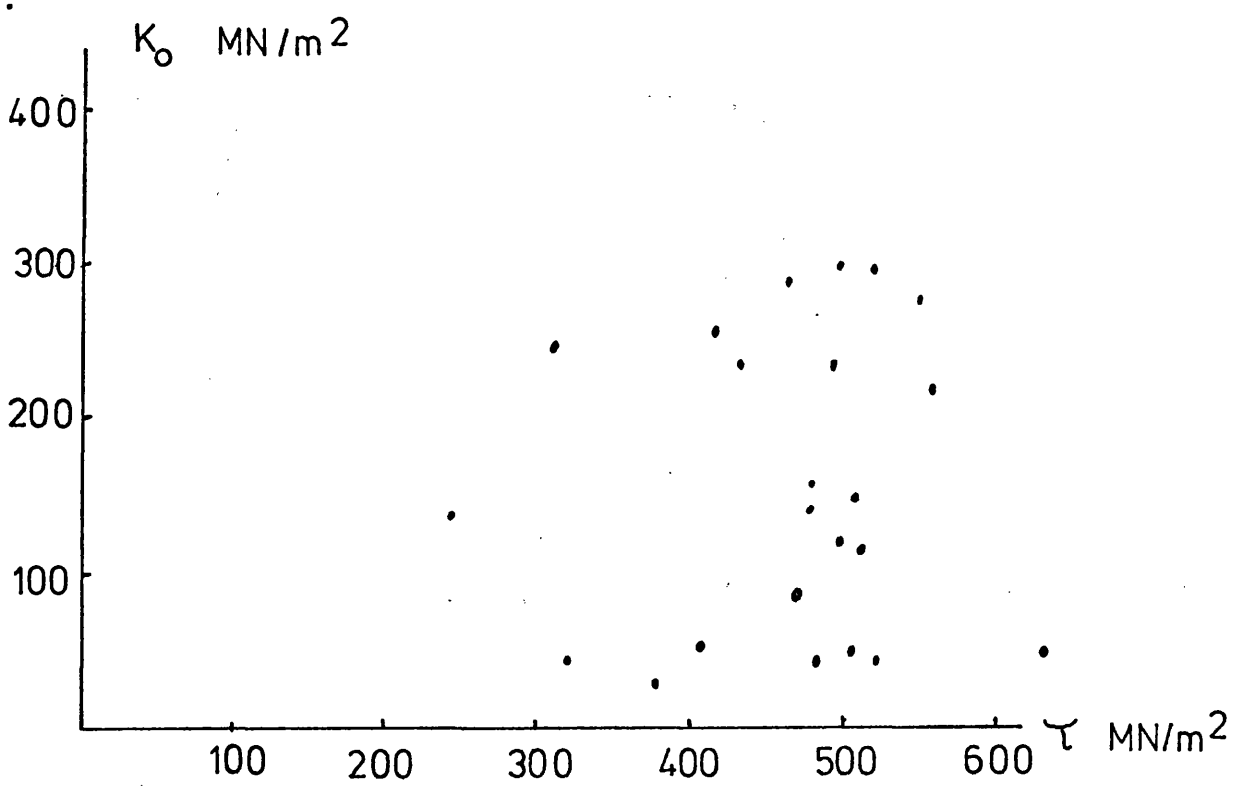

Fig. 2.11a There is no relationship between yield strength, τ, and the stress-corrosion threshold stress, K_o.

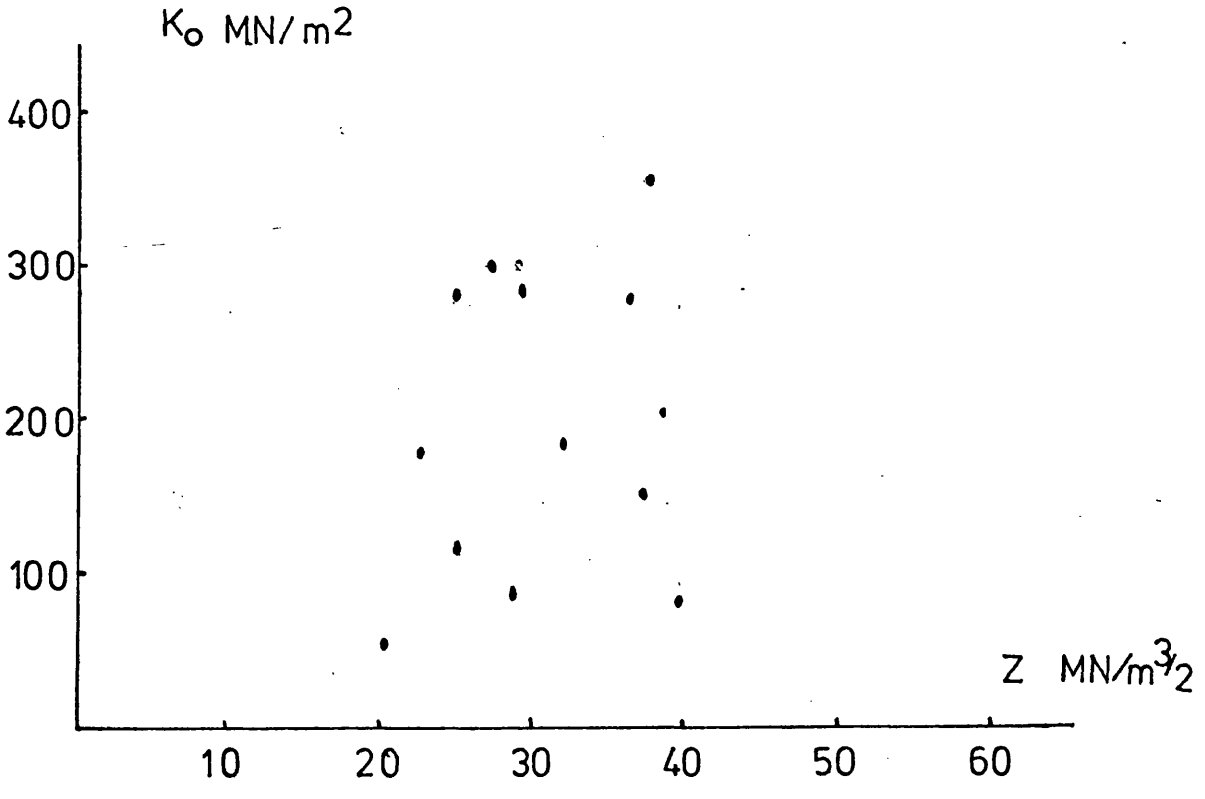

Fig. 2.11b There is no relationship between fracture toughness, Z, and stress-corrosion threshold stress, K_o.

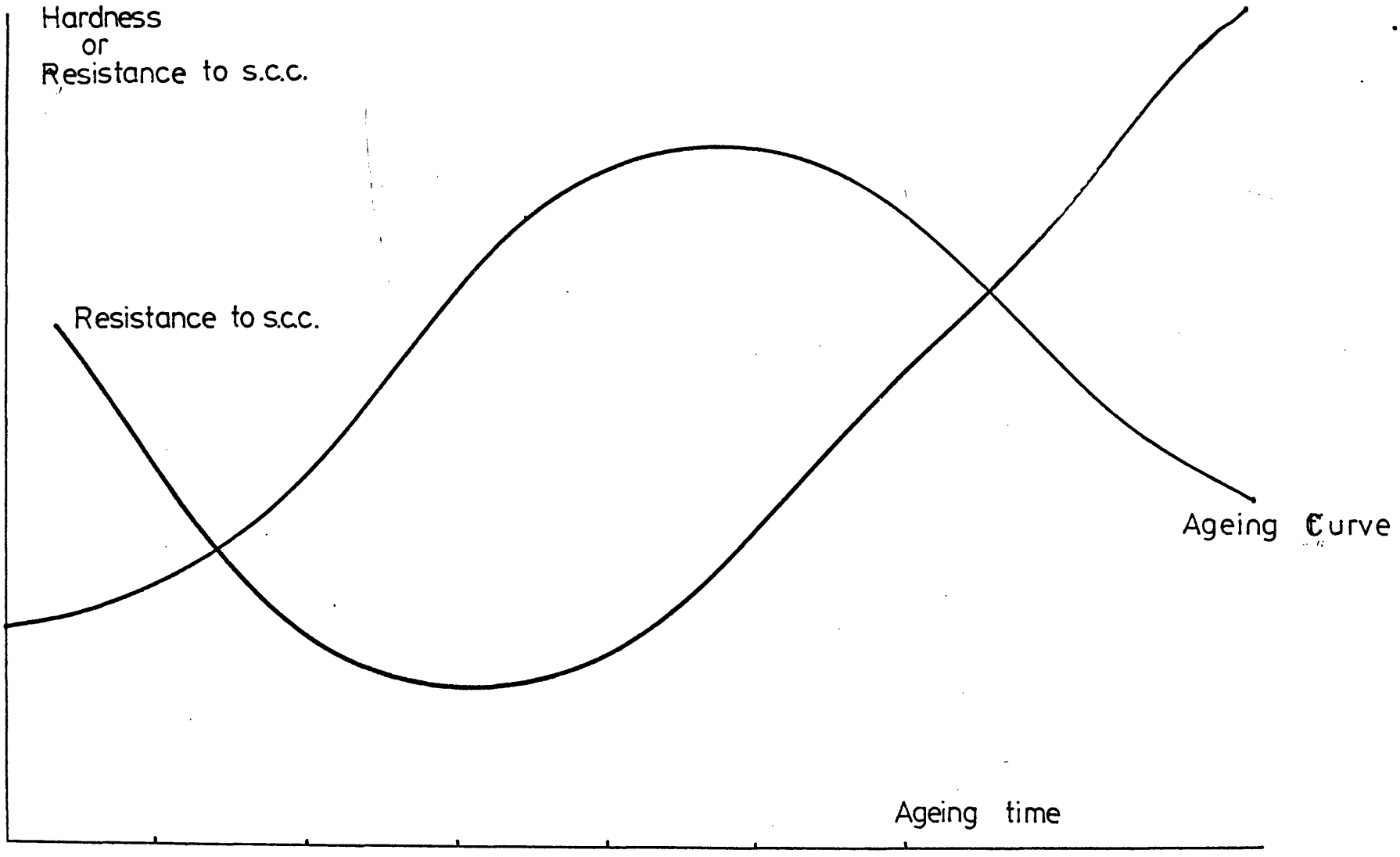

Fig. 2.12. Variation of hardness and stress-corrosion resistance during ageing of precipitation hardening aluminium alloys.

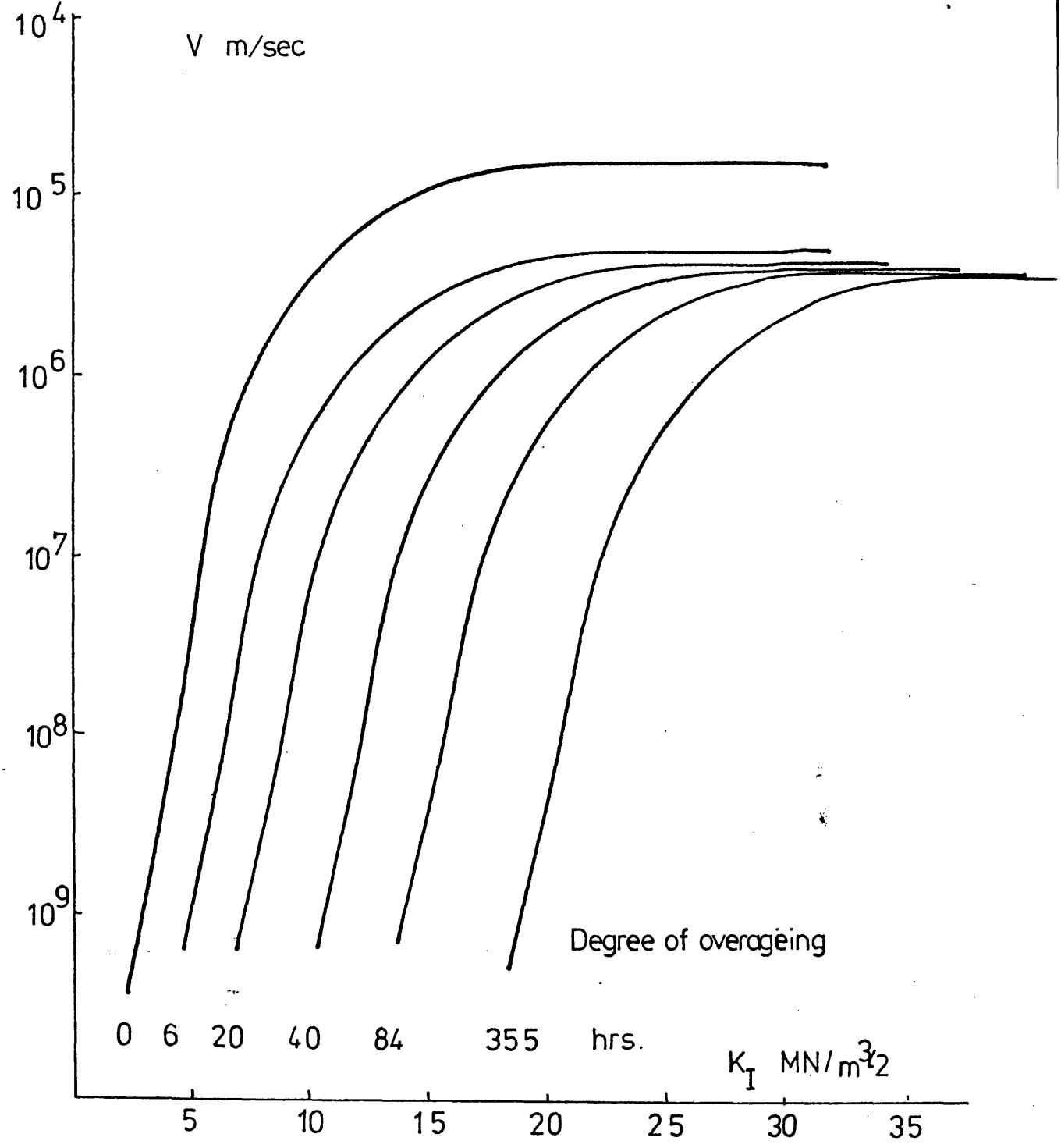

Fig. 2.13 The influence of overageing and stress intensity, K_I, on the stress-corrosion crack velocity, V, for a high strength aluminium alloy.

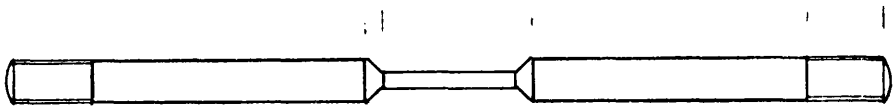

Scale. 1:0·75

Fig 4.1 Environmental test specimen

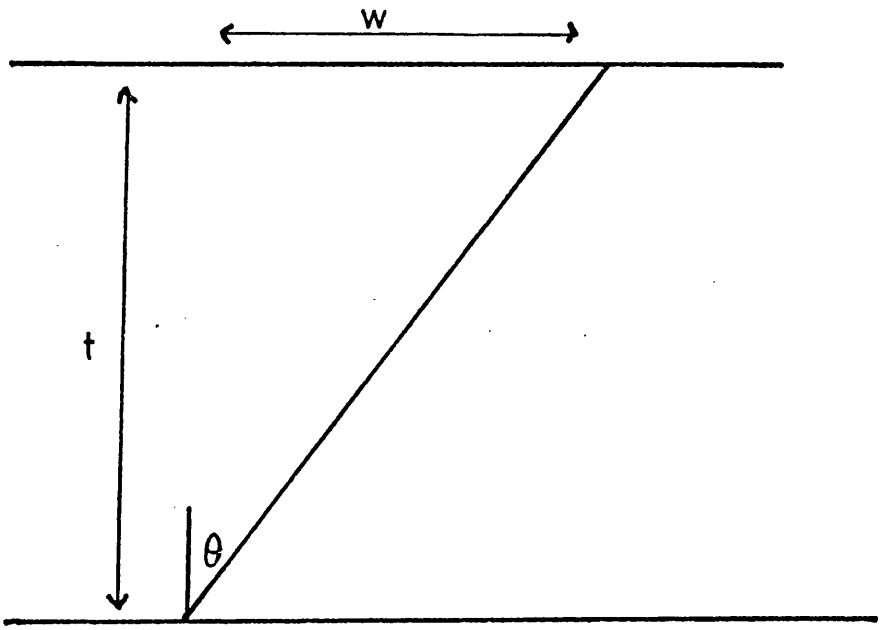

$t = w \tan \theta$

t - foil thickness
W is measured width of object lying at an orientation of θ with respect to the perpendicular through the plan of the foil

Fig. 4.2 Measurement of foil thickness

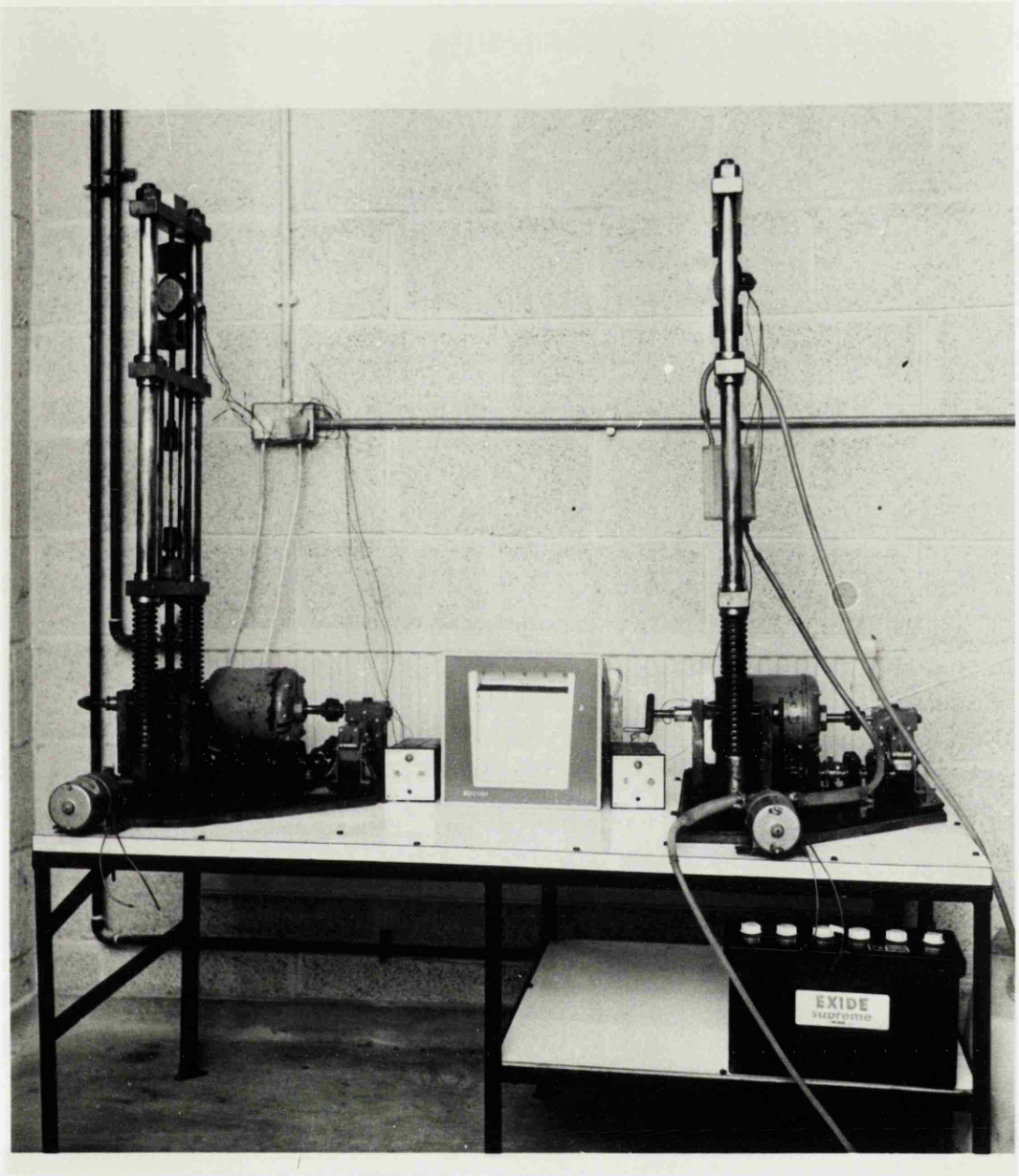

Fig 4.3 Stress-corrosion apparatus

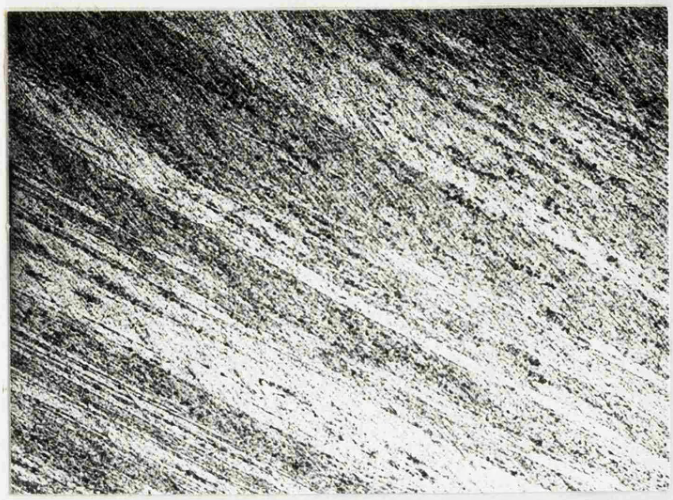

a.

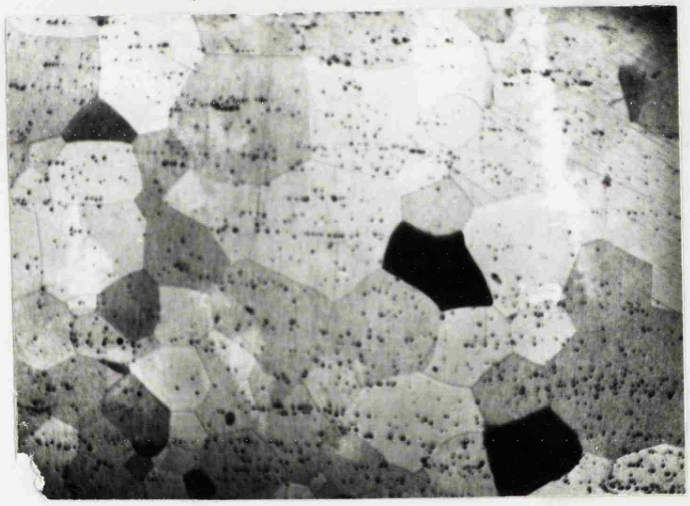

b.

Fig 5.1. Optical micrographs (x50) of
(a) as - received material
(b) after recrystallisation at 550°C for 72 hours

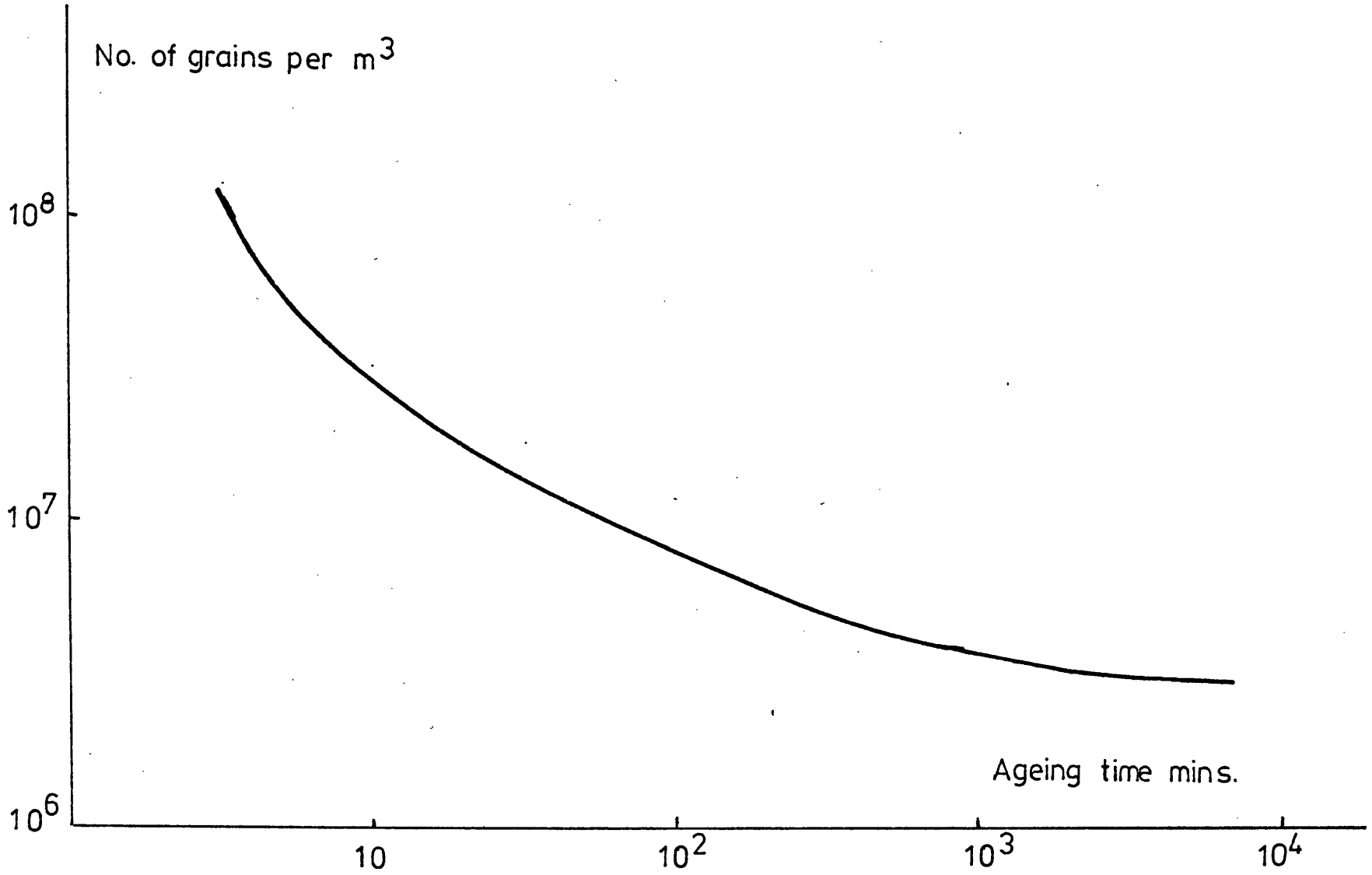

Fig. 5.2 Variation in grain density with ageing time during recrystallisation

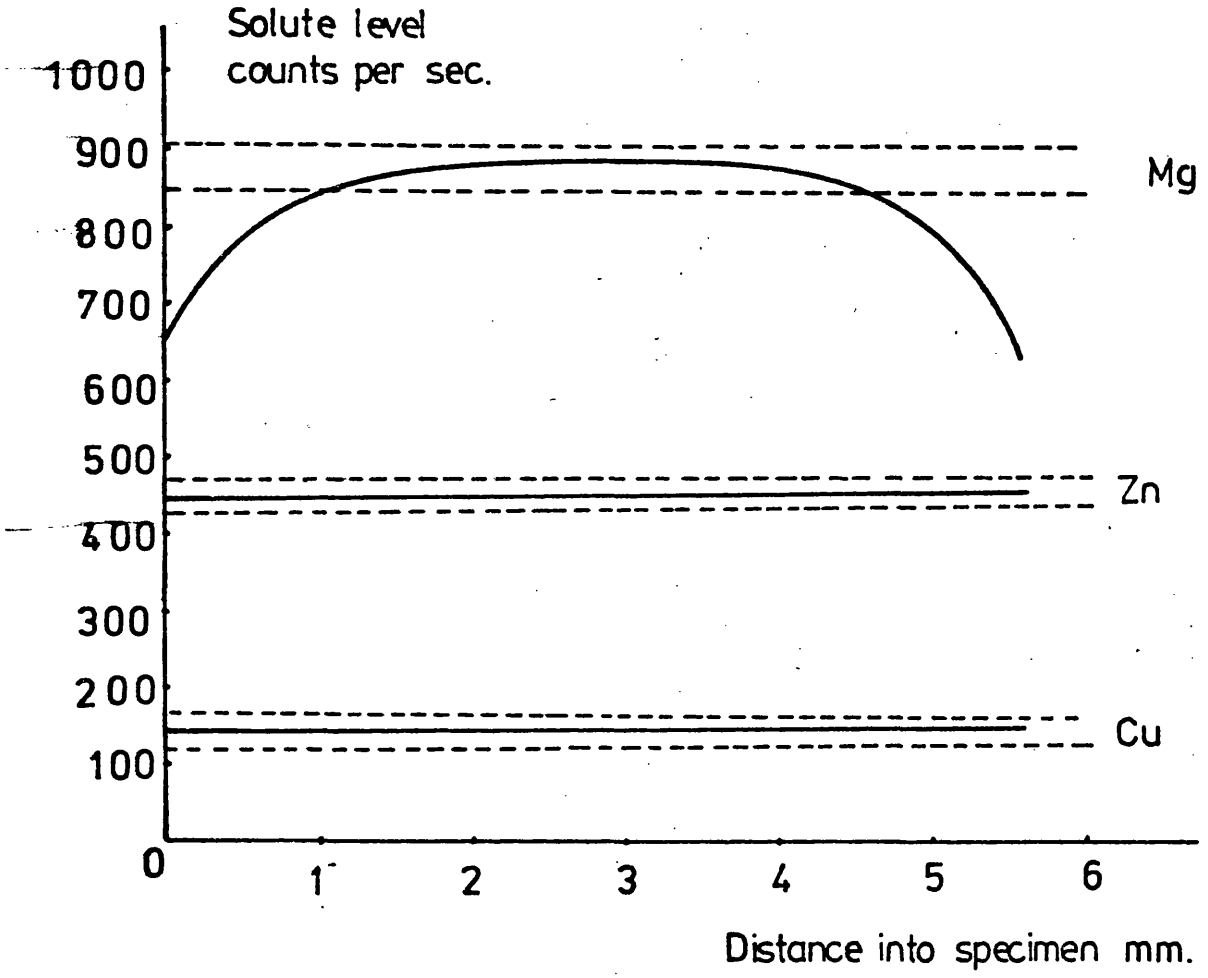

Fig. 5.3. Mg, Zn and Cu distributions across a transverse section of rod before and after recrystallisation, showing magnesium loss at specimen edge during recrystallisation.

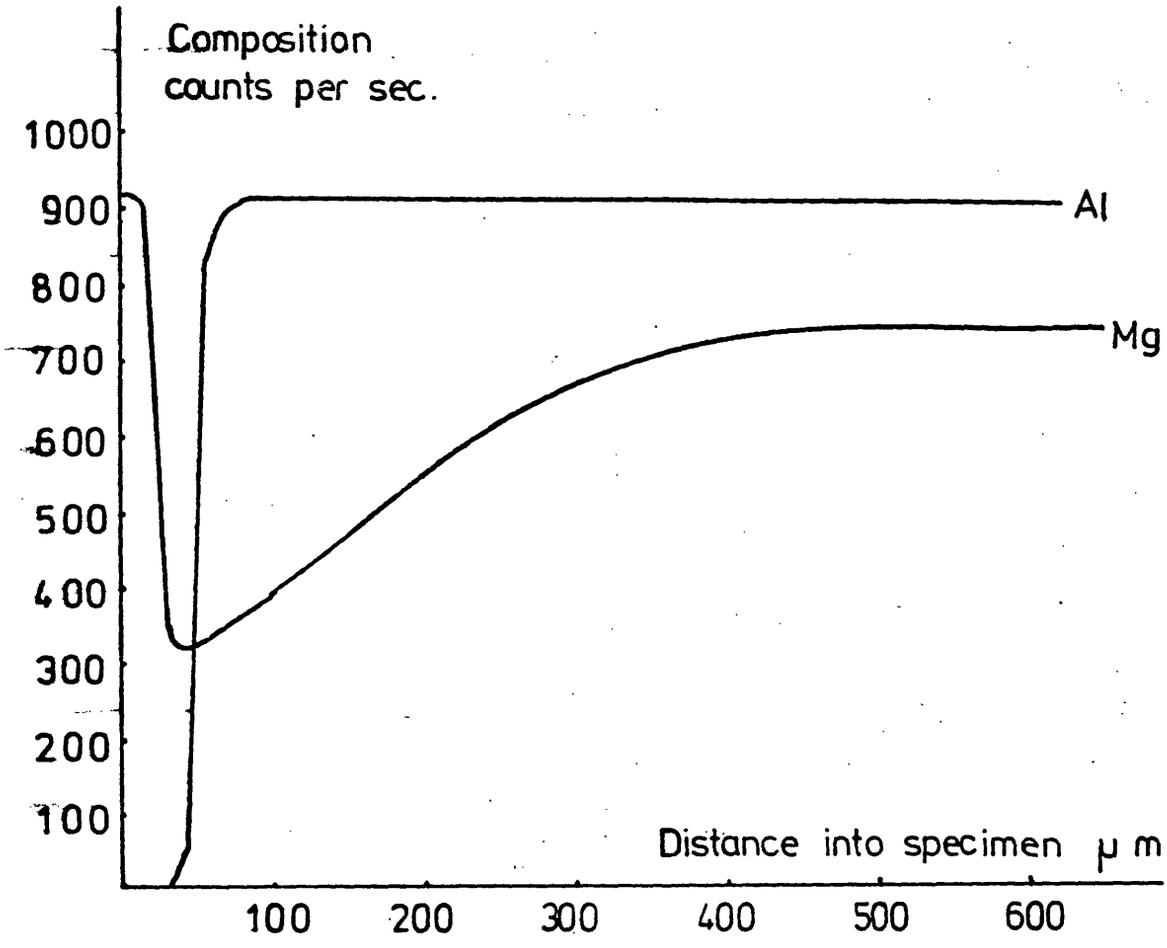

Fig. 5.4. Mg and Al distributions across the recrystallised metal showing Mg segregation in outer oxide layer.

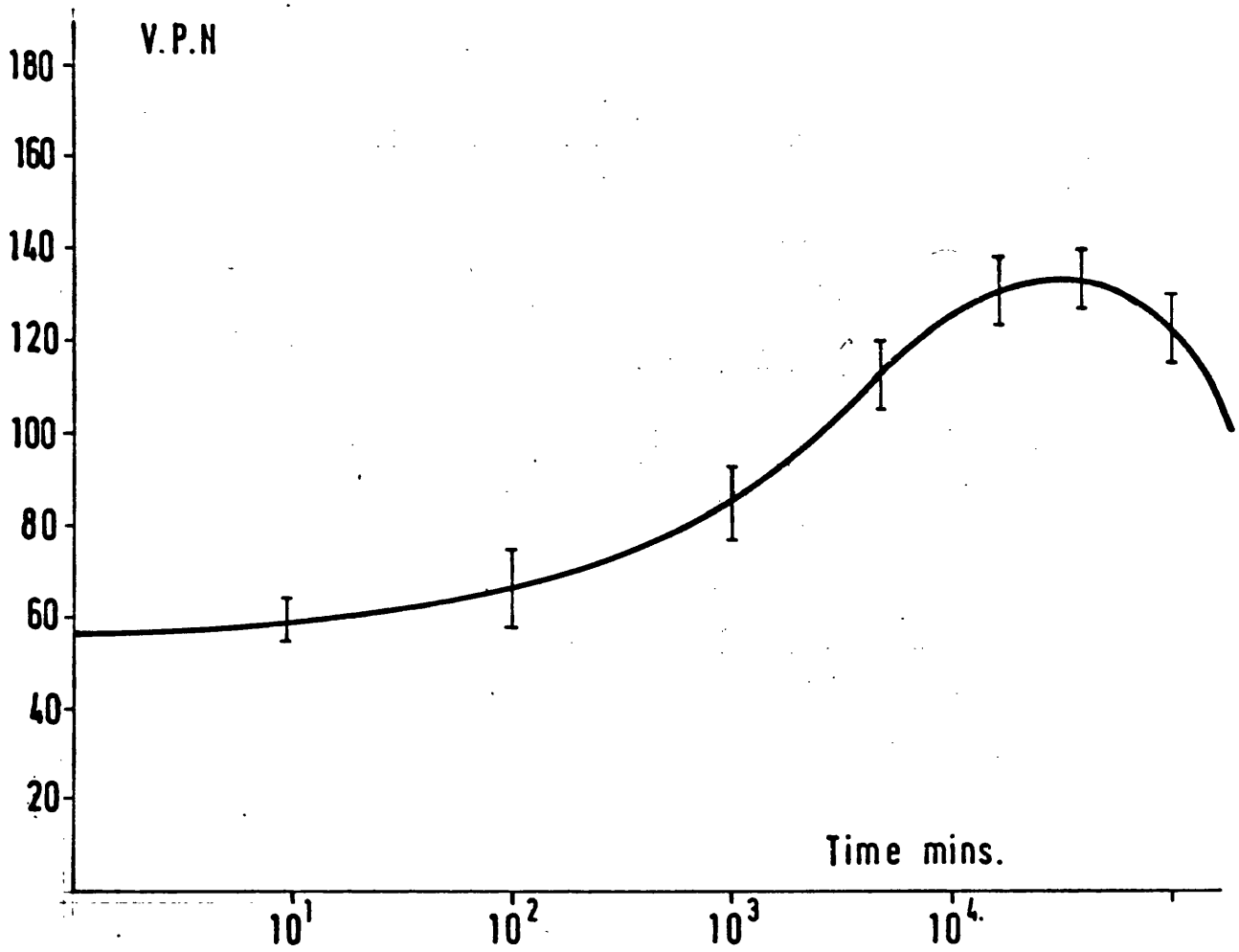

Fig. 5.5. Typical ageing curve for an Al-Zn-Mg alloy-Al 4.5Zn 2.5Mg cold-water quenched and aged 120°C.

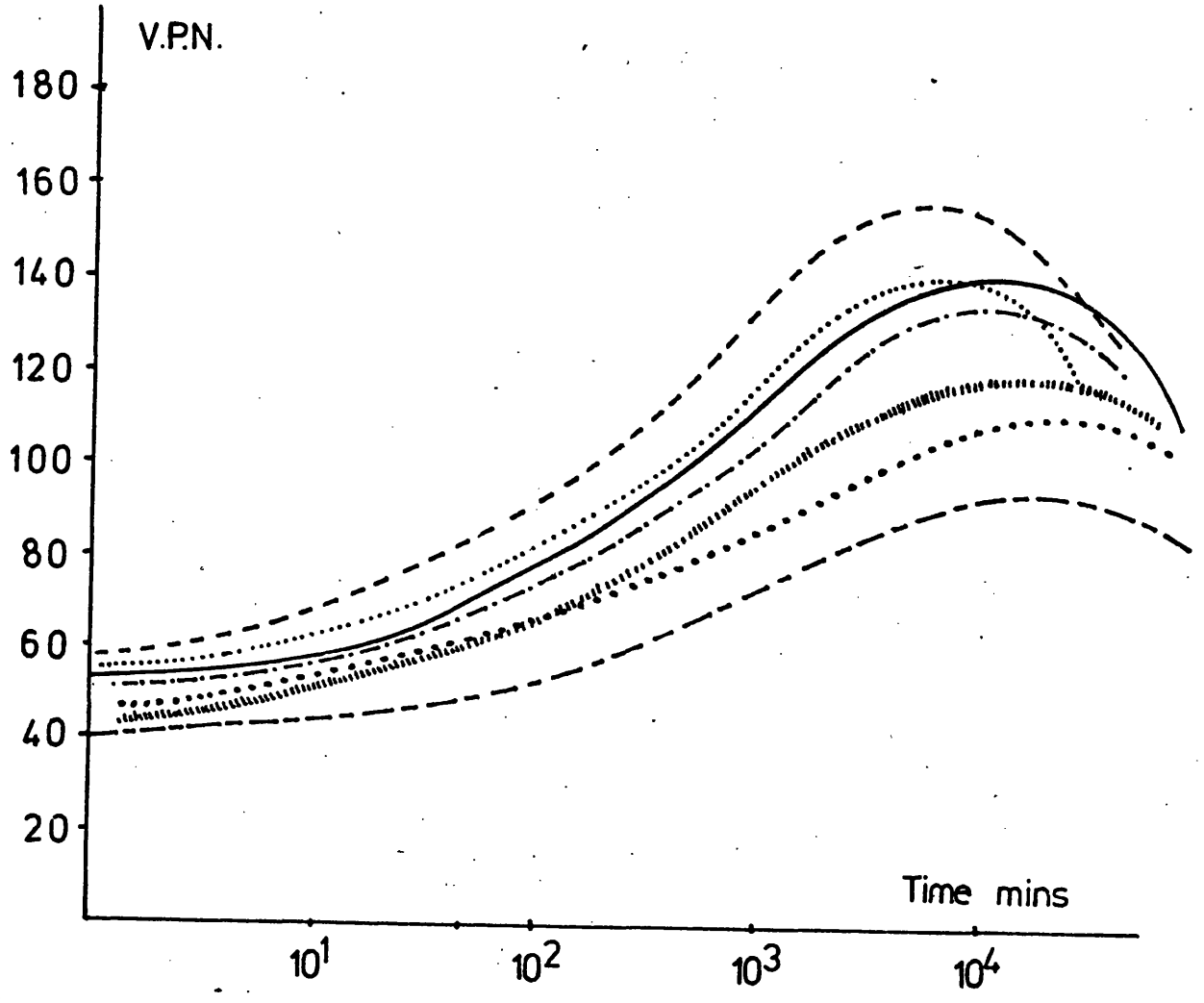

Fig. 5.6. The effect of alloy content on the behaviour of cold-water quenched materials aged at 120°C.

_____ Al 4.5Zn 2.5Mg
_ _ _ _ _ _ Al 5.0Zn 3.0Mg
_ _ _ _ _ Al 4.0Zn 2.0Mg
_ . _ . _ . _ Al 5.0Zn 2.0Mg
. . . . . Al 4.0Zn 3.0Mg
. . . . . Al 4.5Zn 2.5Mg 0.22Cu
. . . . . Al 4.5Zn 2.5Mg 0.15Cu

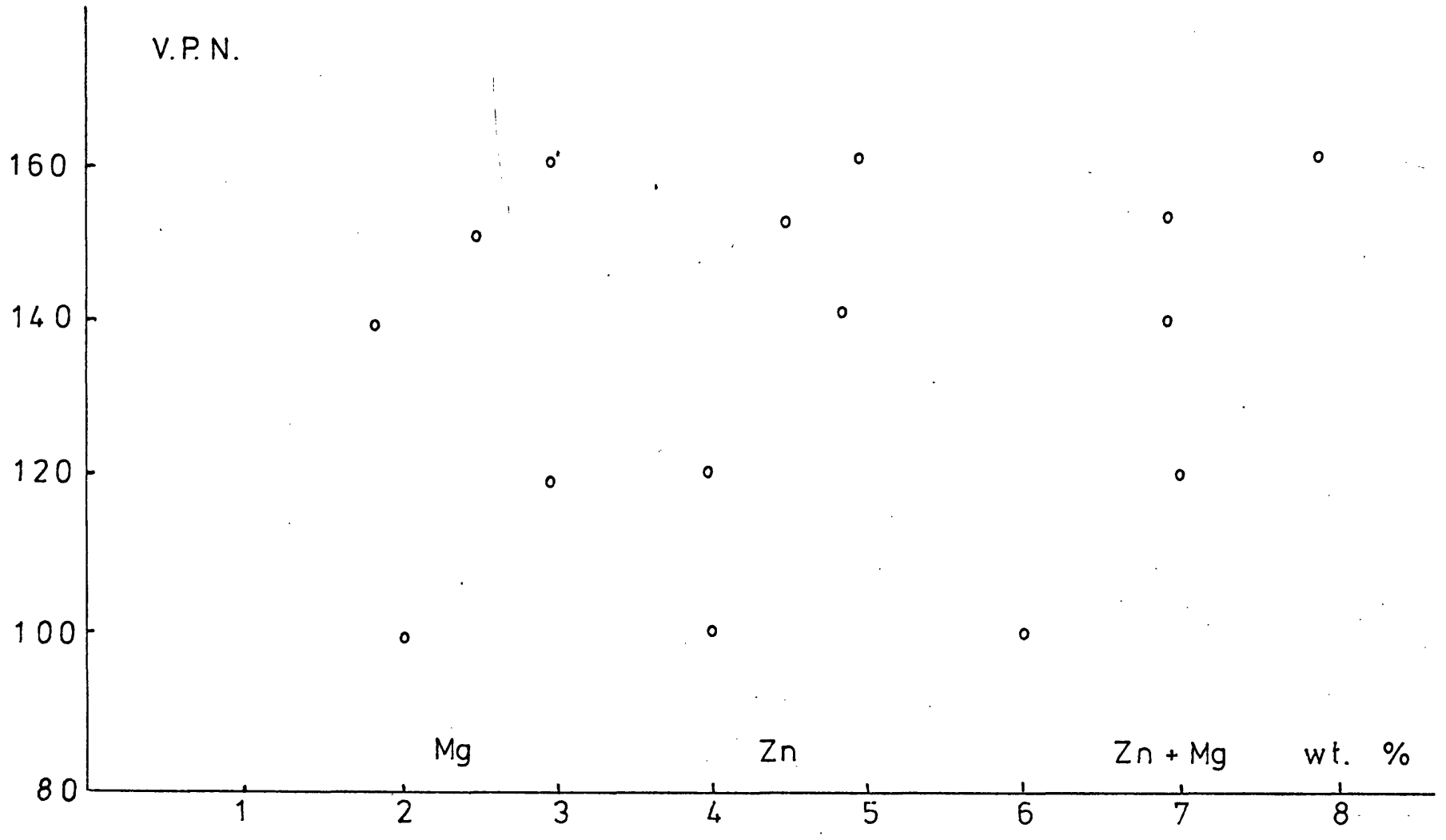

Fig. 5.7 The influence of alloy composition on the peak hardness for CWQ alloys aged at 120°C

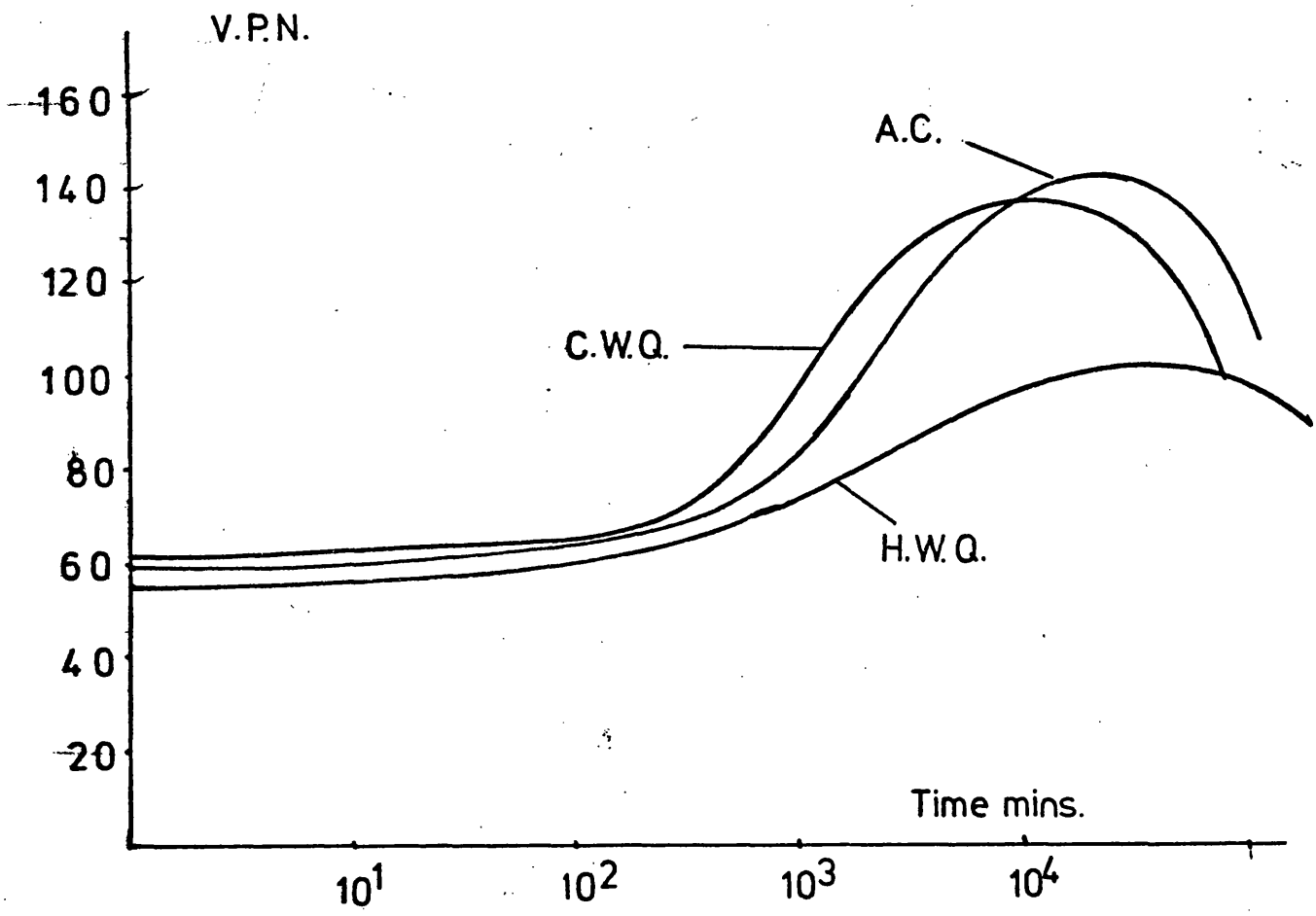

Fig. 5.8. The effect of quench-rate on the ageing behaviour of a typical alloy (Al 4.5Zn 2.5Mg aged at 120°C).

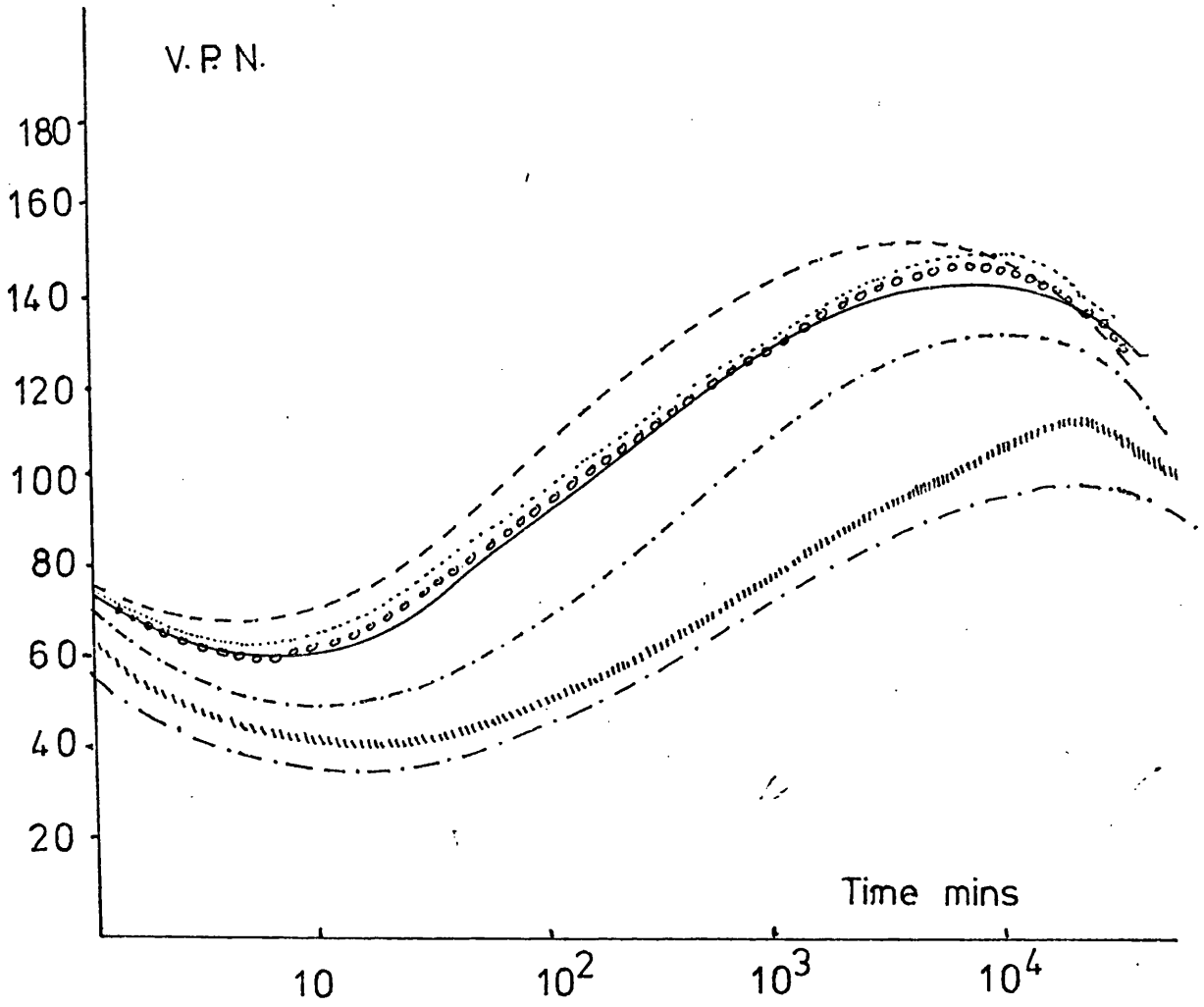

Fig. 5.9 Ageing curves for air-cooled alloys aged at 120°C

——— Al 4.5 Zn 2.5Mg.
– – – – – – Al 5.0 Zn 3.0Mg.
—·—·— Al 4.0 Zn 2.0Mg.
—·—·—·— Al 5.0 Zn 2.0Mg
····· Al 4.0 Zn 2.5Mg.
oooooooo Al 4.5 Zn 2.5Mg. 0.15 Cu.
····· Al 4.5 Zn 2.5Mg. 0.2 Cu.

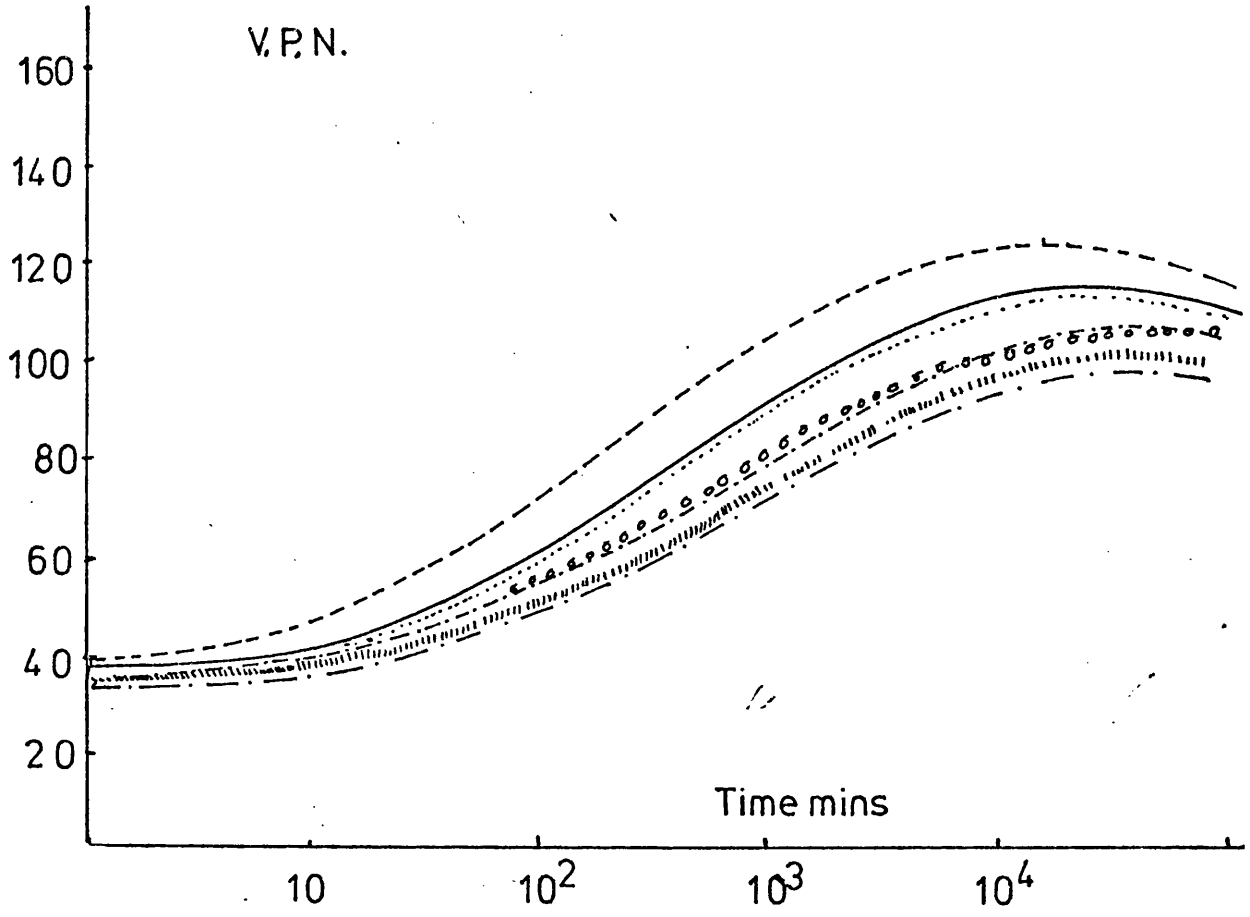

Fig. 5.10 Ageing Curves for hot-water quenched alloy aged at 120°C

————	Al 4.5 Zn 2.5 Mg	—·—·—·	Al 5.0 Zn 2.0 Mg
- - - - - -	Al 5.0 Zn 3.0 Mg	·····	Al 4.0 Zn 3.0 Mg
—·—·—	Al 4.0 Zn 2.0 Mg	oooooooo	Al 4.5 Zn 2.5 Mg. 0.15 Cu

..... Al 4.5 Zn 2.5 Mg 0.2 Cu

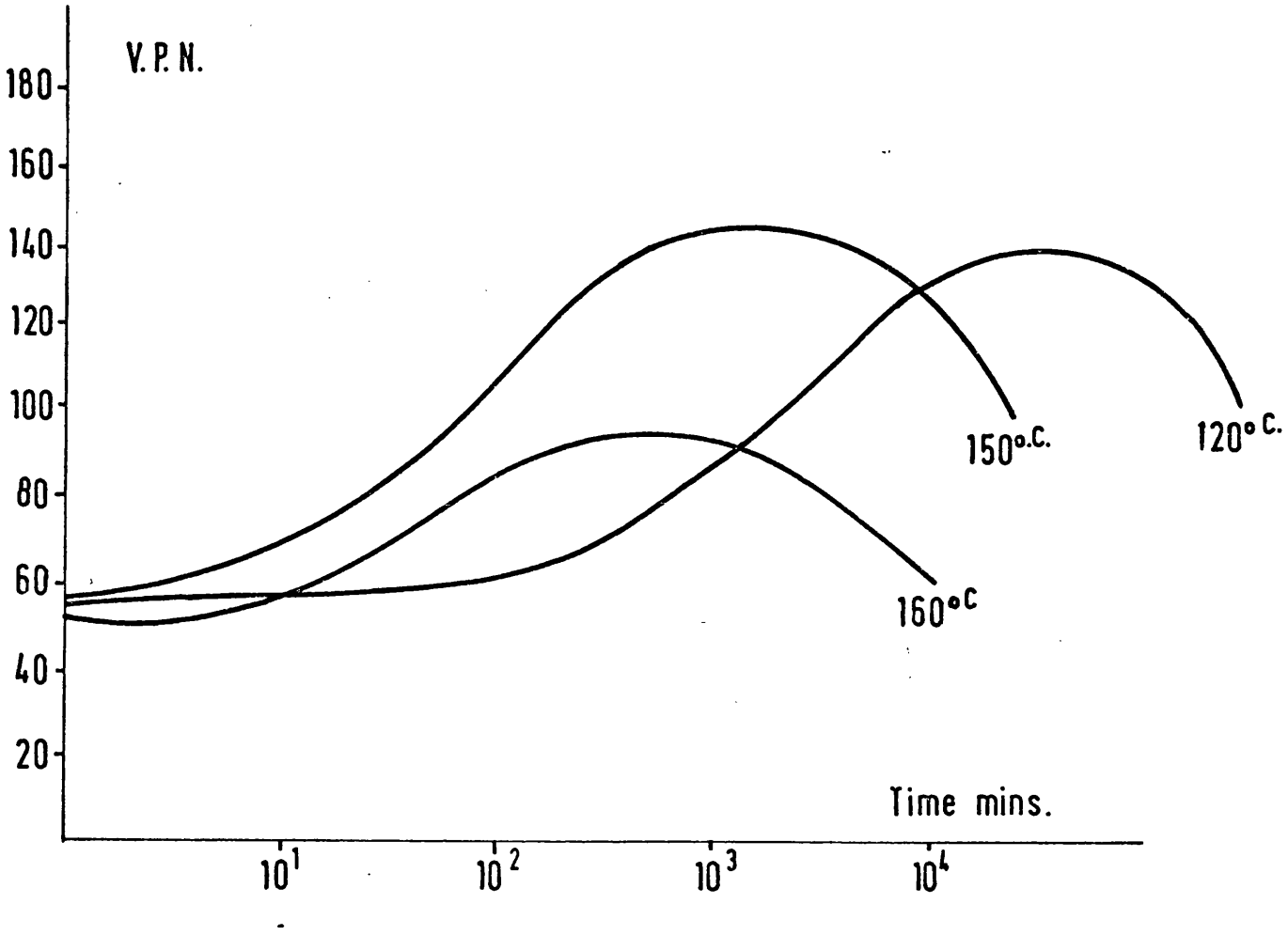

Fig 5.11. The effect of ageing temperature on the ageing behaviour of a typical alloy (Al 4.5Zn 2.5Mg cold-water quenched).

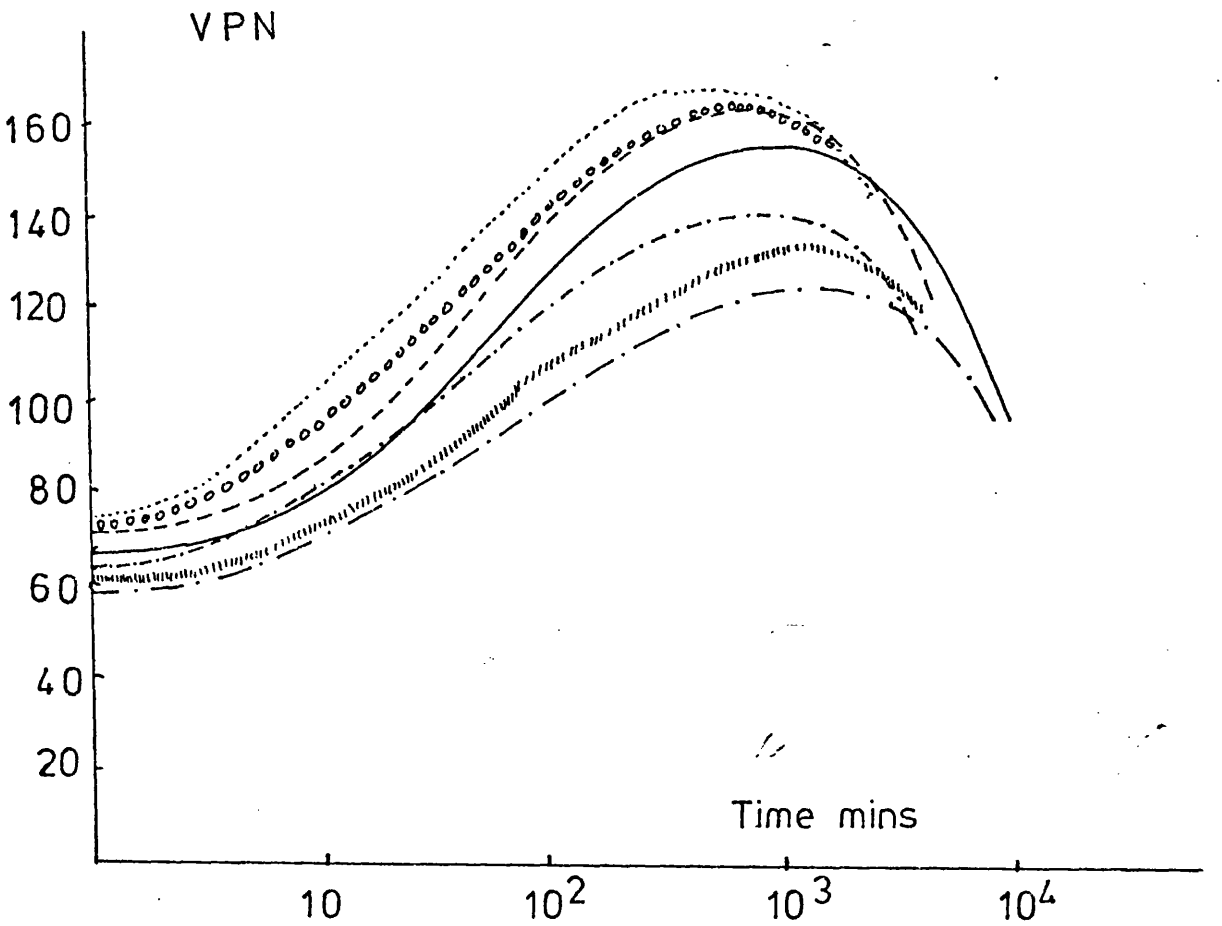

Fig. 5.12 Ageing Curves for cold-water quenched alloy aged at 150°C

——— Al 4.5 Zn 2.5 Mg.
- - - - - - - Al 5.0 Zn 3.0 Mg.
—·—·— Al 4.0 Zn 2.0 Mg.
—·—·—·— Al 5.0 Zn 2.0 Mg
····· Al 4.0 Zn 3.0 Mg
°°°°°°°°°° Al 4.5 Zn 2.5 Mg. 0.15 Cu
..... Al 4.5 Zn 2.5 Mg. 0.2 Cu.

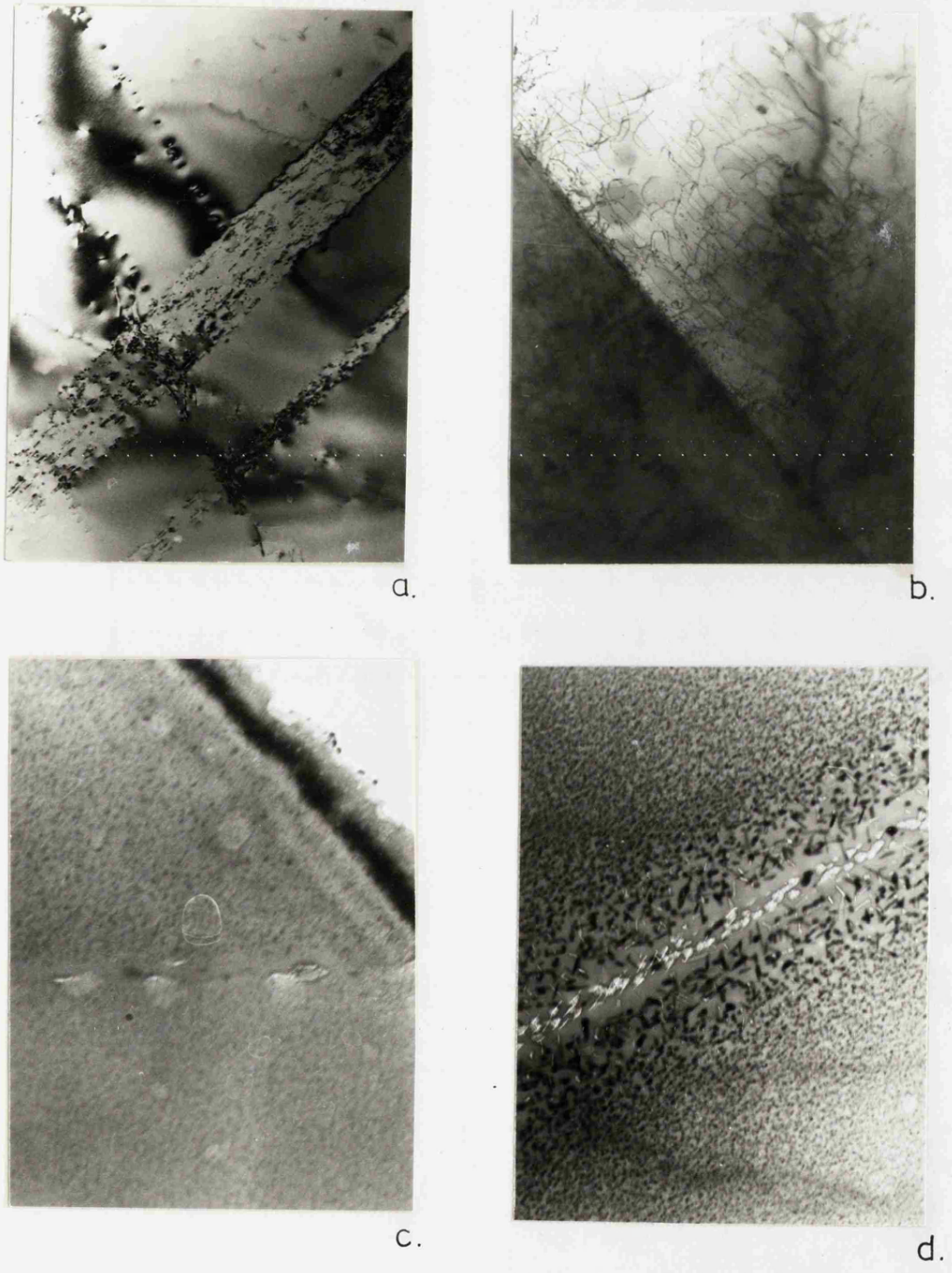

Fig 5.13 The effect of ageing on the development of microstructure; alloy N765 CWQ.
(a) banded dislocation network solution treated x77,000
(b) grain-boundary, solution treated x 20,000
(c) grain-boundary, peak hardness x77,000
(d) grain-boundary, overaged x 20,000

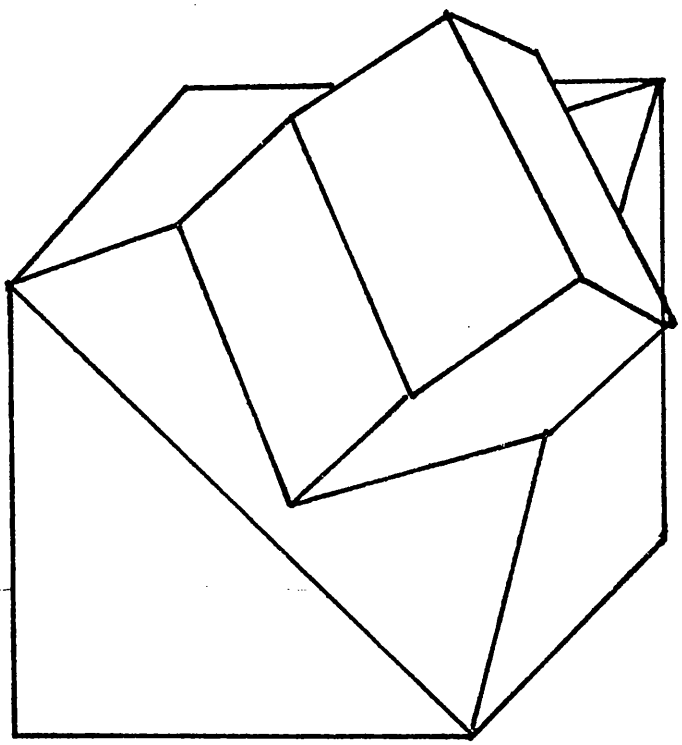

Fig. 5.14 Orientation relationship, η, to aluminium matrix

$(1\bar{2}0)_{\eta}$ //$(1\bar{1}1)_{A1}$; $(001)_{\eta}$ //$(110)_{A1}$

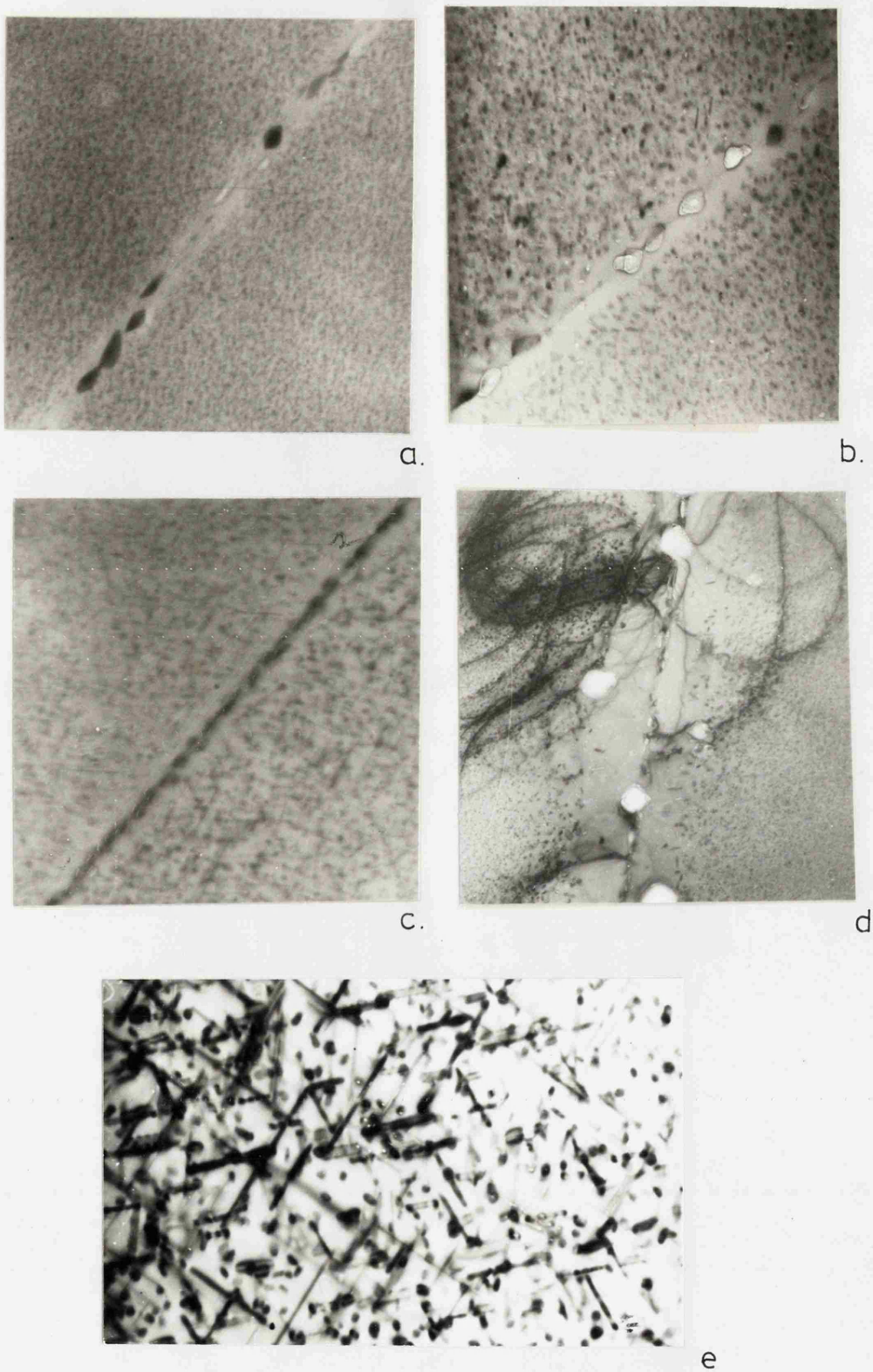

Fig 5.15 The influence of composition on the microstructure of CWQ alloys
(a) alloy N766 peak hardness x 77,000
(b) N766 overaged x 12,000
(c) alloy N767 peak hardness x 77,000
(d) N767 overaged x 12,000
(e) matrix precipitation in N767 overaged x 77,000

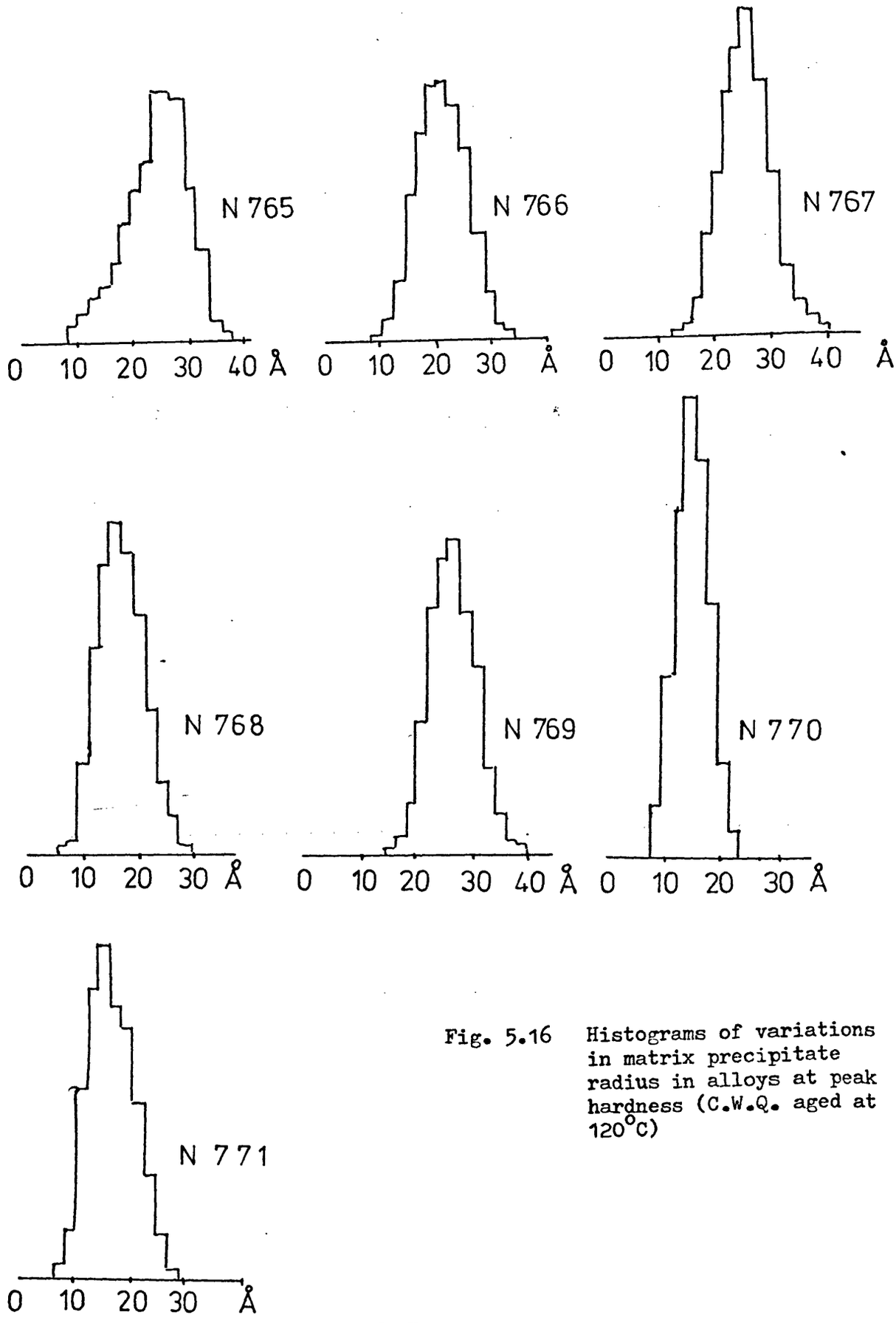

Fig. 5.16 Histograms of variations in matrix precipitate radius in alloys at peak hardness (C.W.Q. aged at 120°C)

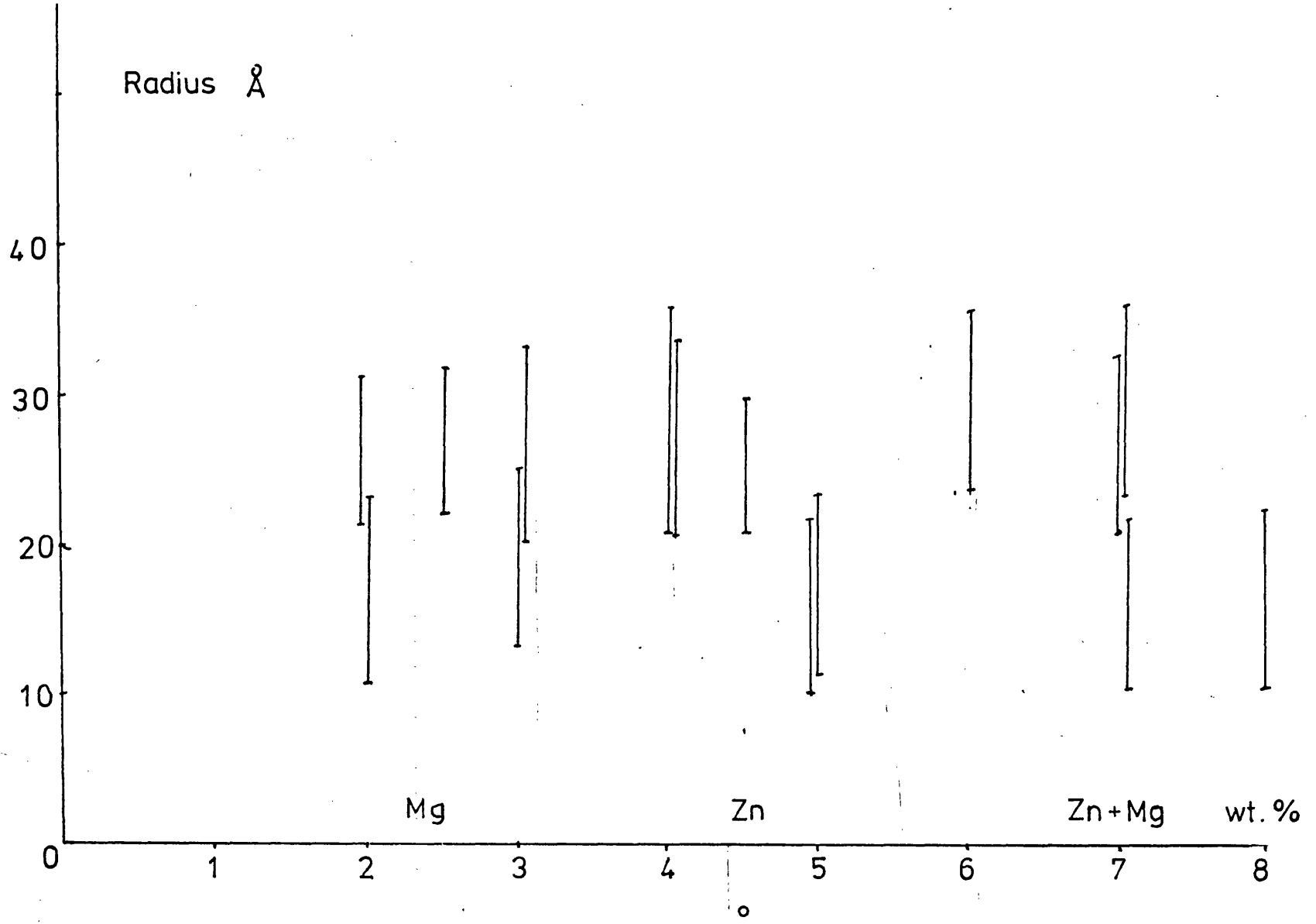

Fig. 5.17 Variation in matrix precipitate radius, Å, with alloy composition. CWQ alloys aged 120°C at peak hardness.

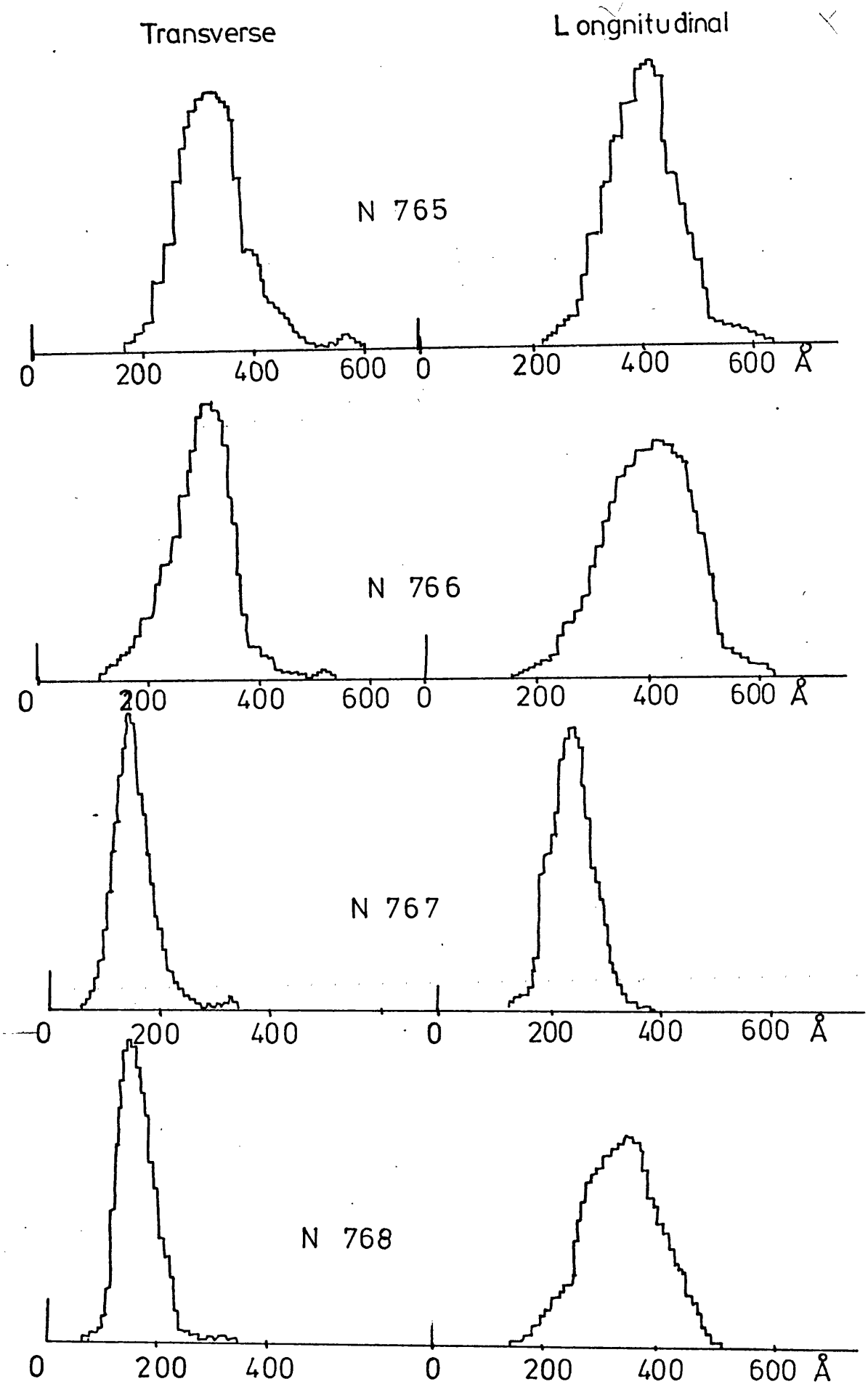

Fig. 5.18(a) Grain-boundary precipitate size distribution

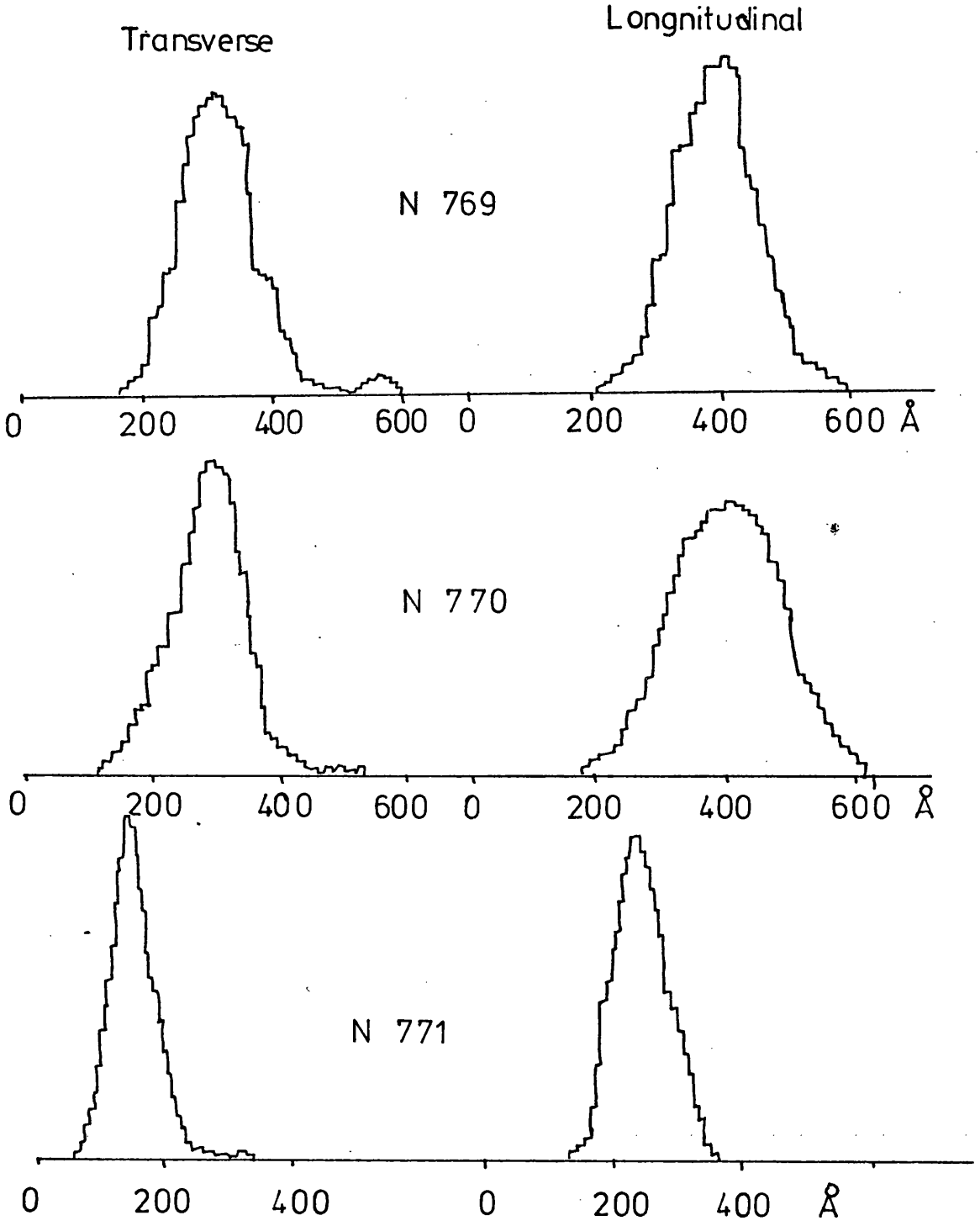

Fig. 5.18b. Grain-boundary precipitate size distribution in transverse and longitudinal directions for CWQ alloy aged at 120°C at peak hardness

a.

b.

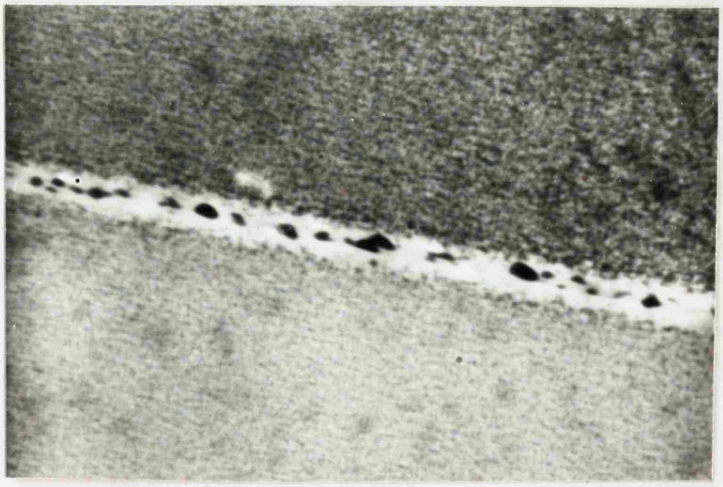

c.

Fig 5.19 The variation of the microstructure of alloy N765 with quench rate
(a) Air-cooled peak hardness x 30,000
(b) Air-cooled overaged x 30,000
(c) hot-water-quenched at peak hardness x 20,000

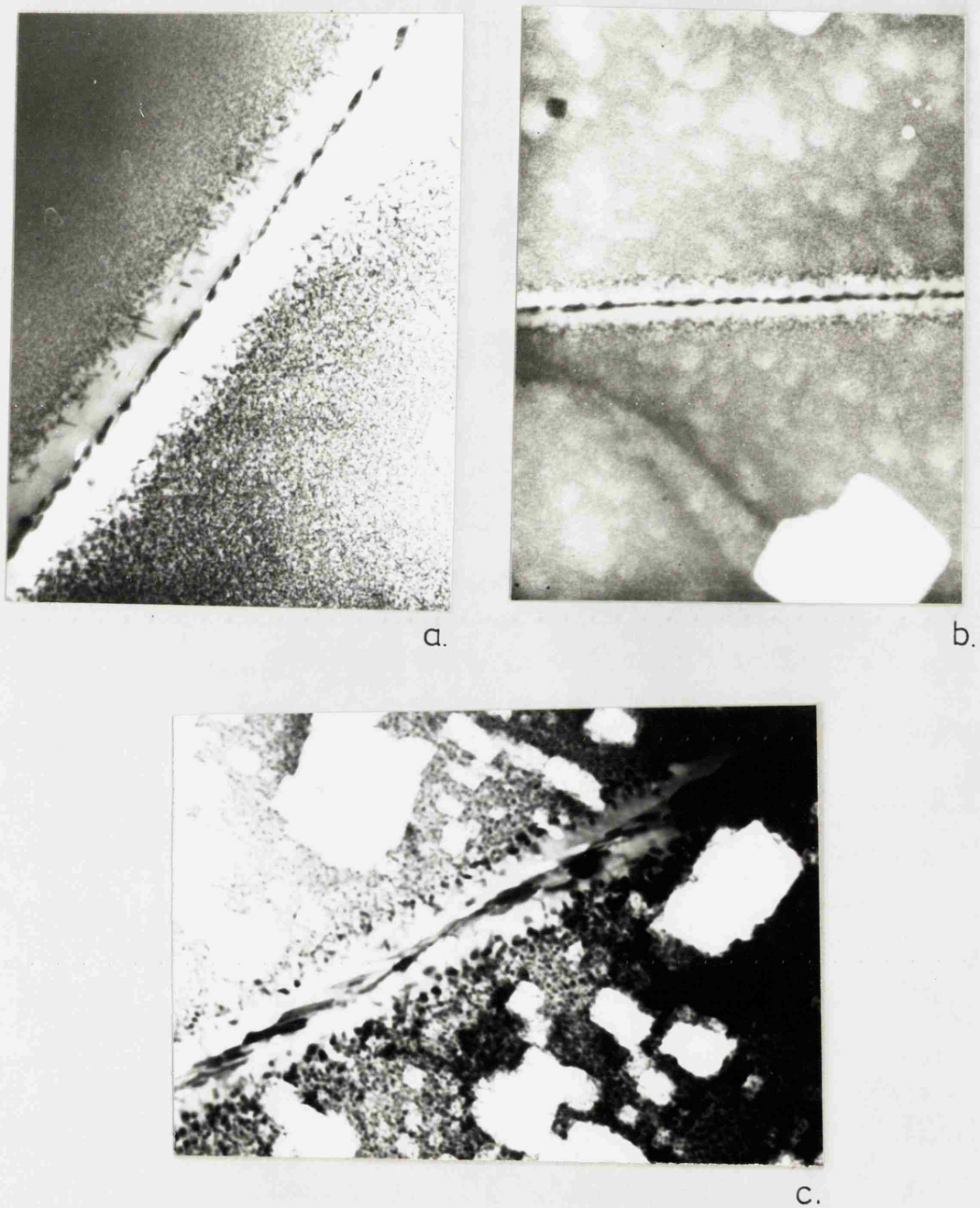

Fig 5.20. The microstructure of alloys aged at 150°C to peak hardness
(a) N765 x 20,000
(b) N766 x 20,000
(c) N771 x 30,000

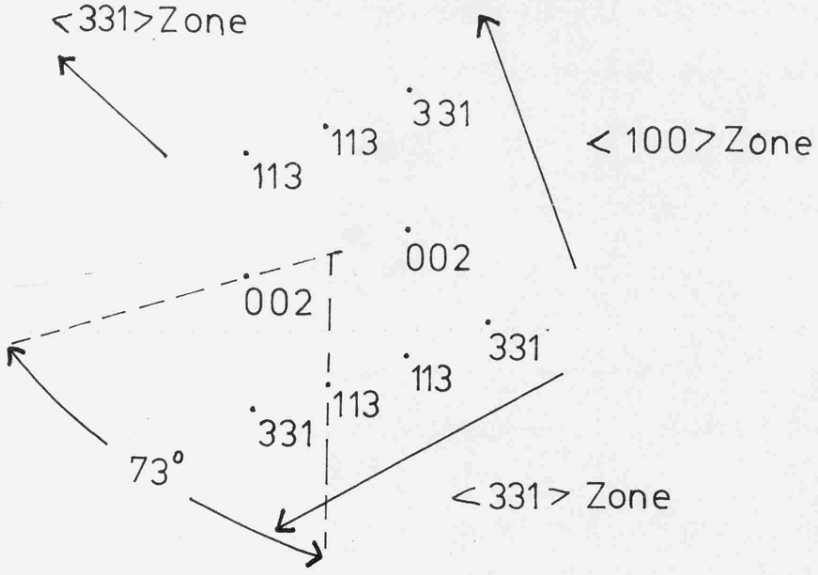

Zone axis = 013

Fig 5.21. Kikuchi line patterns

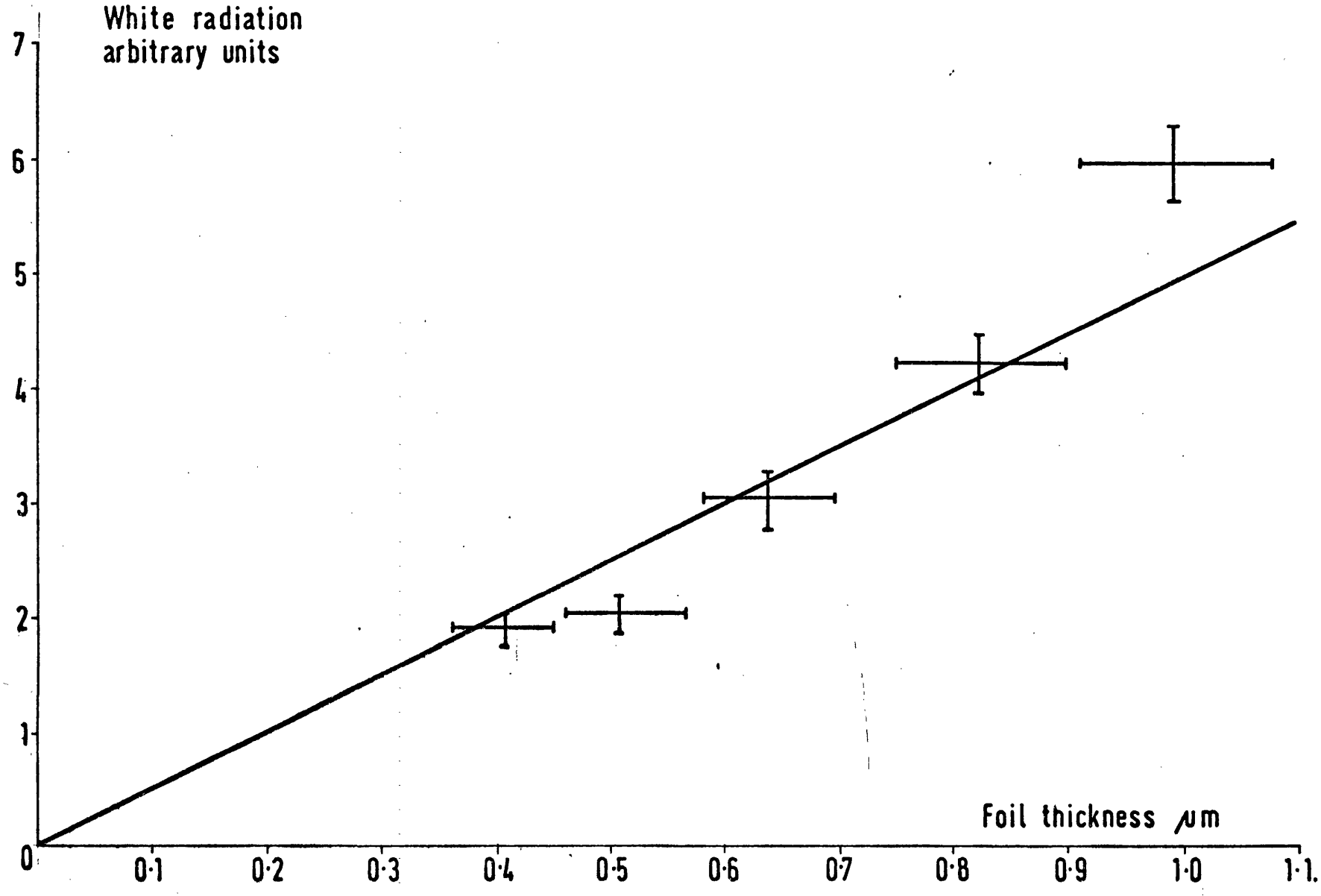

Fig 5.22. Calibration curve for quantitative precipitate-density measurements; white radiation, x-ray level vs. foil thickness.

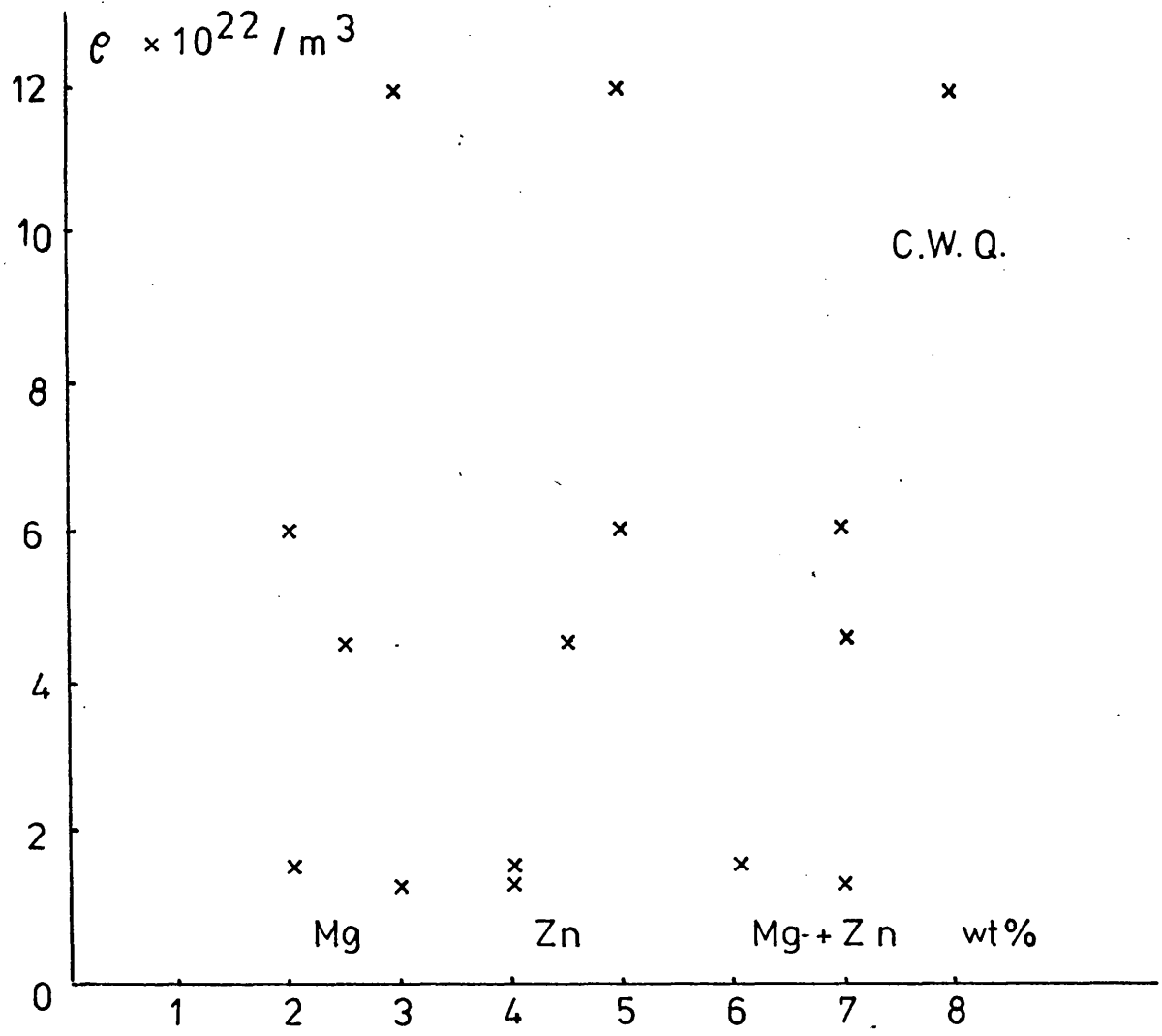

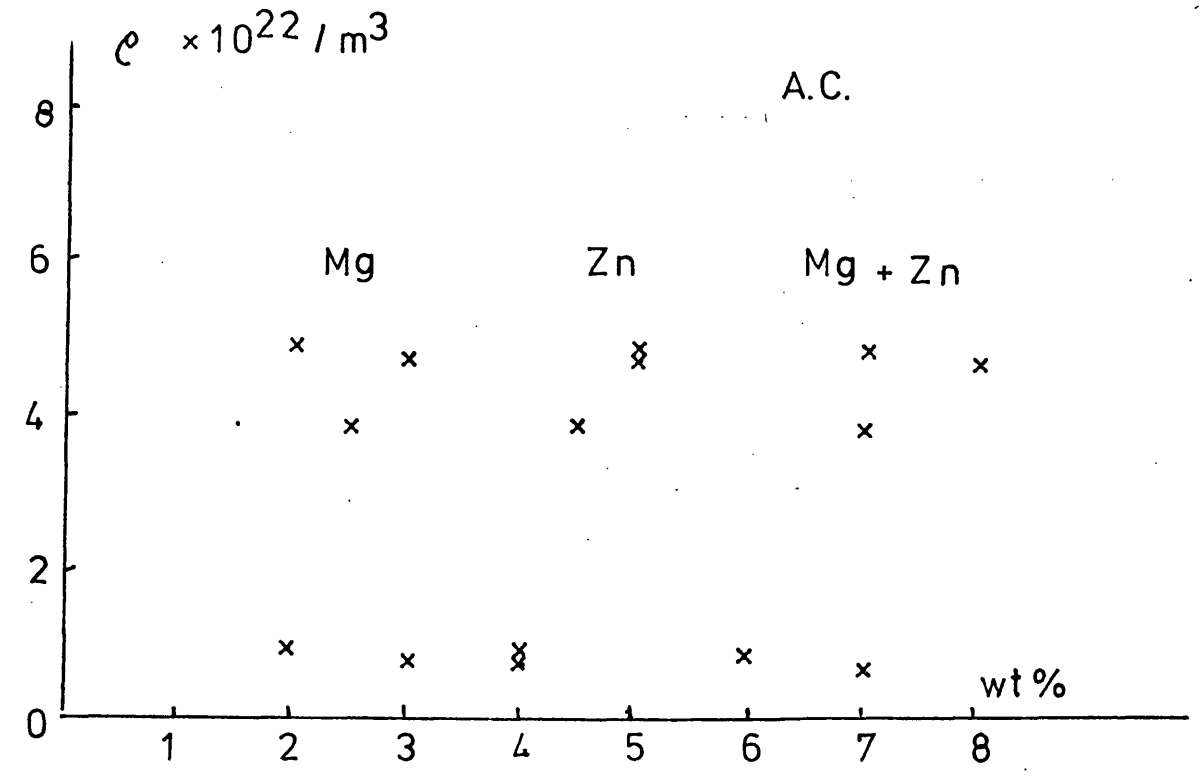

Fig. 5.23 Variation of precipitate density with composition at peak hardness for CWQ and AC alloys.

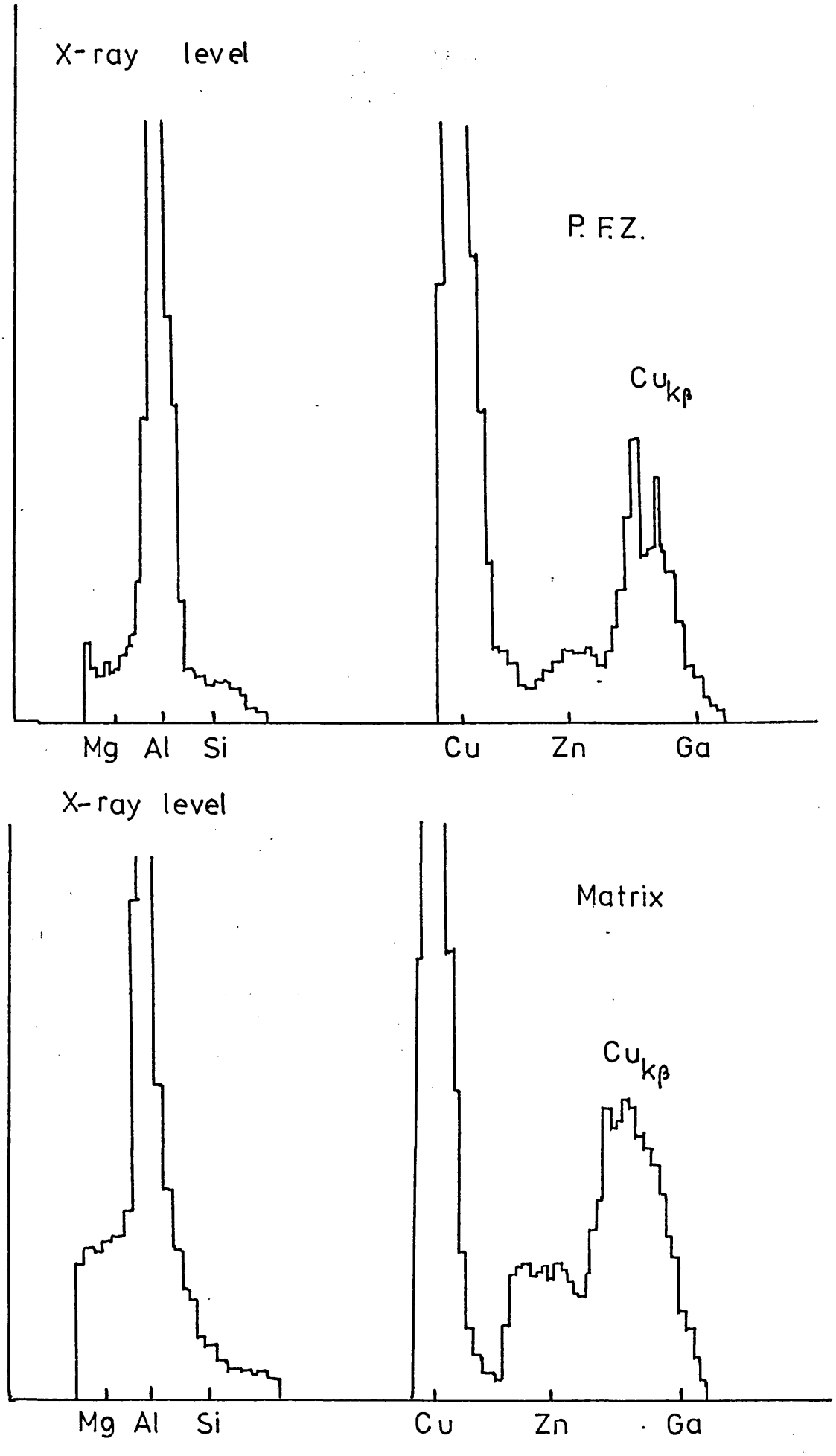

Fig. 5.24 X-ray spectra from the PFZ and the matrix taken from alloy N765 CWQ in the peak-hardness condition.

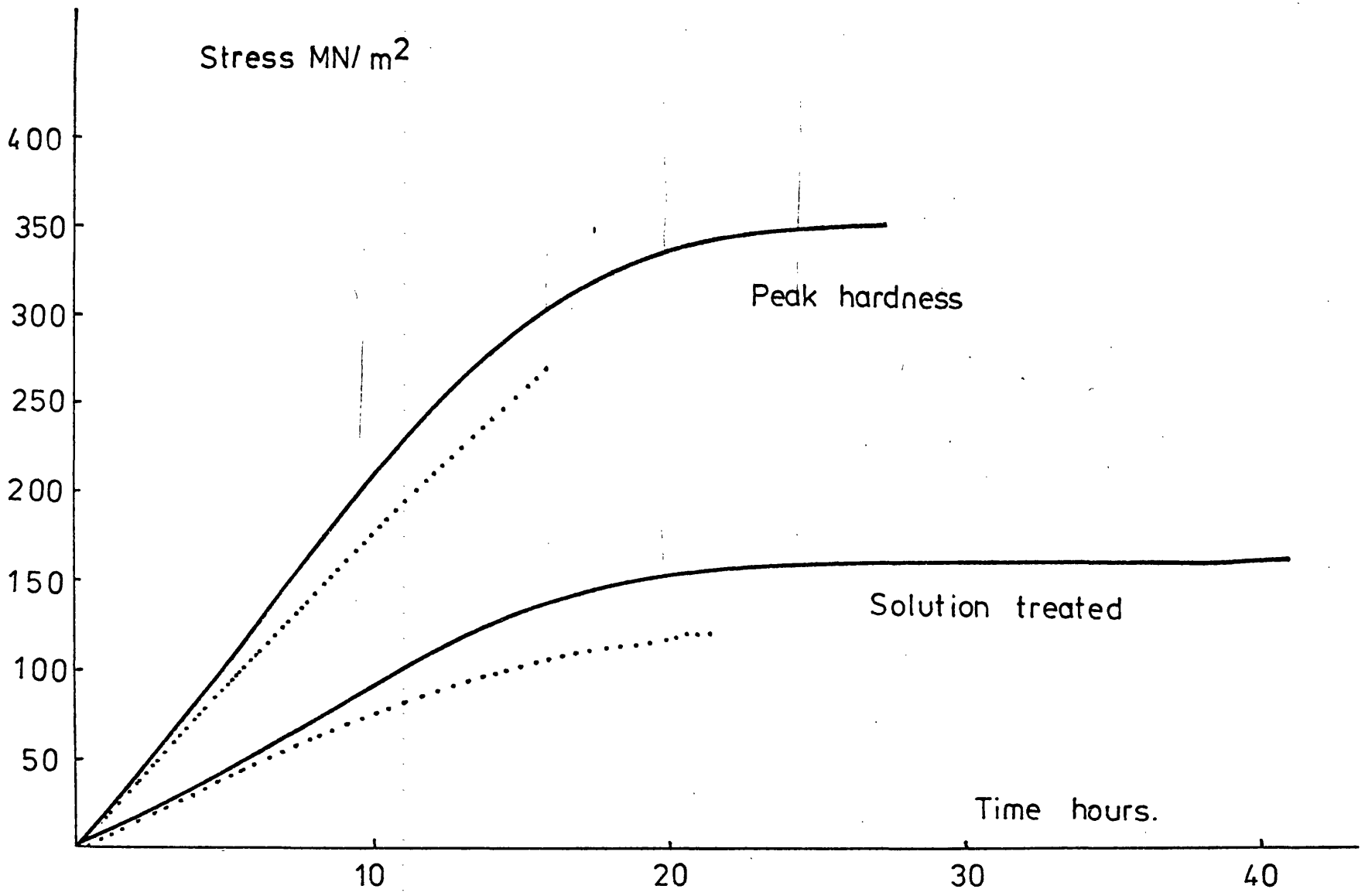

Fig. 5.25 Tensile test data for alloy A14.5Zn 2.5Mg in air (full curve) and in salt-water (dotted curve). Curves for peak-hardness and solution-treated conditions are shown.

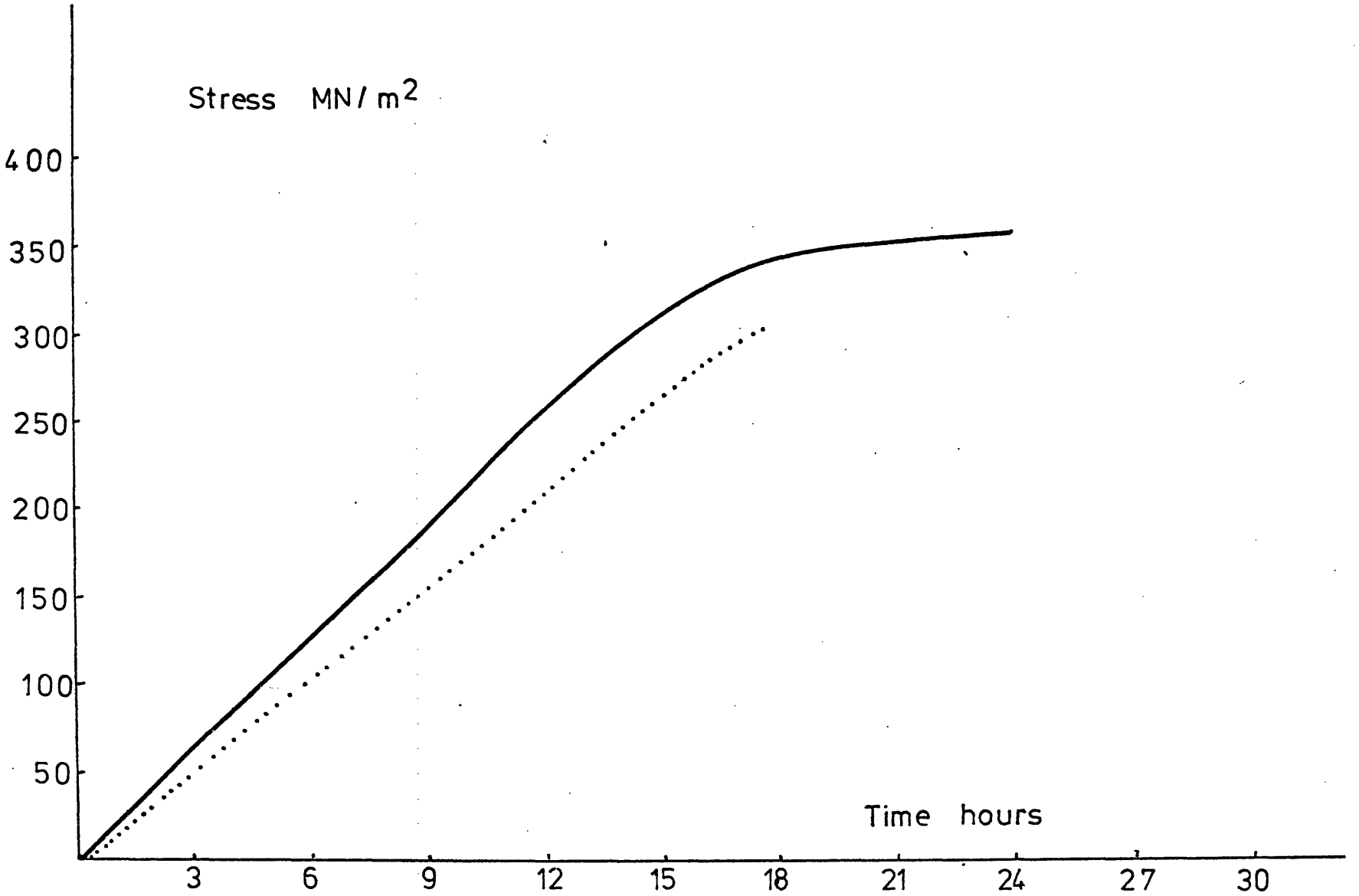

Fig. 5.26 Tensile test data for overaged alloy Al5.0Zn 3.0Mg in air (full curve) and salt-water (dotted curve).

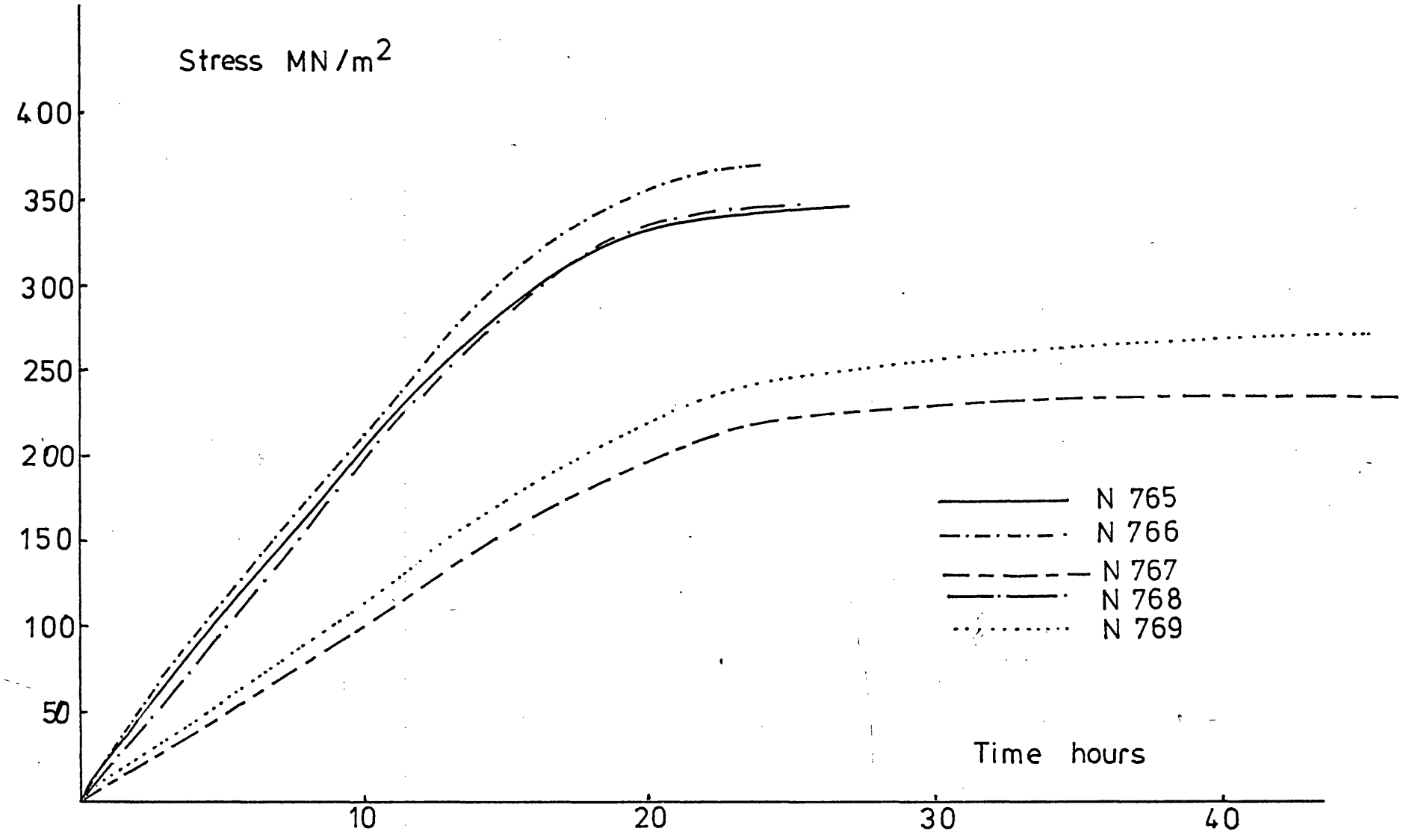

Fig. 5.27a. Tensile test data for CWQ alloys at peak-hardness in air.

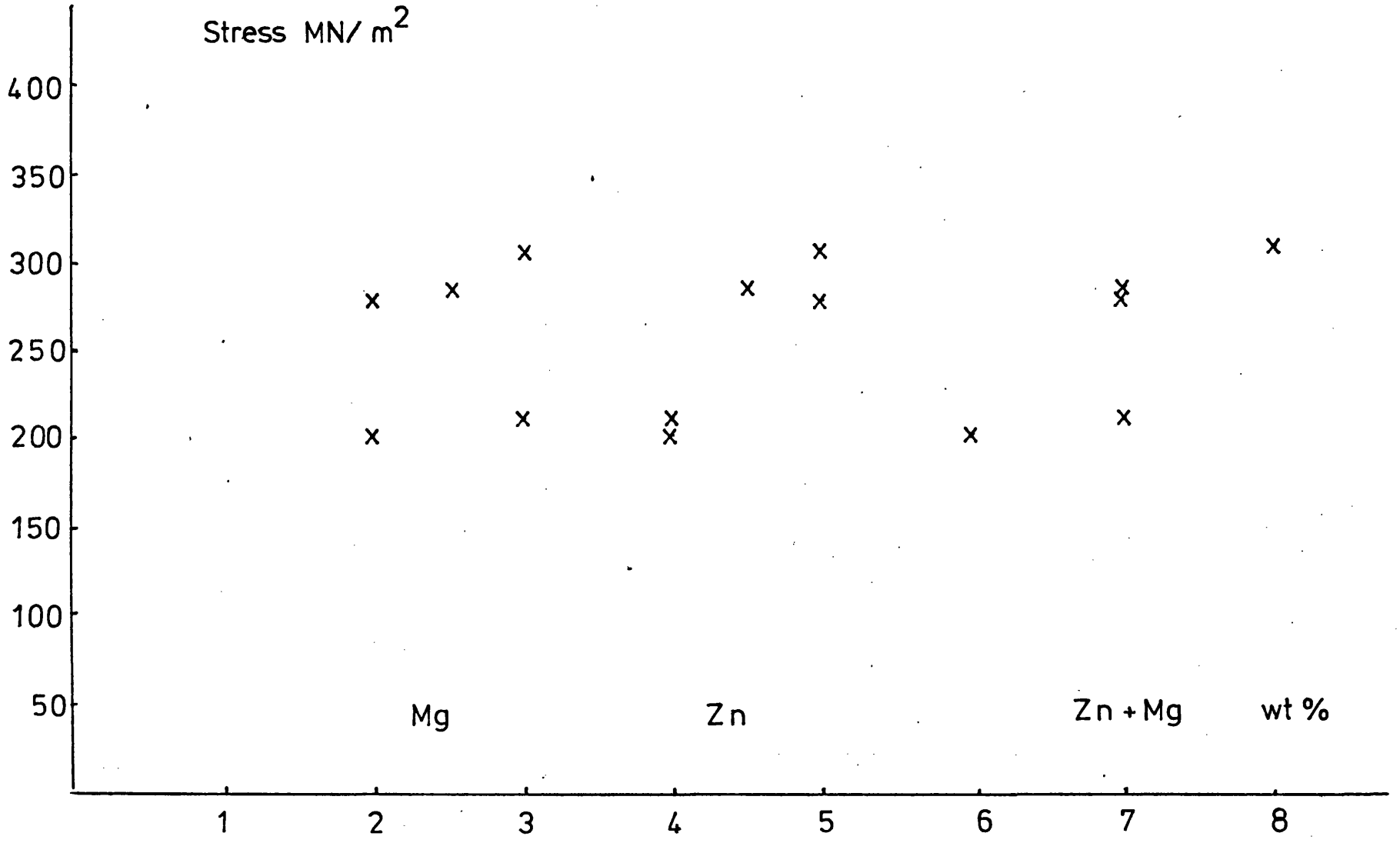

Fig. 5.27b. Variation of yield stress with composition for CWQ alloys at peak-hardness

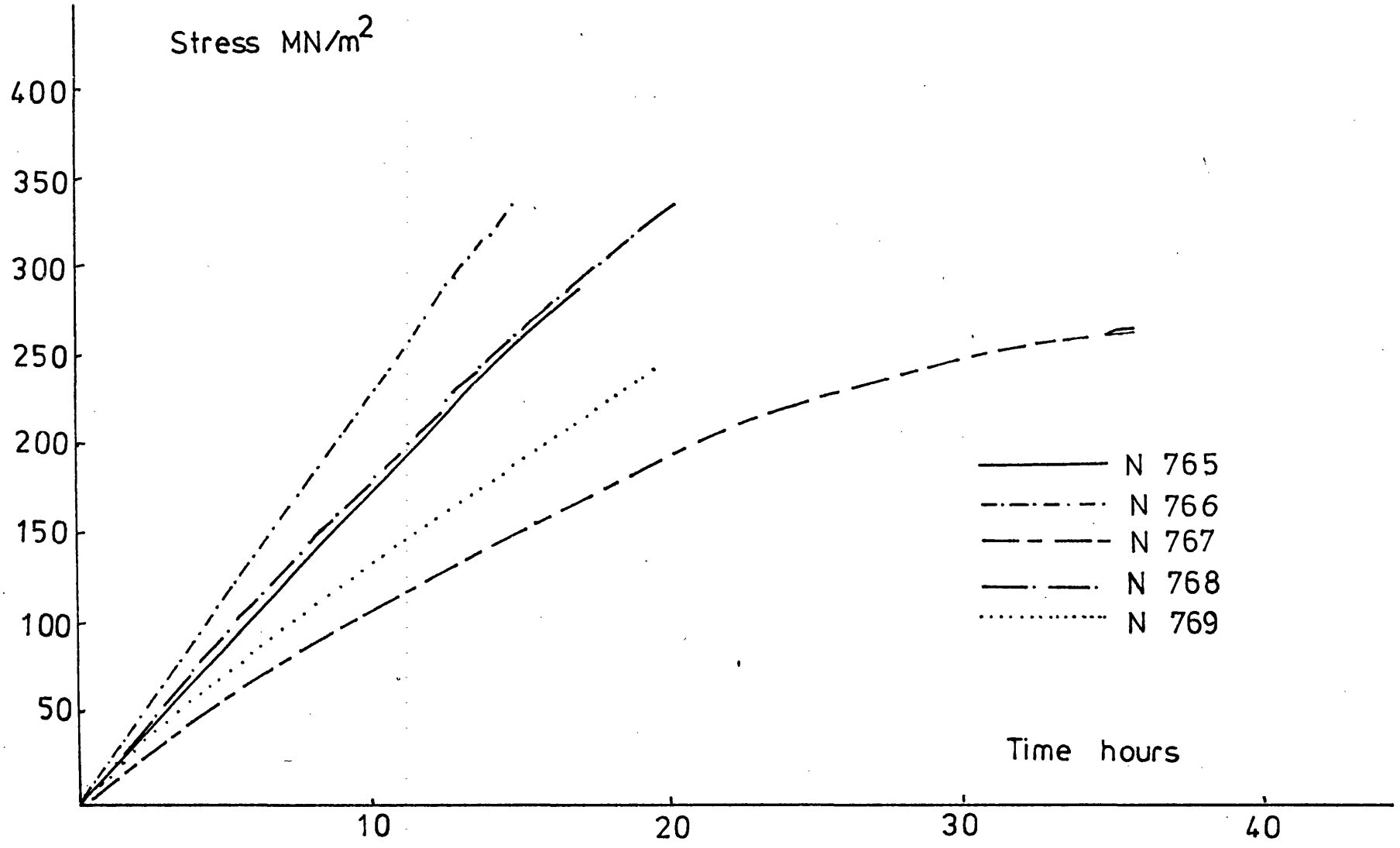

Fig 5.28a Tensile data in salt-water for CWQ alloys at peak hardness

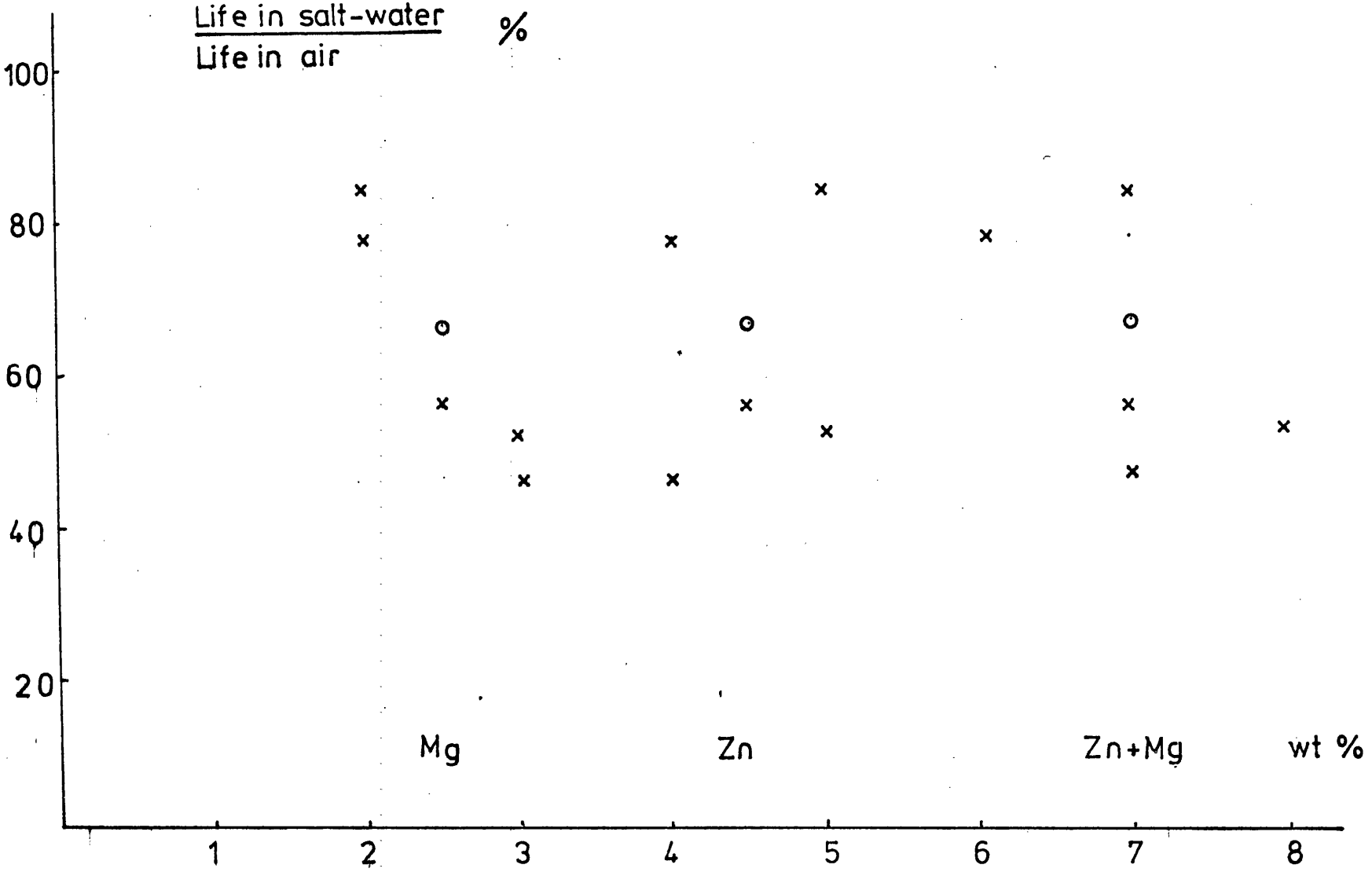

Fig. 5.28b Variation of resistance to stress-corrosion with composition for CWQ alloy at peak hardness (0 indicates a copper-bearing alloy)

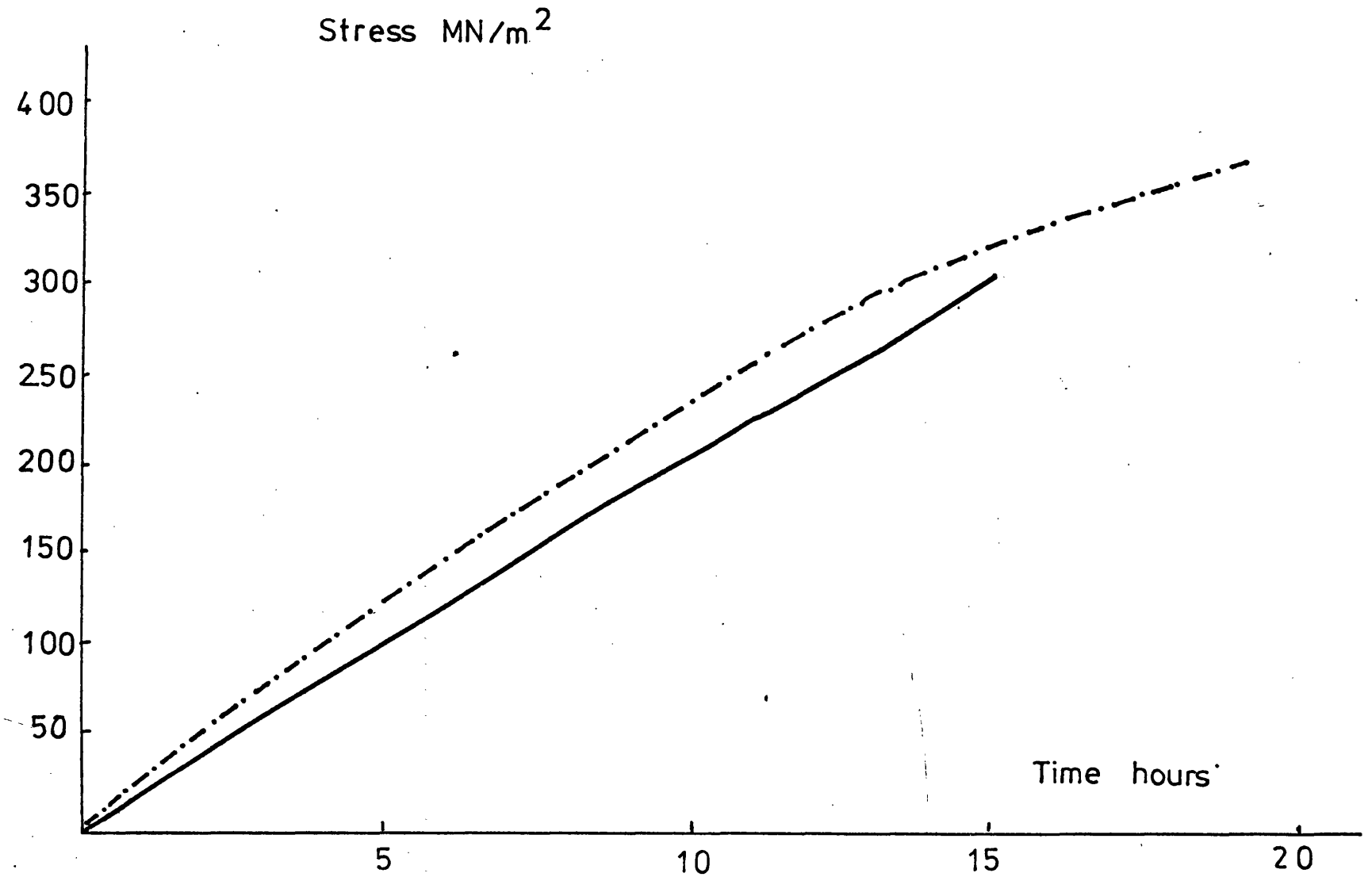

Fig. 5.29 The influence of copper on the tensile behaviour in salt-water; alloys A14.5Zn 2.5Mg (solid line) and A14.5Zn 2.5Mg 0.15 Cu (dotted curve) in peak-hardness condition..

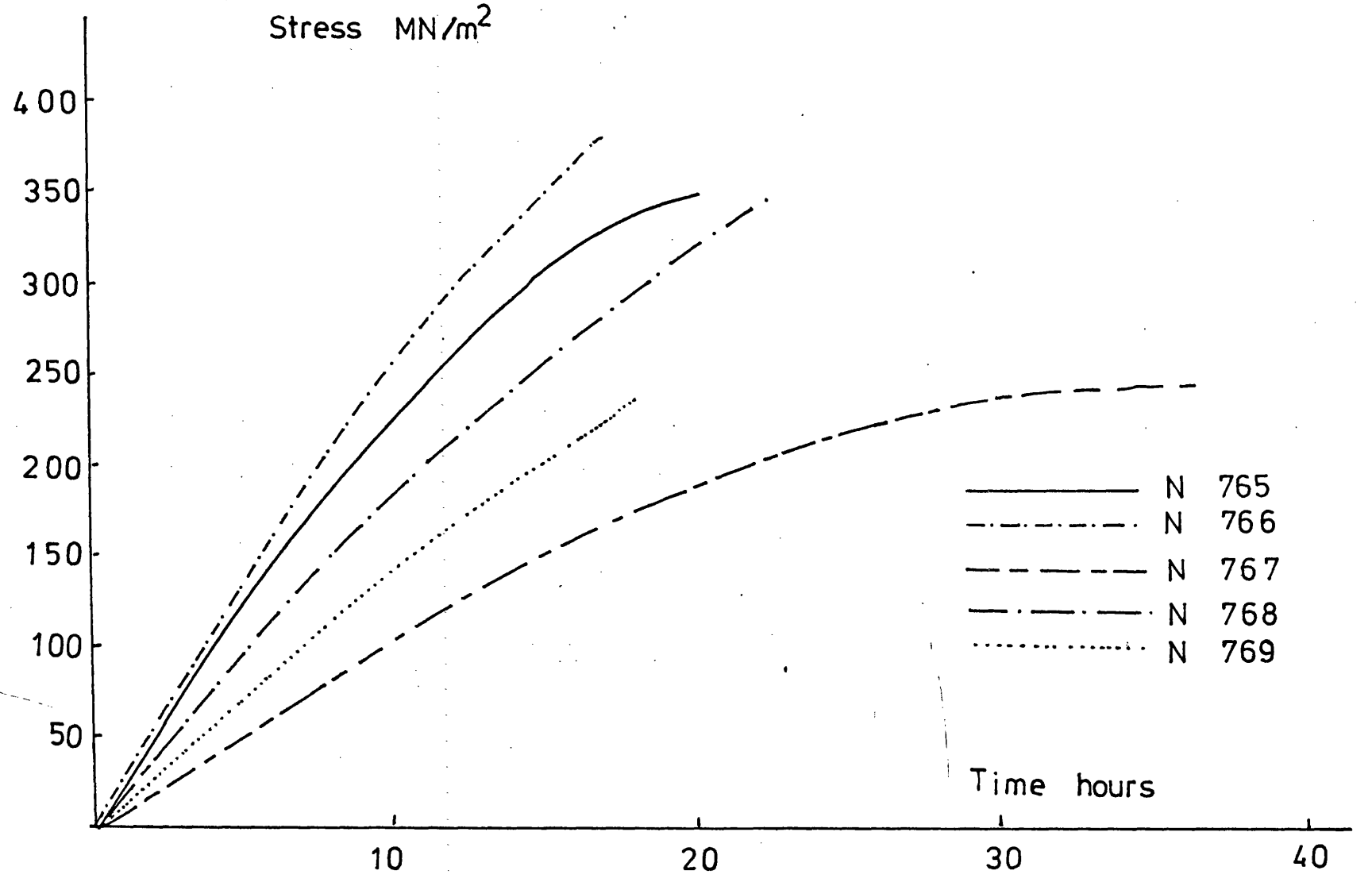

Fig 5.30 Tensile tests in salt-water for air-cooled alloys at peak hardness

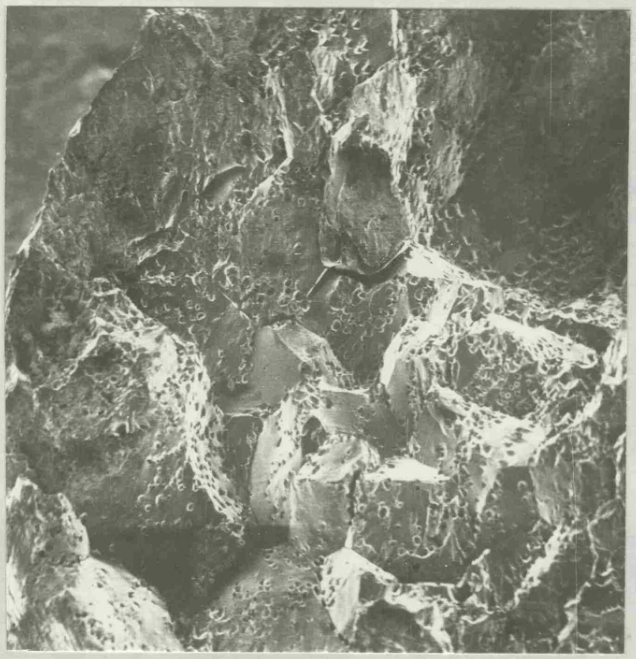

a

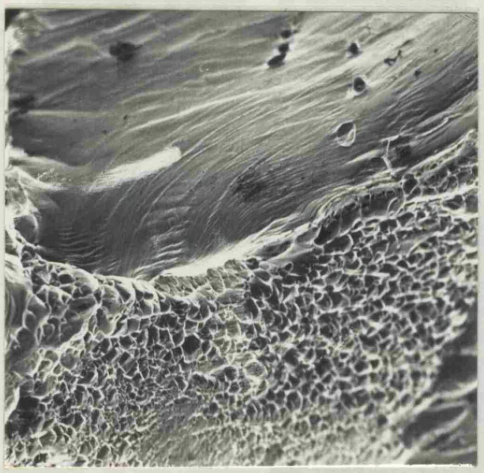

b.

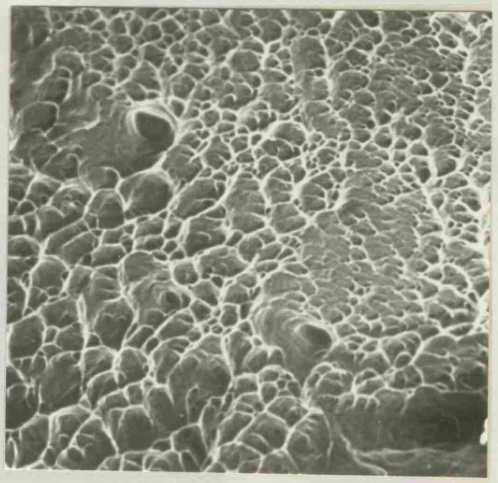

c.

Fig 5.31 Typical scanning electron micrographs of the tensile fracture surfaces of air-tested material alloy N765 CWQ
(a) x 50
(b) x 150
(c) x 400

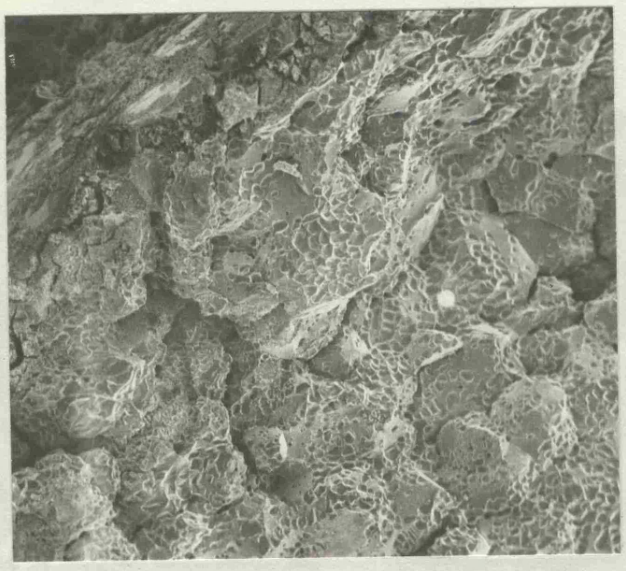

a.

b.

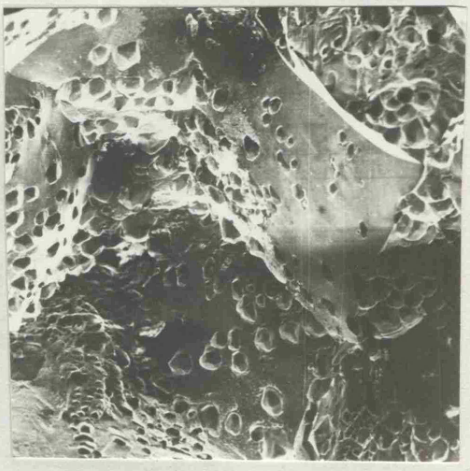

c.

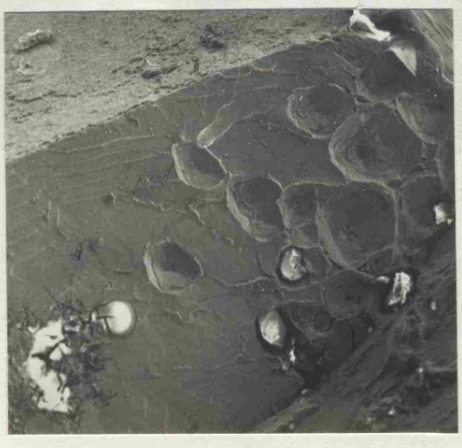

d.

Fig 5.32. Typical features found on stress-corroded fracture surfaces
(a) General features x 50
(b) Corrosion on the outer surface x 150
(c) Crack penetrating from surface x 70
(d) More cracks x 120

a.

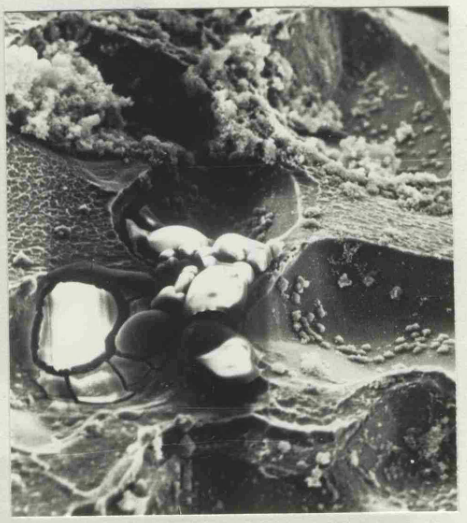

b.

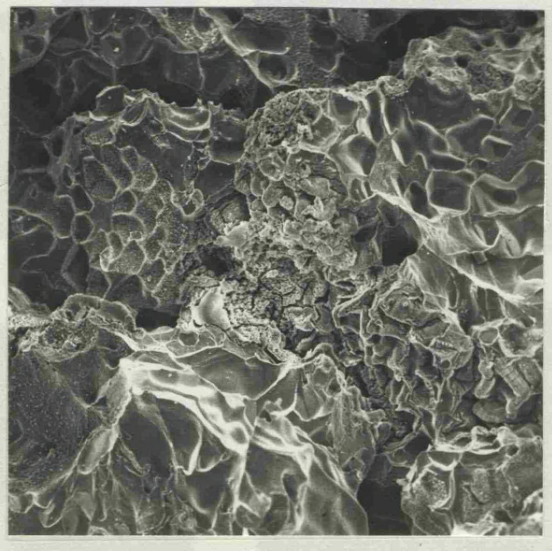

c.

Fig 5.33 Corrosion product
(a) 'Mud-crack' corrosion product x 150
(b) Corrosion product found near head of advancing stress-corrosion crack, x 750
(c) typical distribution of corrosion product x 220

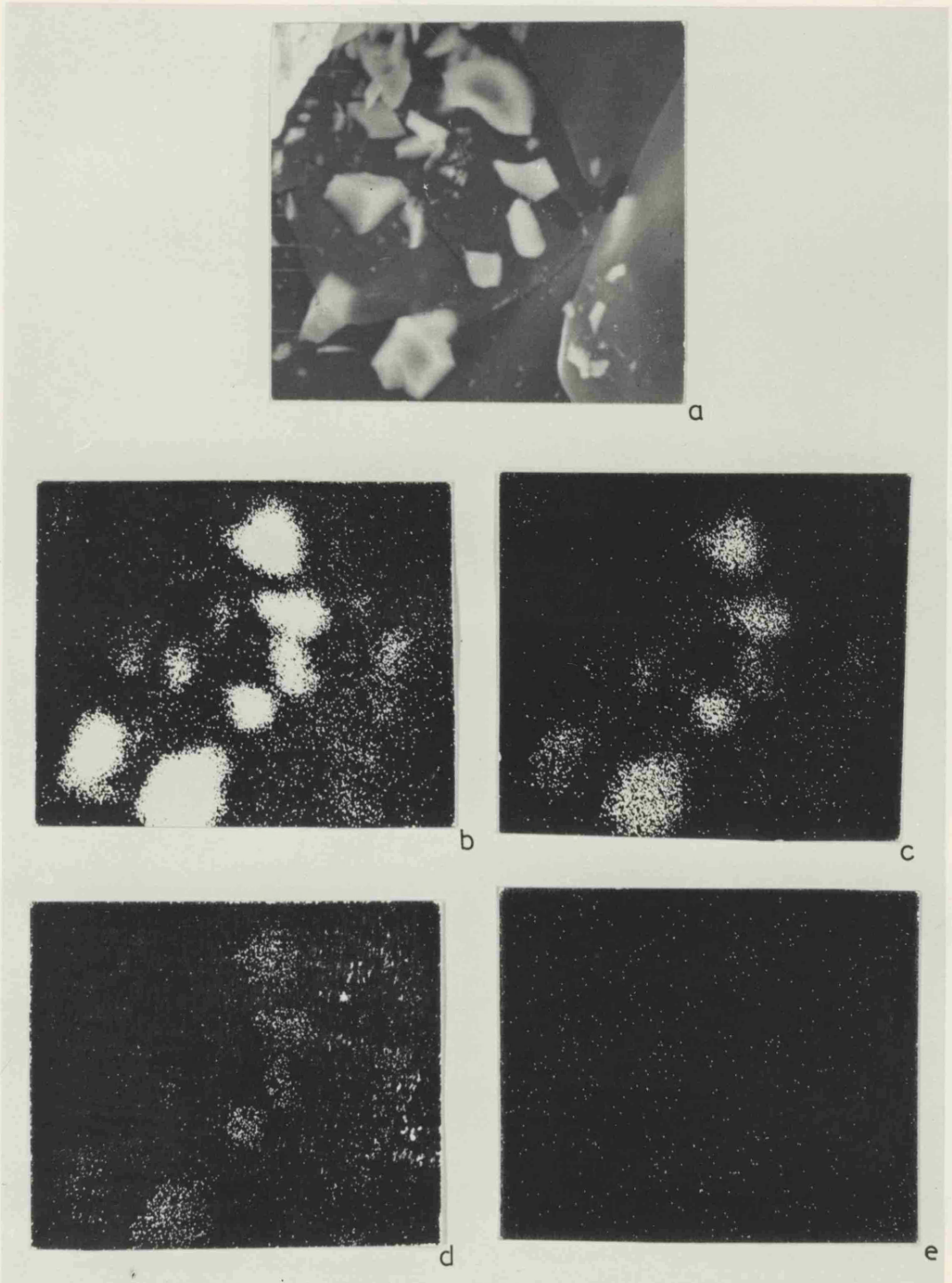

Fig 5.34. Electron probe microanalysis results on "mud-crack" corrosion product;
(a) electron picture
(b) Al
(c) Mg
(d) O and
(e) Zn distributions, X1000.

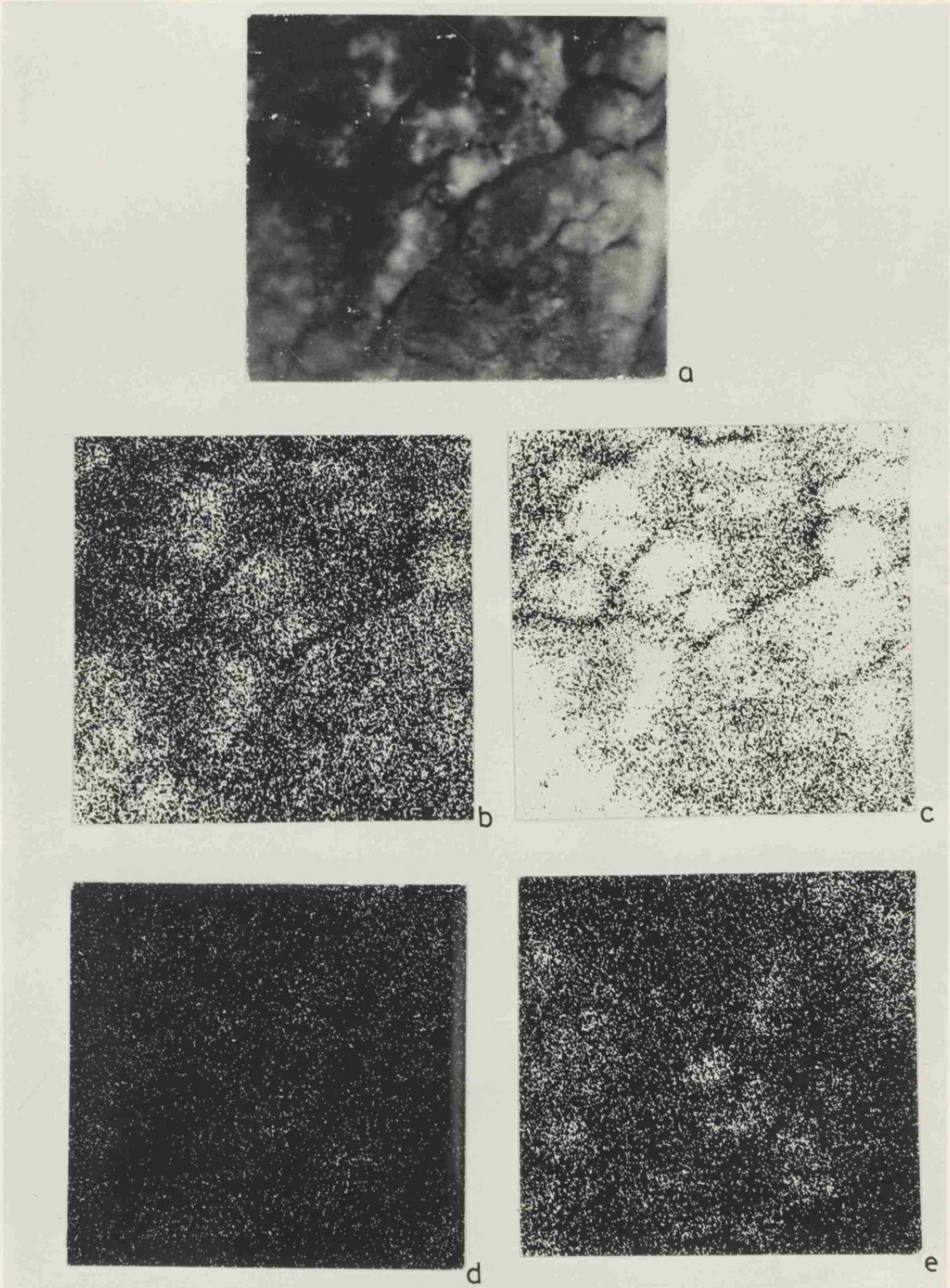

Fig 5.35. Electron probe microanalysis results on corrosion product found hear the crack tip;
(a) electron picture,
(b) Al,
(c) Mg,
(d) O and
(e) Zn distributions, X1400.

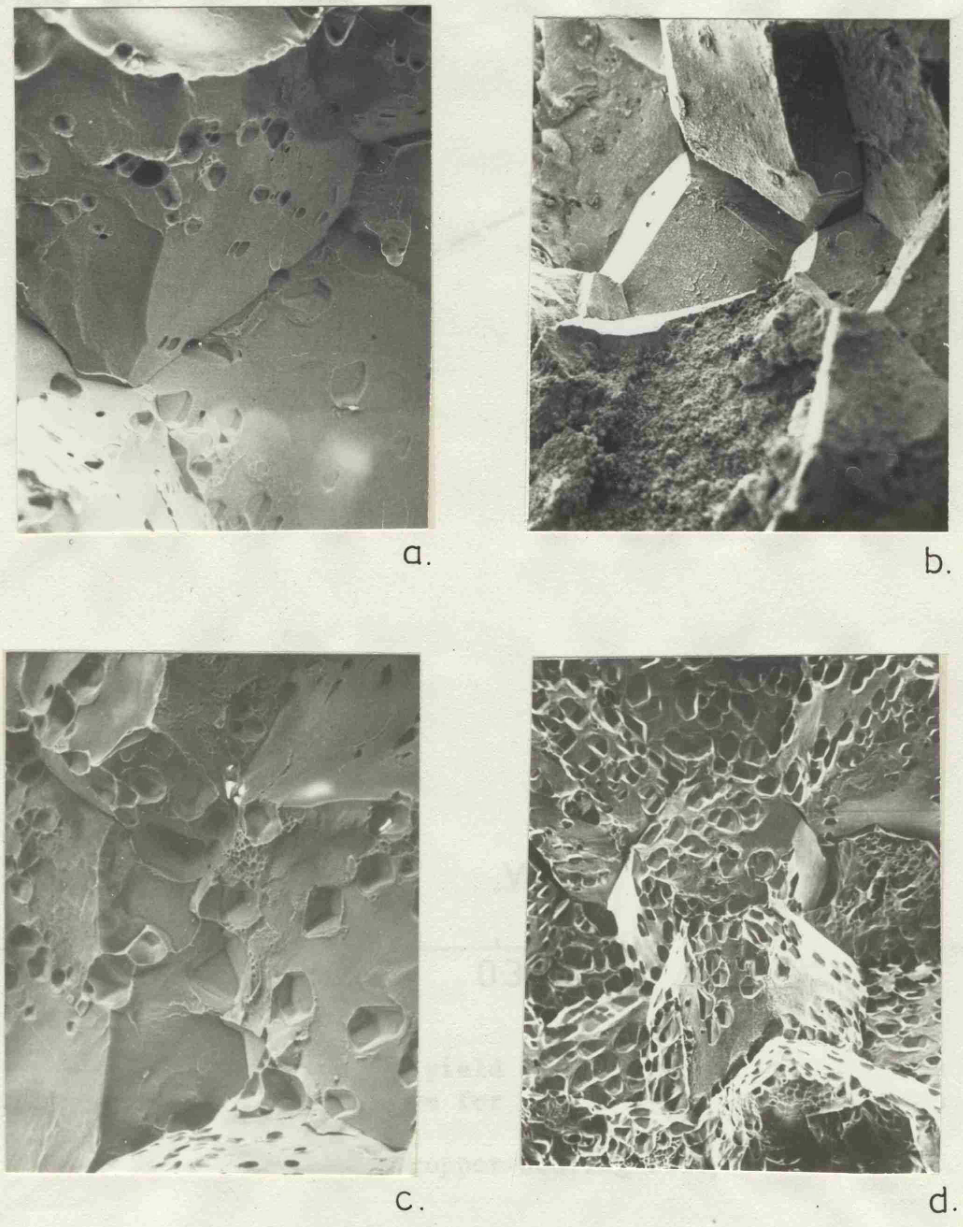

Fig 5.36 The influence of heat treatment on the tensile fracture surfaces; alloy N765
(a) solution-treated x 150
(b) solution-treated x 50
(c) Overaged x 770
(d) air-cooled peak hardness x 70

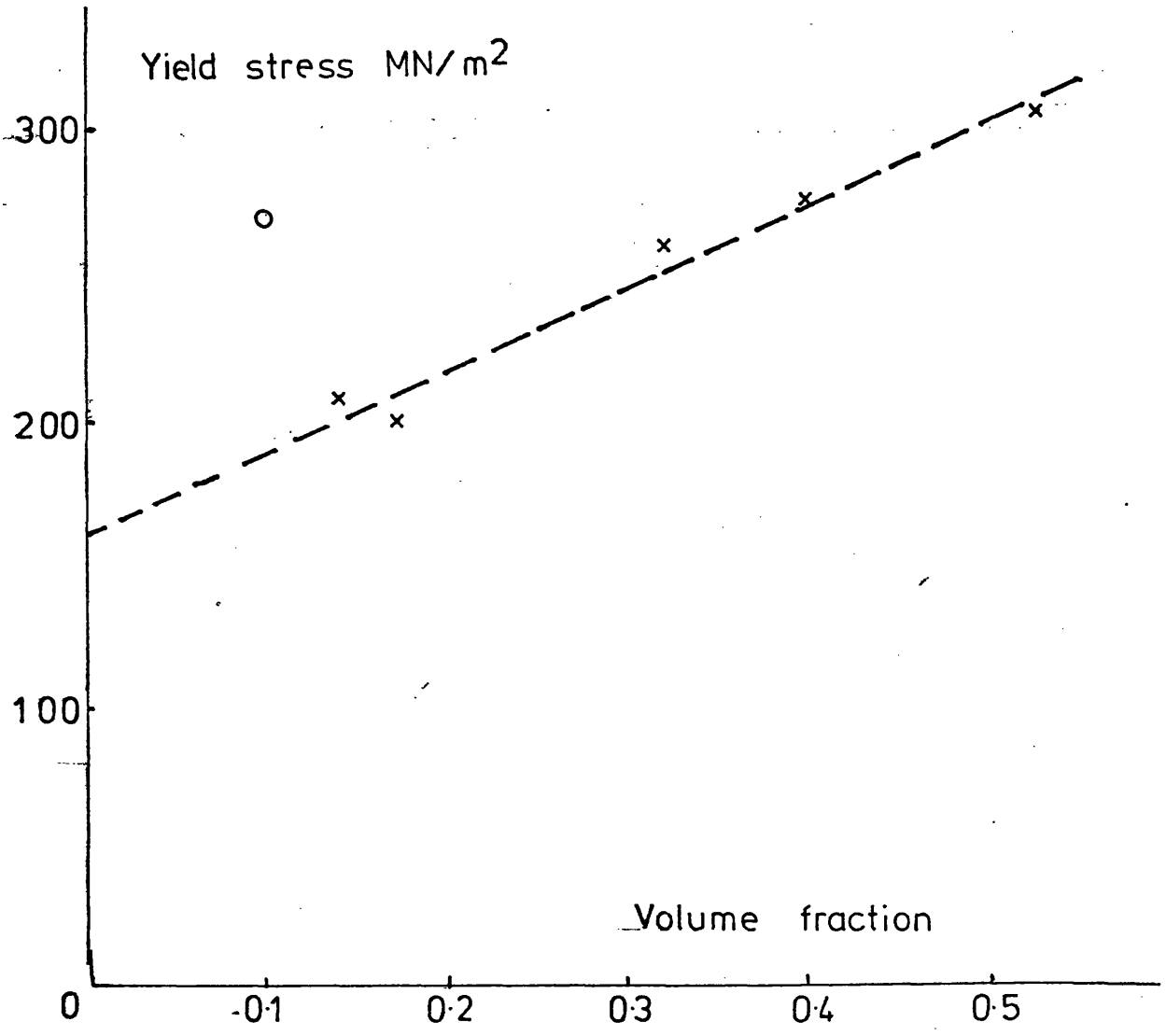

Fig 6.1 Variation of yield stress with volume fraction of precipitate for CWQ alloys at peak hardness aged 120°C.
O indicates copper-bearing alloy.

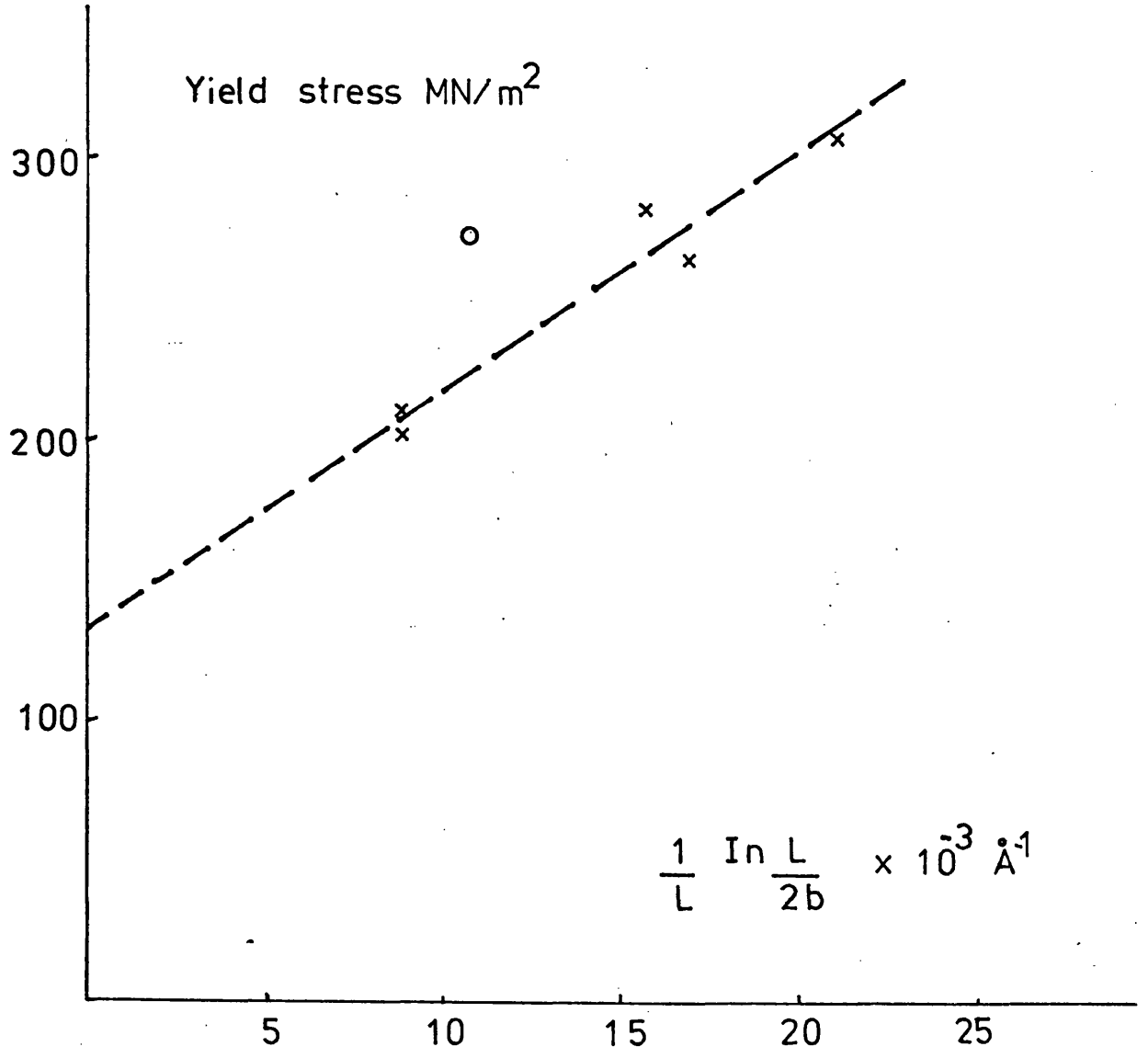

Fig. 6.2 Variation of yield stress with the Orowan function, $\frac{1}{L}$ In $\frac{L}{2b}$, for CWQ alloys aged at 120°C to peak hardness.
O indicates copper-bearing alloy.

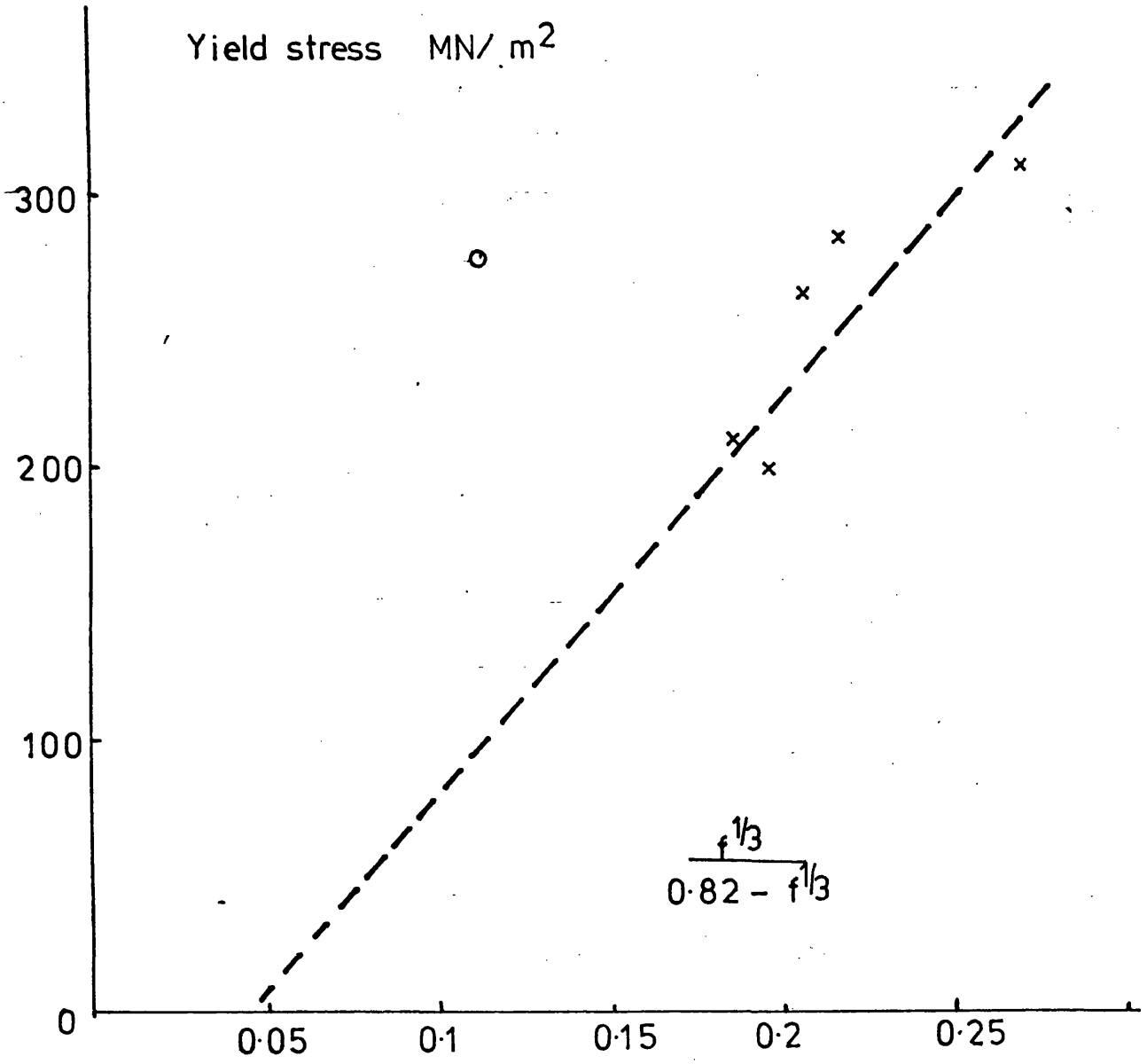

Fig 6.3 Variation of yield stress with Ansell and Lenel's function for CWQ alloys aged to peak hardness at 120°C.
0 indicates a copper-bearing alloy.

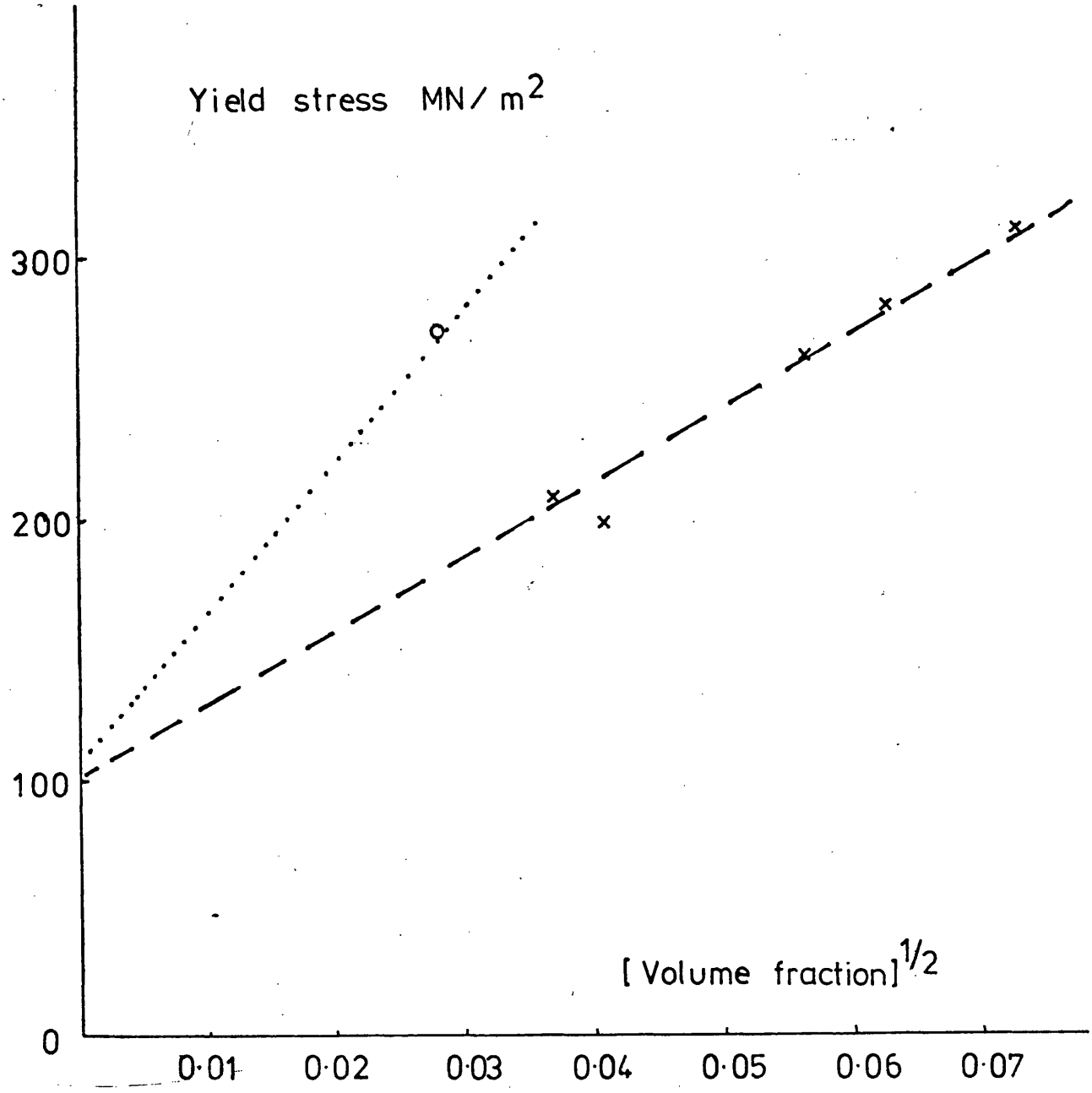

Fig. 6.4 Variation of yield stress with the square root of volume fraction of matrix precipitate for CWQ alloys aged at 120°C to peak hardness.
O indicates copper-bearing alloy.

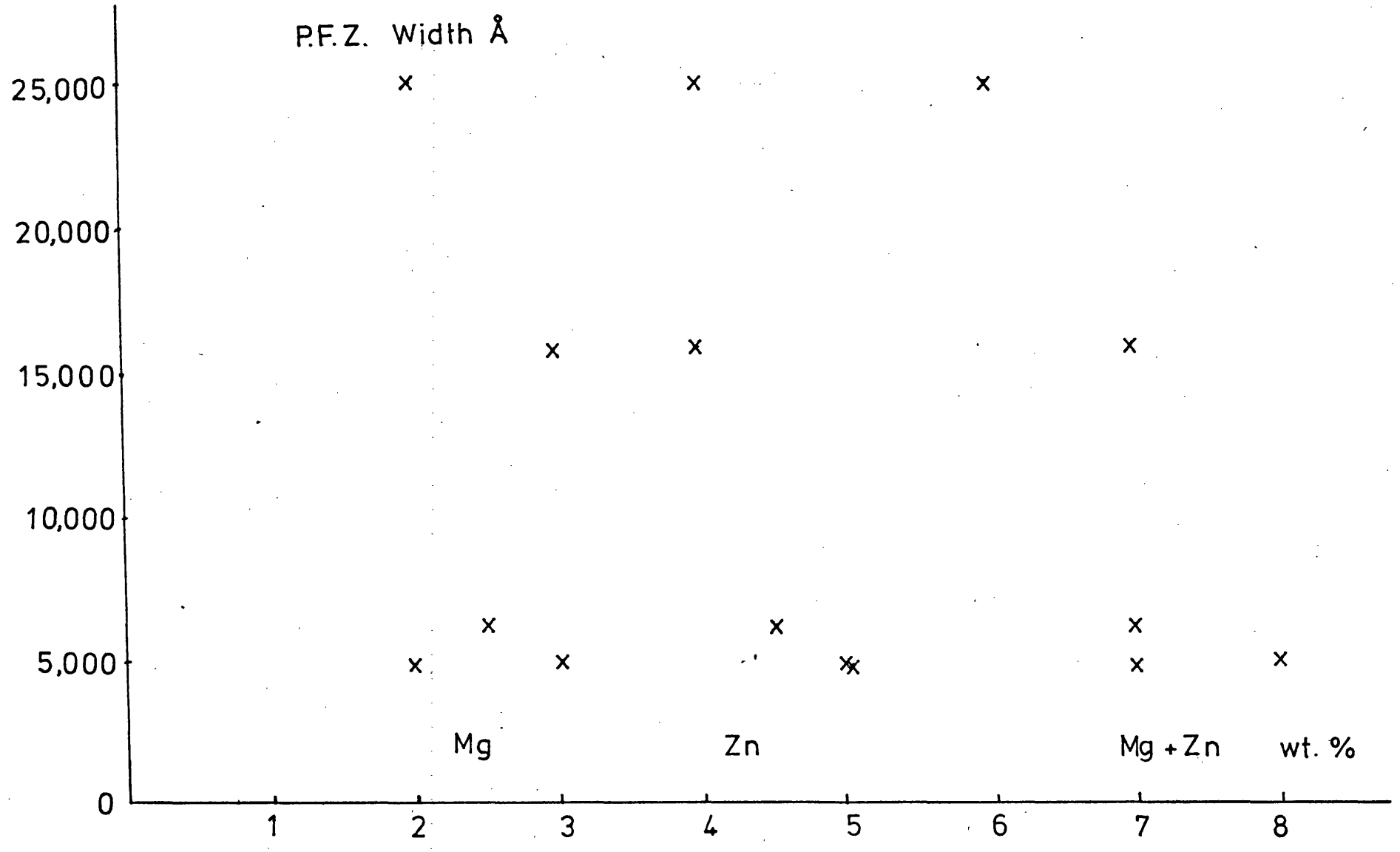

Fig. 6.5 Variation of PFZ Width with alloy composition for CWQ alloys aged at 150°C to peak hardness, illustrating dependence on zinc content.

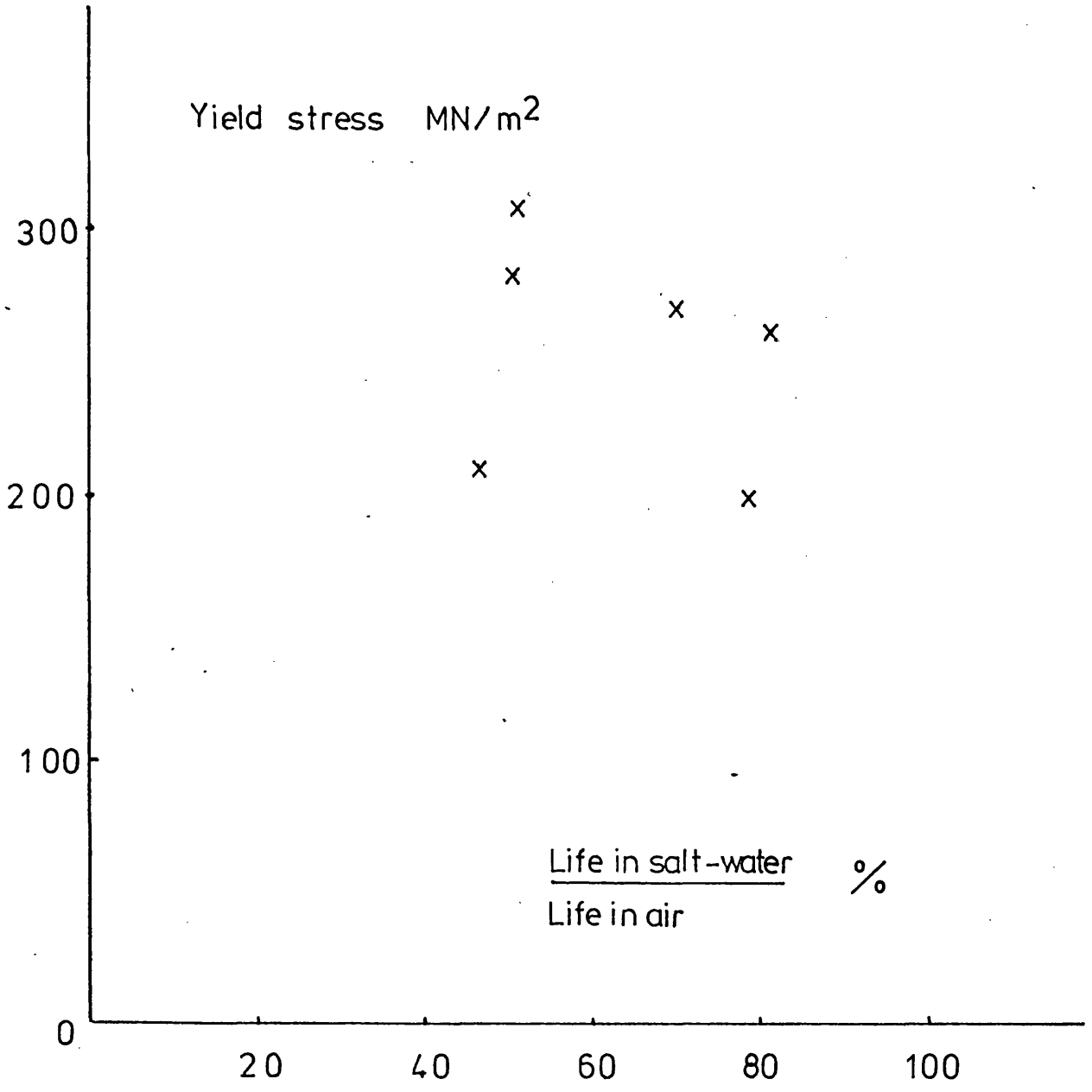

Fig 6.6 Variation of yield stress with stress-corrosion susceptibility.

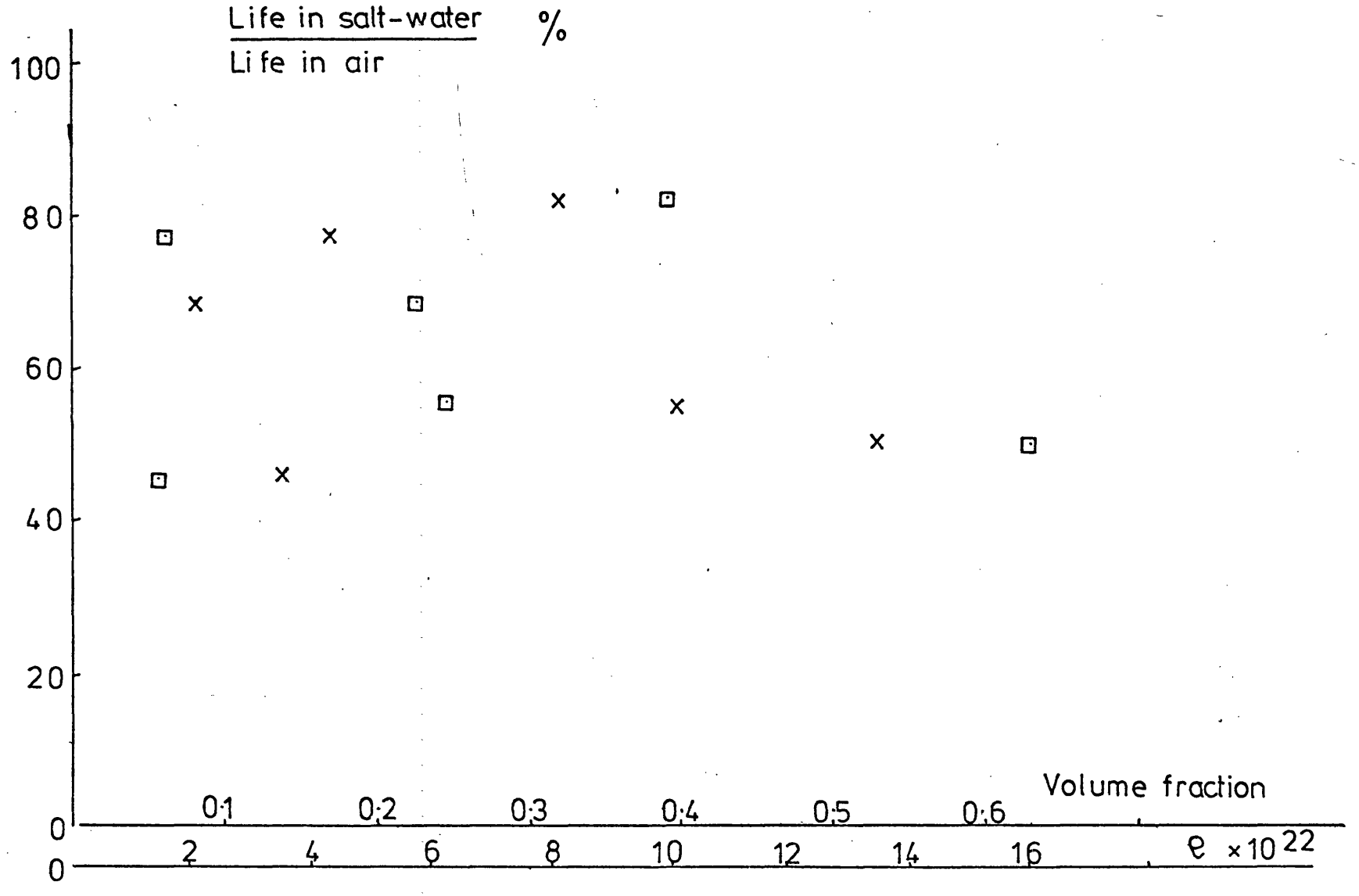

Fig. 6.7 Variation in susceptibility to stress-corrosion environment with matrix precipitate density, ϑ, (O) and volume fraction of precipitate (X).

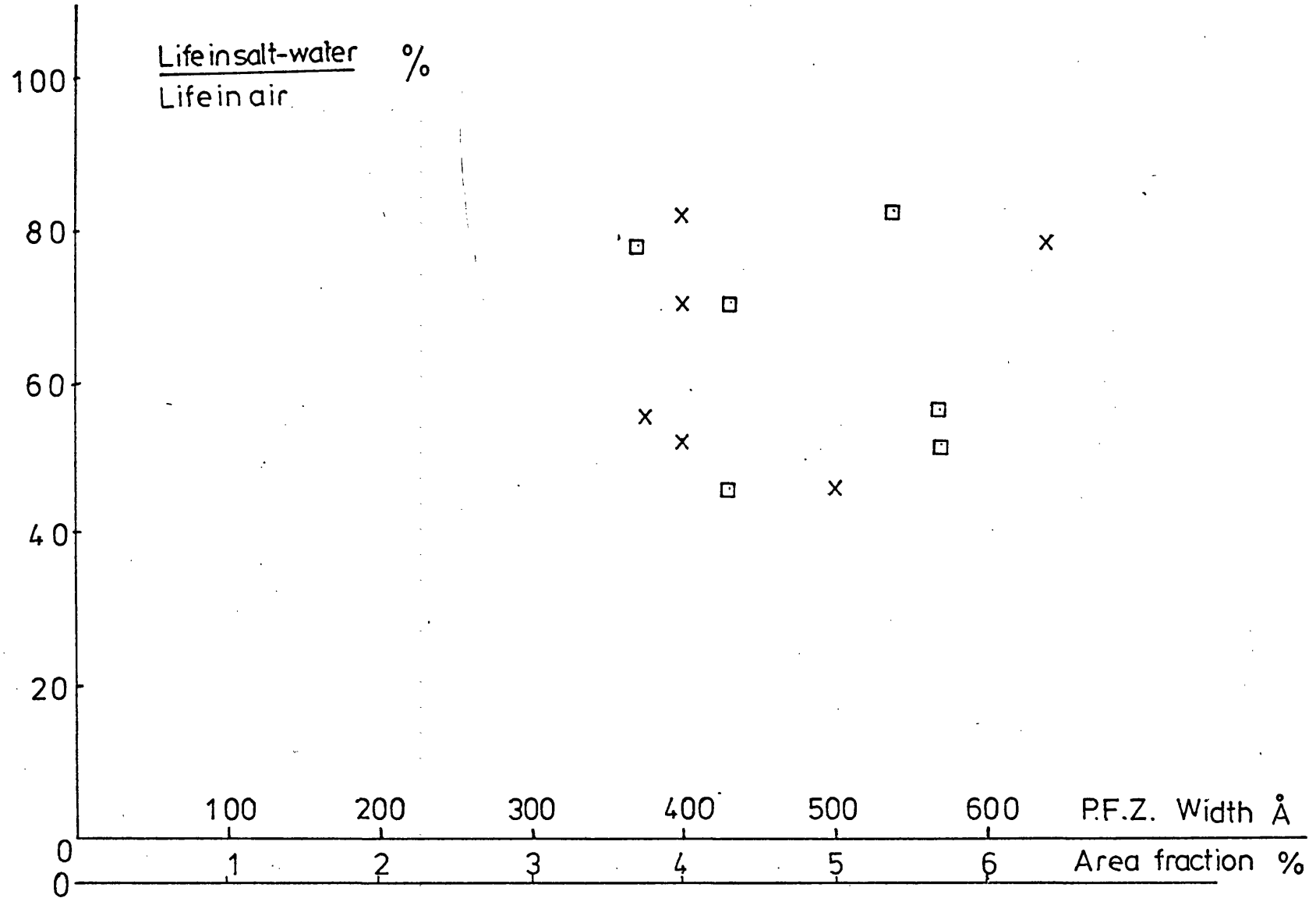

Fig. 6.8 Variation in susceptibility to salt-water environment with PFZ width (X) and area-fraction of grain-boundary precipitates(□).

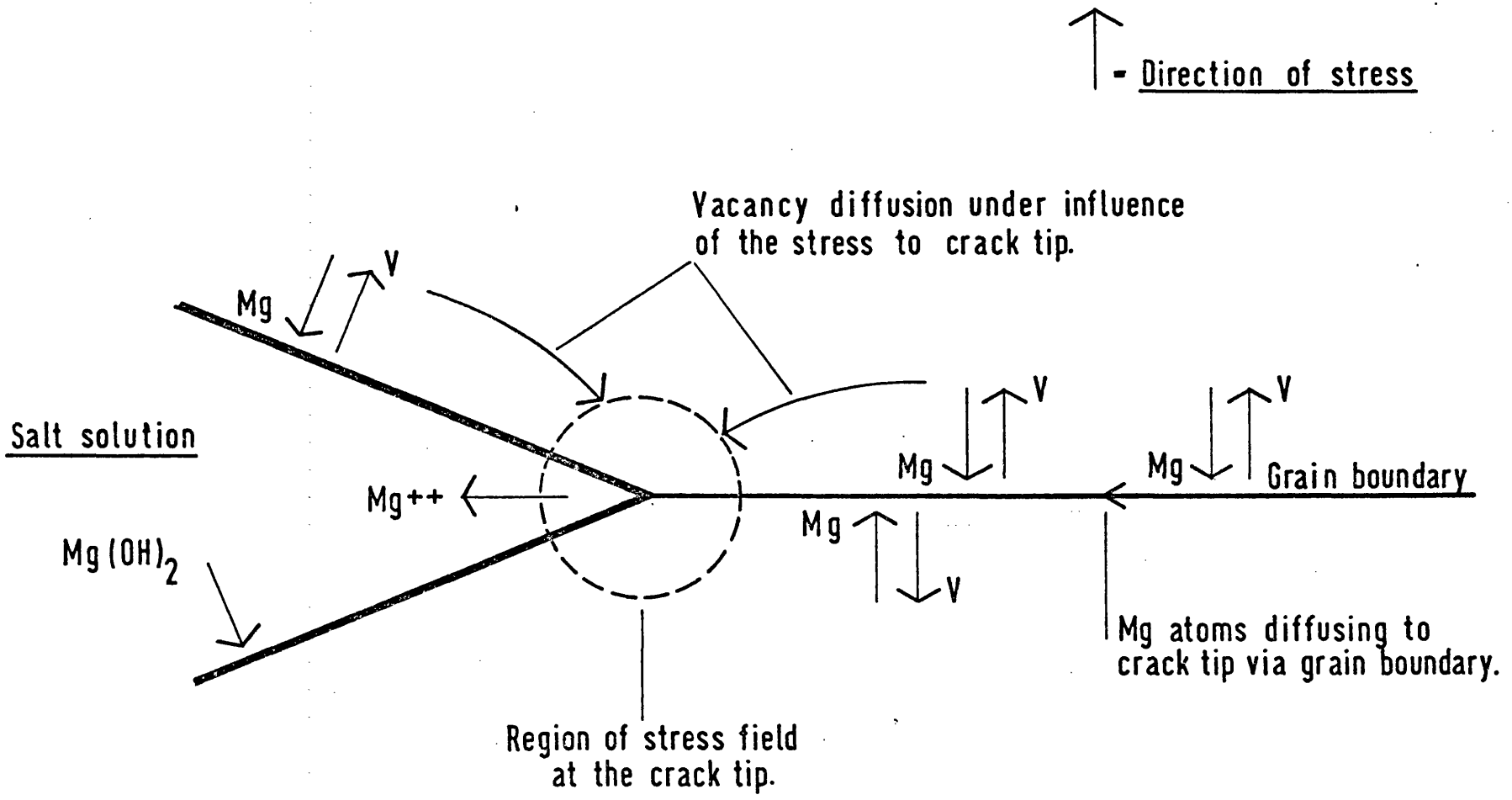

Fig. 6.9 Processes occurring at the crack-tip in the "vacancy" model of stress-corrosion cracking.